A Novel Approach to Touch Voltage Risk Assessment for Gas Pipelines in Shared Transmission Corridors

Keith Man-Kei Chan

2023

A Novel Approach to Touch Voltage Risk Assessment for Gas Pipelines in Shared Transmission Corridors

Keith Man-Kei Chan

A thesis submitted to Auckland University of Technology
in fulfilment of the requirements for the degree of
Doctor of Philosophy (PhD)

Supervisors:
Dr. Craig Anthony Baguley (Deceased)
Prof. Tek Tjing Lie
Prof. Udaya Kumara Madawala

School of Engineering
November 2023

Abstract

Touch voltage hazards are more likely to occur along long-distance pipelines within shared corridors with transmission lines. These hazards pose risks during routine pipeline maintenance when earthing must be temporarily disconnected. Existing probabilistic risk assessments tend to be simplistic and may overestimate risk. This research proposes an advanced probabilistic risk assessment method that integrates a year-long dataset of soil resistivity measurements. By developing soil resistivity models and generating touch voltage hazard profiles over time, a probability reduction factor is introduced to enhance risk assessment accuracy. This factor provides pipeline operators with a data-driven approach to determine the necessity of risk mitigation measures. A case study conducted in a shared gas pipeline and transmission line corridor validates the effectiveness of this approach. The findings demonstrate how modifying factors such as the number of workdays per year and temporary protection settings can help achieve acceptable risk levels.

Table of Contents

LIST OF FIGURES

List of Table

Abbreviations, Symbols, and Nomenclature

Abbreviations	Meaning
AC	Alternating Current
ALARP	As Low As Reasonably Practicable
ANN	Artificial Neural Network
CCITT	Consultative Committee for International Telephony and Telegraphy
CDEGS	Current Distribution, Electromagnetic Fields, Grounding and Soil Structure Analysis
CP	Cathodic Protection
DSP	Digital Signal Processing
EGVR	Earth Grid Voltage Rise
FFT	Fast Fourier Transform
EPR	Earth Potential Rise
ERT	electrical resistivity tomography
FOP	Fall-of-Potential
GIP	Grid Injection Point
GPR	Ground Penetrating Radar
GXP	Grid Exit Point
H0	Null Hypothesis
H1	Alternative Hypothesis
HiFreq	Electromagnetic Fields Analysis
ICC	Intraclass Correlation Coefficient
IEEE	Institute of Electrical and Electronics Engineers
IET	Institution of Engineering and Technology
ITU	International Telecommunication Union
NIWA	National Institute of Water and Atmospheric Research
PRF	Probability reduction factor
Q-Q	Quantile-to-Quantile
RESAP	Soil Resistivity Analysis
RMS	Root Mean Square
SESCAD	Safe Engineering Services & Technologies Limited Computer-Aided Design
Std	Standard

Symbol and Units	Description
%	Percentage
≈	Approximately Equal to
°C	Degree Celsius, scale based on zero for the freezing point of water and 100 degrees for the boiling point
A	Ampere
c	10^{-2} units
e	Euler's number
Hz	Frequency Unit in Cycles per second
k	10^{3} units
m	10^{-3} units, or length unit in metre
P	Probability of a scenario (dimensionless)
p	Probability value (dimensionless)
R	Resistance measured in Ω
s	Second
t	duration of an event (year)
T	Observation period (year)
u	Number of occurrences in a year (count)
V	Volt
ζ	Occurrence count of an event per year (count)
λ	Arrival rate of an event (count per year)
ξ	Annualised Probability of Human Presence on a Hazard Day (dimensionless)
π	Ratio of a circle's circumference to the diameter (dimensionless)
ρ	Ohm metre, Ω·m or Ω-m
σ	Standard deviation
Ω	Ohm

Publication

K. M. K. Chan, C. A. Baguley, U. K. Madawala, “A Novel Approach to Touch Voltage Risk Assessment for Gas Pipelines in Shared Transmission Corridors,” IET Sci. Meas. Technol., vol. 17, pp. 27-36, 2023.

Attestation

I hereby declare that this thesis is the result of my personal ideas and efforts and, to the best of my knowledge, does not contain any material that has been previously published by any other person. All complementary sources and efforts have been mentioned in the citations, references and acknowledgements provided. I also declare that the thesis, or any part of it, has not been previously submitted for the award of any other degree in any other institution of higher learning.

Keith Man-Kei Chan _____

In Memory of Craig Anthony Baguley

(8 February 1969 to 30 January 2023)

"The pursuit of a PhD degree is a life-changing experience."

Dr. Criag Baguley left us forever on 30 January 2023. The author was his first and last primary-supervised Ph. D. student. The author first encountered him during a Power Electronics class in 2012, where he substituted for a lecturer in 2012.

Craig's daily routine at AUT typically began at 7 AM and finished at 7 PM. His mornings were dedicated to administrative tasks, homework assessments, and course material preparation. He maintained an open-door policy, often assisting a long queue of students and providing guidance and support regardless of their background, race, religion, and academic achievement.

Although Craig was a devoutly religious man, he maintained his faith secretly at AUT. Craig's brother described him as a 'quiet man.' Craig devoted himself to humanitarian work with his wife Tina every Saturday, delivering essential goods to island countries in need. Every Sunday morning, Craig dedicated his time to attending Mass. He loved singing and was a member of the choir at the Cathedral of St Patrick and St Joseph. In his private life, he was an amateur boxer, and his muscular upper body remained concealed beneath his shirt.

During this research period, Craig's mother battled a vascular disease. She had one foot amputated, prompting him to make frequent trips to a nearby hospital every day, located just one kilometre away from his office. Heartbreakingly, his mother passed away at the end of this research data collection phase.

On the day of the research journal's publication, Craig did not show up at work. Only a few knew it was linked to his battle with Glioblastoma multiforme, an extremely aggressive and lethal form of brain tumour. Sadly, only 25% of patients survive more than one year, and 5% of patients survive more than five years.

The author visited him at home and discovered a shared graduation year of 1993 from the University of Auckland. The author later discovered that some of his friends had been classmates with Craig during their studies for a Bachelor of Commerce in the 1990s.

Craig's health rapidly deteriorated before Christmas 2022. On 30 January 2023, he passed away peacefully at home while the North Island of New Zealand experienced widespread catastrophic floods caused by heavy rain. He is now resting in peace with his mother at Waikumete Cemetery.

Ave Maria, gratia plena,
Dominus tecum,
benedicta tu in mulieribus,
et benedictus fructus ventris tui, Iesus.
Sancta Maria, Mater Dei,
ora pro nobis peccatoribus,
nunc et in hora mortis nostrae.
Amen.

Acknowledgements

I want to express my sincere gratitude to my respected supervisors, Prof. Tek Lie, Prof. Udaya Madawala, and as well as Dr. Rodney Urban, for their support throughout my research journey. I would also like to express my sincere appreciation to our sponsor, BECA (NZ) Limited, and the Callaghan Innovation Funding, whose financial and resource support made this research endeavour possible. Last but certainly not least, I extend my gratitude to Dr. Craig Anthony Baguley for bringing me on board this remarkable journey.

Before embarking on the path to a PhD, Craig and I discussed introducing new teaching topics in electrical earthing and lightning protection. I vividly remember Craig saying, "The pursuit of a PhD degree is a life-changing experience." His words brought a smile to my face, as I had never seriously considered pursuing a PhD at the time. However, it reminded me of the promise I made to my parents many years ago before leaving for London to become a medical doctor. Ironically, my path led me into the realms of particle physics, electronics, and computer science. Consequently, I made the odd decision to take the plunge and embark on a different kind of doctorate journey.

Craig and I spent a year searching for an industrial sponsor before securing funding from Callaghan Innovation. Our efforts included two trips to Christchurch in pursuit of sponsorship. We also approached my former employer for support, but the new General Manager declined our proposal. Fortunately, we sought assistance from Dr. Rodney Urban, Director of BECA (NZ) Limited and leader of its Electrical Earthing Team. During our discussions, Dr. Urban highlighted that probabilistic risk assessment was an underutilised area of study, which aligned with my expertise in lightning protection and earthing system design. He played a key role in securing the funding and, along with his Electrical Earthing Team, facilitated access to the CDEGS earthing software and other valuable resources at his office to support our research.

Before the COVID-19 pandemic emerged, certain distribution network operators, who were my former clients, had willingly agreed to assist in collecting data within their operational areas.

Regrettably, due to the implementation of health and safety measures prompted by the pandemic, all these plans had to be abandoned. I express my profound gratitude to my friend's parents, Mr. Hok Ming Chan and Ms. Chi Ying Lee, who unconditionally provided access to their land for research during the period of travel restrictions. It came as a surprise that their land is conveniently located adjacent to a genuine transmission shared corridor. This unexpected transmission shared corridor allowed for making the hypothetical case study more realistic.

I would also like to acknowledge the support of my electrician apprentice, Mr. William Cheng. He kindly allowed me to use his café, conveniently located between BECA and AUT, as my temporary office during the periods of travel restrictions across New Zealand.

This research faced a series of significant challenges, which Craig and I tackled one by one. Tragically, at the beginning of 2022, Craig lost his mother, and not long after, he also passed away. Before his passing, he asked me to complete this research, and fulfilling his wish has become my way of honouring his legacy.

I dedicate this research to the memory of Dr. Craig Anthony Baguley, whose guidance and vision continue to inspire me.

Hail Mary, full of grace,
the Lord is with thee.
Blessed art thou amongst women,
and blessed is the fruit of thy womb,
Jesus.
Holy Mary, Mother of God,
pray for us sinners,
and in the hour of our death.
Amen.

Chapter 1 - Introduction

The earthing system of a power grid plays a critical role in ensuring electrical safety by providing a controlled path for fault currents and mitigating touch and step voltage hazards. Soil resistivity, a key factor influencing earthing system performance, varies seasonally due to environmental conditions such as moisture and temperature fluctuations. Conventional earthing system design relies on conservative assumptions that do not fully account for these variations, potentially leading to inaccurate risk assessments. While probabilistic risk assessment methods offer a statistical approach to evaluating the acceptance criteria of electrical shock hazards, existing models do not sufficiently address the seasonal effects on touch voltage hazards, particularly during maintenance activities on gas pipelines.

This research investigates the impact of seasonal soil resistivity variations on touch voltage hazards encountered by maintenance workers on gas pipelines. A novel probabilistic risk assessment framework is introduced to quantify the influence of these seasonal changes, improving the understanding of risks during maintenance activities. The study contributes new knowledge by refining risk assessment methodologies, leading to a more accurate evaluation of touch voltage hazards specific to gas pipeline maintenance.

This chapter presents the background of earthing system design, the development of a probabilistic risk assessment approach, the research purpose, key research questions, contributions to knowledge, and the overall structure of the study, concluding with an outline of the thesis.

1.1 Earthing System of the Power Grid

The earthing system is one of the essential parts of the power grid. The components of an earthing system consist of an earth grid, earth electrodes, earth conductors such as overhead earth wires, cable sheaths and the soil [1]. The primary purpose of an earthing system is to provide a safe environment during power system earth faults by allowing the fault current to discharge into the earth before the protective relay system operates to interrupt the delivery of electrical energy [2]. Most countries use earthed neutral for power transmission and distribution systems. The neutral

can be directly connected to the earth or connected to the earth through a Neutral Earthing Resistor or Reactor to limit the maximum fault current. The benefits of an earthed neutral include during a single phase to earth fault, the risk of system over-voltages can be minimised, thus reducing the chance of insulation failure, ensuring sufficient earth fault current to reliably operate the protective relaying systems and simplifying the insulation requirements for primary equipment.

Hence, soil is often used to conduct the neutral and fault currents. To distinguish between these two types of currents, the neutral current typically flows between the grounding systems of the power source and the load, whereas the fault current flows from the point of fault to the grounding system of the circuit's source. Nevertheless, as current flows through the earth, it spreads to remote earth locations and converges back to the circuit's source, forming a complete circuit. During a single line-to-earth fault condition, a substantial amount of current flows through the fault location, significantly elevating the earth's electrical potential on the ground surface along the path of conduction and in the vicinity of the earthing system [2].

Therefore, despite its cost effectiveness and availability, the drawback of using the earth for conduction is that a potential difference between two points on the earth's surface can reach a level capable of causing an electric shock to animals or humans when two extremities simultaneously come into contact with two different earth potentials.

Depending on magnitude of the potential difference across the ground, the electric shock can be hazardous because the current that passes through a living object, known as body current [3], could cause damage to the living tissue or interrupt vital biological functioning, such as the heartbeat [4]. For example, suppose a power system earth fault occurs while a person is touching an earthed metallic structure. In this case, fault current may flow from the structure through the body to the ground, causing an electric shock. The potential difference between the hand and feet is called touch voltage. Similarly, the electric shock caused by the potential difference between two feet is called step voltage [2, 5]. The primary hazard from touch and step voltages is ventricular fibrillation, often leading to fatality if the victim is left untreated at once [4, 6].

The earth potential rise hazards are not limited to the power system installation. These hazards can be transferred outside the power system installation because the nearby metallic structure can become an alternative path for the earth current. The current that splits into the metallic structure can also create an electric shock that harms the living being. Therefore, a thorough consideration of earth potential rise hazards is essential in the design of any non-power system structures located near power system components.

1.2 Design of Earthing System

In the design phase of power system installations, computer simulations help predict the influence of earth potential rise associated with power system installations and nearby structures such as pipelines, railways, lamp posts, or fences. Computer simulation software is commonly used for this purpose, and it simulates the effects of various electrical phenomena on earthing systems, soil, and metallic structures such as fences. In addition, the touch and step voltages can be analysed under different scenarios, to evaluate the effectiveness of the different hazard mitigation methods.

To design a safe earthing system using computer software, representative soil resistivity data is of paramount importance during the design stage for determining tolerable human limits of touch and step voltages. However, soil resistivity varies due to multiple factors, such as moisture content, temperature, and soil composition, making it challenging to obtain accurate measurements that precisely represent the soil.

To overcome this challenge, designers typically apply conservative assumptions when selecting soil resistivity values for earthing system designs. For example, a horizontally layered soil resistivity model with higher resistivity values in each layer can represent a worst-case scenario where the earthing system must handle a significant prospective fault current. In this scenario, the design anticipates higher earthing resistance due to the high resistivity assumptions. However, after the earth grid is installed, the actual earthing system resistance is often measured to be lower than predicted by the simulation. This occurs because the conservative model includes an additional margin to account for soil resistivity uncertainty. The reduced as-built resistance allows

sufficient fault current to flow, ensuring that the high-speed protection system detects faults and activates the circuit breaker, meeting performance specifications.

Similarly, designers may also assume a low soil resistivity value to obtain lower tolerable voltage limits for assessing human safety against touch and step voltages during a fault condition. By combining these two conservative assumptions, designers can confidently ensure that the actual touch and step voltages will be significantly lower than its design, and humans can sustain that touch and step voltages well below the heart fibrillation threshold during a fault condition of the associated power system.

While soil resistivity varies geographically and over time due to changes in soil properties, the conservative approach applied in the earthing system design, which typically assumes a worst-case scenario of high soil resistivity, may not be appropriate for evaluating the safety of non-power system infrastructure in the vicinity from the fault site or the source of the fault because their earthing system is not necessarily connected to the power system earth grid. Therefore, periodic review of soil resistivity is necessary to ensure that the assumed conservative soil resistivity value does not mislead the hazard identification process.

1.3 Probabilistic Risk Assessment Method

Risk is recognised as a natural part of our daily lives. Risk refers to the possibility of experiencing harm, loss, or undesired outcomes in various situations [7]. Risk assessment is a systematic process that involves identifying, analysing, and evaluating potential hazards or risks associated with a particular activity [8]. The objective of risk assessment is to understand the nature and extent of the risks involved and to provide information that can be used to make informed decisions regarding the identified risks.

The risk assessment for earthing system safety typically involves several key steps, including hazard identification, risk analysis, and risk evaluation. First, potential hazards are identified and documented in the hazard identification step. Next, in the risk analysis step, the likelihood and consequences of each identified hazard are assessed, and the level of risk associated with each

hazard is determined. Finally, the risk analysis results are evaluated in the risk evaluation step, and decisions are made about mitigating or managing the identified hazards.

Quantitative and qualitative risk analysis are commonly used methodologies for assessing and analysing risk. Qualitative risk analysis involves identifying and assessing risks based on subjective judgments, reoccurrences and expert opinions [9, 10, 11]. This method does not use numerical values to measure risk but instead evaluates risk based on severity, frequency, and impact. Therefore, using qualitative risk analysis makes it difficult to define a clear guideline on how the risk can be accepted or rejected.

On the other hand, quantitative risk analysis involves using numerical values to measure the likelihood and consequences of a specific risk [12]. This method utilises statistical data, mathematical models, and simulations to evaluate the risk and determine the probability of specific outcomes. Therefore, the quantitative risk analysis provides a more precise and accurate representation of the hazards. The other benefit of quantitative risk analysis is that the stakeholder can prioritise allocating resources and efforts to address the identified risk.

Probabilistic risk analysis is a commonly used quantitative method for analysing risk [11]. The assessment involves using mathematical models and simulations to determine the probability and consequences of specific fault scenarios. The probabilistic risk analysis in this thesis is the probability of heart fibrillation due to electric shock. The goal is to provide the basis for risk evaluation and decisions about the identified hazards.

1.4 Purpose of Research

Under normal operation, the underground pipelines may be electrically isolated from the earthing system. During electrical fault conditions or lightning events, the pipelines must be electrically connected to the earthing system through a surge arrester to reduce the risk of insulation breakdown of the pipeline gaskets and the protective coatings. However, for the pipelines undergoing routine maintenance, the electrical coupling mechanisms, such as the surge arrester to the earthing system, must temporarily be disabled to allow specific pipeline tests to be undertaken correctly [12, 13]. During an electrical fault associated with nearby transmission lines,

the absence of the surge arrester can cause the potential difference between the pipeline and the immediate earth to be high enough to create a harmful electric shock to the workers [2, 13].

The touch voltage hazards can be eliminated by taking mitigation actions, such as installing gradient control conductors or earth mats [2]. However, these can incur high costs for existing long-distance transmission-class pipelines [8]. On the other hand, some test procedures may involve temporary disconnection of the pipeline earth system; therefore, the test is carried out under the exposure of electrical shock risk. To encounter this unavoidable risk, if the mitigation cost is disproportionated to the benefit obtained or the exposure to the risk is a part of the work procedure, the risk can be accepted by comparing the quantified probabilistic risk level with the pre-defined probability threshold under the principle of 'As Low As Reasonably Practicable' [5, 7, 8, 14] .

The current probabilistic risk analysis using the Poisson distribution [1] to model the risk assumes that hazardous earth fault events can occur randomly every day within an observation period. However, this calculation does not take into account the effects of soil resistivity variations [5, 12]. When soil resistivity variations are considered, it introduces the possibility that hazardous events may not occur daily. The sensitivity of body current to earth current is affected by the properties of the soil resistivity. For example, on a hot and dry day, the earth's surface with high contact resistance can significantly reduce the current flowing through a human body to a safe level in the event of an earth fault.

By integrating soil resistivity variation into the risk assessment, it becomes possible to consider how different soil conditions may influence the occurrence and severity of hazardous earth fault incidents. A more comprehensive assessment of the risks associated with earth fault events can provide effective risk management or hazard mitigation to the specific conditions and properties of the soil in a given location.

The effect of the seasonal soil resistivity variation is recognised and can affect hazards caused by the earth potential rise [5, 15, 16]; these hazards include the touch and step voltages. However, due to the lack of continuous historical data about the soil resistivity model for the particular soil,

the touch and step voltage hazards induced by the conduction of body current during the earth fault event cannot be accurately established. The adverse effects of inaccurate hazard identification due to variations in soil resistivity are often masked by excessive conservative considerations in design and routine safety assessment.

Excessive conservatism in design can serve as a double-edged blade. On one hand, it ensures safety by assuming worst-case conditions, such as persistently high soil resistivity, which aligns with the threshold for human fatality in hazards like touch voltage. On the other hand, it can lead to overly restrictive risk assessments and the false identification of hazards. Conservative assumptions may overestimate risk, preventing the acceptance of certain risks that could be considered tolerable under a more realistic assessment of soil resistivity dynamics.

While the worst-case approach guarantees safety by accounting for conditions where human fatality thresholds might be reached, it often disregards the natural variability of soil resistivity due to seasonal and environmental factors. This static, highly resistive model, while protective, does not reflect actual temporal and spatial variations in soil conditions. Consequently, hazards may be over-predicted, leading to unnecessarily rigid designs and inefficient resource allocation.

To address these limitations, this thesis proposes a novel risk assessment approach that integrates real-world soil resistivity variations into touch voltage evaluations. A year-long dataset of periodic Wenner test measurements is used to develop soil resistivity models that capture seasonal changes. These models enable the estimation of body current exposure under varying soil conditions, ensuring that the calculated risk aligns with critical human safety thresholds. By incorporating dynamic soil resistivity into the assessment, this method improves the accuracy of risk quantification.

To further refine the risk assessment, statistical distributions are applied to calculate a probability reduction factor, quantifying the proportion of days within the observation period when touch voltage risks are present. This factor is then incorporated into the probabilistic risk calculation, which traditionally considers only the frequencies and durations of human contact and earth faults [12]. The result is a more precise and realistic risk assessment that maintains safety margins while

allowing greater flexibility in risk management. This approach aligns with the ALARP principle by balancing safety and efficiency, reducing the inefficiencies of overly conservative designs while ensuring compliance with human fatality thresholds.

1.5 Research Questions

In the areas of soil resistivity modelling and probabilistic risk analysis, a series of fundamental questions arise, each designed to address the complexities of electrical safety in the context of underground pipelines. Because these pipelines are critical assets in energy transportation and infrastructure, it is critical to understand the basic principles that govern safe operation to introduce improvement to the existing methods in hazard identification and risk assessment. These questions are listed below:

1. What are the essential requirements for soil data collection to meet the criteria for soil resistivity modelling?
2. What is the minimum sample size needed for a robust statistical analysis?
3. How does the variation of soil resistivity impact the occurrence of touch voltage hazards?
4. How can the varying soil resistivity be effectively integrated into the current probabilistic residual risk assessment?
5. How can pipeline asset operators implement safety management utilizing the proposed risk calculation method to ensure compliance with the As Low As Reasonably Practicable principle?

1.6 Contributions to Knowledge

This research introduces several significant contributions to the understanding and management of earth potential rise hazards, particularly in the context of gas pipeline maintenance. The key contributions are outlined below:

Consideration of Seasonal Soil Resistivity Variations

- Gas pipeline operators often face challenges due to limited knowledge and resources for addressing earth potential rise hazards. Existing information, such as updated prospective fault levels, is often not readily available.
- The first major contribution of this research is the consideration of seasonal variation in soil resistivity over an extended period. This addresses the limitations of current methods and enhances the accuracy of hazard identification for earth potential rise. The research outcome provides a better understanding of how seasonal changes in soil resistivity impact touch voltage hazards, improving the overall risk assessment.

1. Introduction of the Probability Reduction Factor (*PRF*)
    - Current probabilistic risk assessment methods primarily focus on the coincidence of contact and fault scenarios but do not fully incorporate the critical probability of ventricular fibrillation in the context of touch voltage hazards.
    - The second contribution is the introduction of a *PRF* that accounts for the probability of ventricular fibrillation, based on soil resistivity monitoring. This novel variable refines the existing probabilistic residual risk calculations, making them more representative of realistic touch voltage hazards. The *PRF* enables the development of a dynamic risk model that provides an acceptance boundary of risk, considering both prospective fault levels and the duration of maintenance personnel exposure. Furthermore, soil resistivity monitoring leads to a better understanding of the variation in touch voltage hazards.
2. Enhanced Risk Representation for Maintenance Personnel
    - In situations where planned outages or reductions in fault protection settings are not feasible, the third contribution is the introduction of an improved risk assessment approach that enables pipeline asset operators to make better-informed decisions, consistent with the As Low As Reasonably Practicable (ALARP) principle.
    - By integrating the proposed *PRF*, this approach allows for a more comprehensive and realistic representation of the risks faced by maintenance personnel. It provides

a basis for identifying potential earth potential rise hazards and helps operators implement targeted safety measures, ensuring adequate protection for workers. This new methodology is a significant advancement in safety and risk assessment practices, contributing to both personnel safety and pipeline integrity.

1.7 Thesis Outline

This thesis is organised as follows:

Chapter 2 presents the background material related to the earth system, underground pipelines, the existing risk assessment methods outlined in industrial standards, and the statistical methods used in this research.

Chapter 3 provides a literature review of the research. The identified research topics include seasonal soil resistivity variation, modelling and simulation, system model simulation, and probabilistic modelling and applications. The scientific knowledge gaps identified from the literature review are summarized in this chapter.

Chapter 4 describes the procedure and results of a 12-month soil resistivity monitoring study.

Chapter 5 details the development of a touch voltage profile using a hypothetical pipeline model.

Chapter 6 introduces a novel statistical framework derived from the touch voltage profile. The key innovation, the Probability Reduction Factor (PRF), is demonstrated using a real-life transmission setting. This also illustrates the feasibility of applying this novel risk assessment method for maintenance planning.

Chapter 7 extends the application of the touch voltage profile beyond risk assessment by transforming it into a touch voltage equation with carefully selected predictors. This provides a tool for detecting hazardous touch voltages during emergency maintenance.

Chapter 8 discusses the research contributions and potential future research opportunities.

Chapter 9 concludes the research.

Chapter 2 - Background

This chapter provides the necessary background to support the development of the research. A fundamental understanding of earthing systems is essential, as they play a critical role in ensuring electrical safety in pipeline and transmission line environments. Since earth potential rise during electrical faults directly influences touch and step voltage hazards, an explanation of this phenomenon is included. The assessment of these hazards requires well-defined safety thresholds, so the background also covers the calculations of tolerable touch and step voltages based on established standards [1, 2, 5, 12].

To address the hazards associated with earth potential rise, common hazard mitigation methods are reviewed. The effectiveness of these mitigation strategies depends on accurate soil resistivity data, as soil characteristics influence fault current dissipation. Therefore, various data collection methods for soil resistivity are discussed, highlighting their importance in modelling earthing system performance. Since this research adopts a probabilistic approach to risk assessment, an overview of probabilistic methods and acceptance criteria is also provided. These foundational topics collectively establish the theoretical and practical context for the study's methodology and analysis.

2.1 Earthing Systems

An earthing system provides a pathway for the current to return to the source via the mass earth. The earth current can be a return current of a fault condition, a zero-sequence current of an unbalanced load condition, and a leakage current from the power system components. Power system earthing requires that the earth fault current associated with the power system is detectable so that the protection devices, such as circuit breakers, can effectively be operated to the designated settings. On the other hand, when the fault current flows to the earth, the metallic parts in contact with the earth can be livened to a dangerous level. If a person contacts these livened objects, the person may receive an electric shock as the person's body may provide an alternative conduction path for the fault current due to the potential difference between the two contact points [2, 5]. The severity of the electric shock depends on various factors, such as the duration of

exposure, the path and magnitude of the current through the body, and the person's overall health status and medical condition [18]. For personal safety, the hazards related to earth potential rise can be identified through three contact scenarios that can result in electric shocks. When the conduction path is between one hand and two feet, it is referred to as touch voltage. When the conduction path is between two hands, it is referred to as reached touch voltage. Finally, when the conduction path is between two feet, it is referred to as step voltage [2, 5].

On the other hand, a significant amount of earth current can also be transferred outside the power system facility in a fault condition. Metallic fences, pipelines, and metallic cable sheaths can provide low-resistive paths to split some part of the earth current towards the electrical earthed third-party structures [12, 19]. As a result, the current density around the affected structure may increase during an electrical fault. Depending on the soil conditions and the fault level, the electrical potential gradient on the earth's surface may also become hazardous to humans as the current density increases. By considering these factors and taking appropriate measures, engineers can design an effective earthing system that can limit the potential gradient on the earth's surface to minimise the risks associated with the earth current interference and ensure the safety of the power system facility and neighbouring structures.

Furthermore, understanding soil resistivity is crucial in the design of effective earthing systems for power facilities. Since soil resistivity directly influences the dissipation of the electrical charges from the fault currents into the earth, low-resistivity soil allows for more efficient dispersion of fault currents. In contrast, high-resistivity soil can impede the electrical charges dissipation [2, 5], causing a high potential gradient on the earth surface and diverting the earth current to other metallic structures. The other factors that also affected earthing performance are the choice of electrode material and placement orientation. Therefore, when designing an earthing system, local soil resistivity, along with these other factors, is essential to be taken into account as the effectiveness of the earthing system relies significantly on these elements and quantities. These considerations collectively contribute to ensuring a well-functioning and reliable earthing system. Thus, engineers must conduct sufficient soil resistivity measurements and surveys to determine the appropriate earthing design and ensure the safety of power system facilities and

nearby structures at all times [5]. Eventually, understanding soil resistivity is a critical element of managing electrical hazards associated with fault conditions and ensures the safety and reliability of electrical systems.

2.2 Soil Resistivity Measurement Methods

Measuring soil resistivity is a process of determining the resistance of a soil sample to the flow of electrical current. Various methods have been developed to measure soil resistivity under different environmental conditions and depths accurately. Two commonly used, non-destructive, and cost-effective methods for earthing system analysis are the Wenner and Schlumberger tests, also known as the 4-pin test methods, which do not require drilling or excavation. Another non-destructive approach involves using electromagnetic methods, such as ground-penetrating radar (GPR). The 4-pin test methods and electromagnetic techniques are commonly used in geophysical prospecting to determine the subsurface electrical resistivity of soils and rocks. The strengths and weaknesses of these methods will be discussed in the following sections.

2.2.1 Electromagnetic Method

When it comes to soil resistivity measurement, the electromagnetic method, explicitly using GPR, shown in Figure 2-1, offers significant advantages in terms of both speed and accuracy. GPR is highly sensitive to changes in soil properties, including resistivity, and its penetration depth can be adjusted by varying the radar signal frequency, allowing for the assessment of deeper layers of earth materials and electrical properties [20].

This capability provides the accuracy and precision of soil resistivity measurements and produces the soil model on-site, so post-processing of the soil resistivity data is not required. GPR is commonly used to produce 3D soil models and underground infrastructure identification.

Figure 2-1 Ground-penetrating radar was used to identify the subterranean earth connection within a power station. The photos were taken by the author in 2017.

2.2.2 Schlumberger Test

The Schlumberger array, named after Conrad Schlumberger, the founder of the modern SLB company, has a rich history dating back to the early 1900s. Conard introduced the revolutionary concept of using electrical measurements to map subsurface rock bodies for metal ore mining [21].

In the Schlumberger test, the electrode configuration is arranged symmetrically about a centre point. The potential electrodes are stationed at a fixed distance about the centre of the test traverse, as illustrated in Figure 2-2. Unlike the later development of the Wenner method, where all electrodes are relocated for each measurement, in the Schlumberger array, however, only the current electrodes are moved away from the centre point to adjust the probe spacing for the subsequent measurement. The other characteristic is that the length of each Schlumberger test traverse does not have a fixed length, and the measurements of the apparent soil resistance continue until the potential difference between the two potentials becomes too small to measure

accurately. As a result, the current electrodes are often extended to considerable distances from the centre point of the traverse. This characteristic makes the Schlumberger array particularly well-suited for deeper subsurface investigations [22].

In terms of mathematical interpretation of using the Schlumberger array, it utilizes the inverse square law in its calculations to evaluate apparent soil resistivity. The mathematical expression used to calculate the apparent resistivity ρ commonly used in the industry expressed in (1) is as follows [22]:

$$\rho = \frac{\pi\left(\frac{s^2 - a^2}{4}\right)}{a} R \ [\Omega.m] \tag{1}$$

where,

s is the distance between the current electrode and the nearest potential probe (m),
a is the distance between two potential probes (m),
R is the measured apparent soil resistance (Ω).

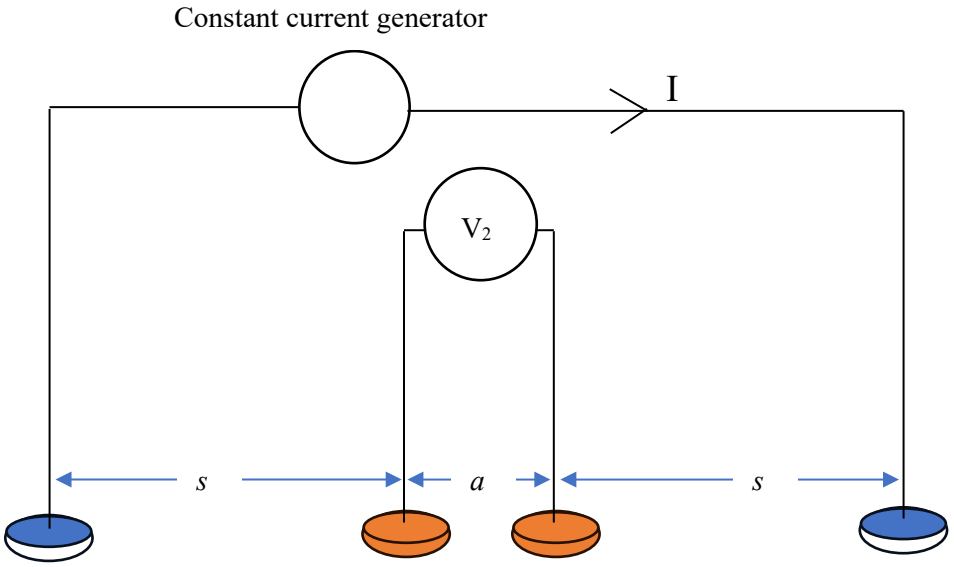

Figure 2-2 The Schlumberger array has four electrodes placed on a line around a common midpoint with two outer current electrodes and two inner fixed potential electrodes.

The Schlumberger method is preferred for geophysical surveys over extensive areas like mining sites. It offers high resolution when probing deep resistivity layer profiles, which makes it especially suitable for tasks involving deep subsurface exploration.

However, the Schlumberger method does come with some drawbacks that make it less suitable for electrical earth potential studies. One of the main limitations is the need for substantial probe spacing when conducting Schlumberger measurements.

In electrical studies, the focus is mainly on understanding the electrical potential in the immediate vicinity of earthing systems, such as power stations or substations, during fault conditions. These studies only required measurements at relatively shallow depths, as the main concern is human safety and the potential for electric shock. The extensive probe spacing characteristic of the Schlumberger array, which is advantageous for deep subsurface exploration, becomes a drawback in this context. It makes it challenging for soil resistivity measurement to obtain reasonable quality at the shallower depths relevant to electrical safety analysis.

Additionally, the mathematical interpretation of Schlumberger measurements involves complex procedures and equations. This complexity made quality control to ensure the reliability of the data collection process difficult.

2.2.3 Wenner Test

The Wenner method was developed based on the particular case of the Schlumberger array, where all electrodes are equally spaced. The Wenner and Schlumberger tests are well-documented in standards and guidelines [1, 5, 22]. The main difference between the two methods is the arrangement of the electrodes used to measure soil electrical resistivity [22]. In the Wenner test, four electrodes are placed evenly in a straight line, as shown in Figure 2-3. Therefore, all four electrodes must be repositioned for every test spacing. The objective of this arrangement is to leverage the symmetrical properties in electrical potential calculations, making the conversion from apparent soil resistance to resistivity more straightforward compared to the calculations required for the Schlumberger method.

Assuming the homogeneous soil resistivity is ρ, the current injection at the two outer probes can be imagined as creating a different path in the earth, as shown in Figure 2-4. Therefore, if a virtual line is drawn to link the points in the ground will form an equipotential plane which is orthogonal to the current paths. Those current paths influence the electrical potential difference between two

voltage probes. Since the soil is homogeneous and the probe arrangement is symmetrically and evenly distributed, the volume of soil measured can be approximated to a truncated cone shape with the tip cut off, as shown in Figure 2-4.

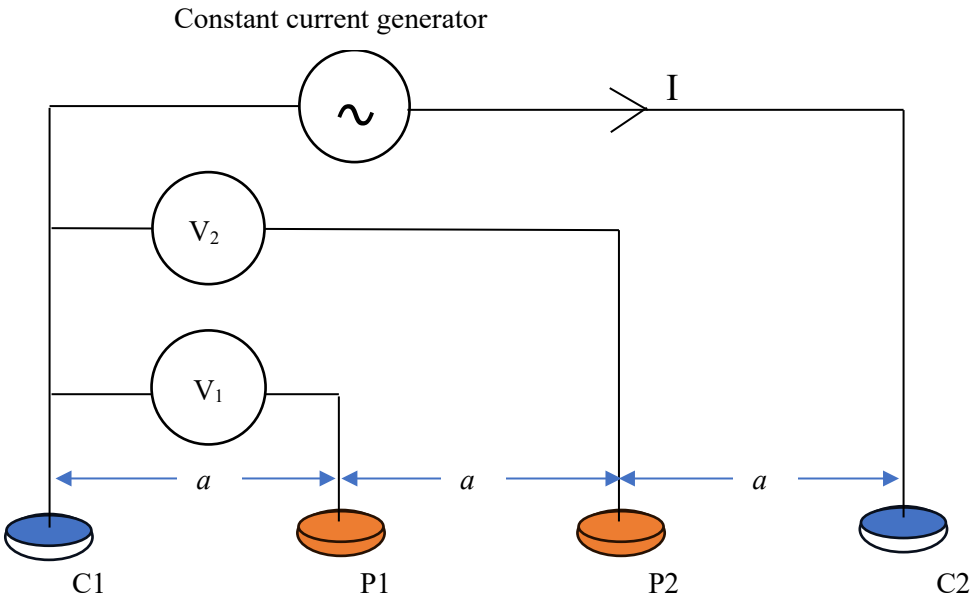

Figure 2-3 The setup of the Wenner Test. The off-frequency constant current signal is injected into the ground through the hemispherical electrodes.

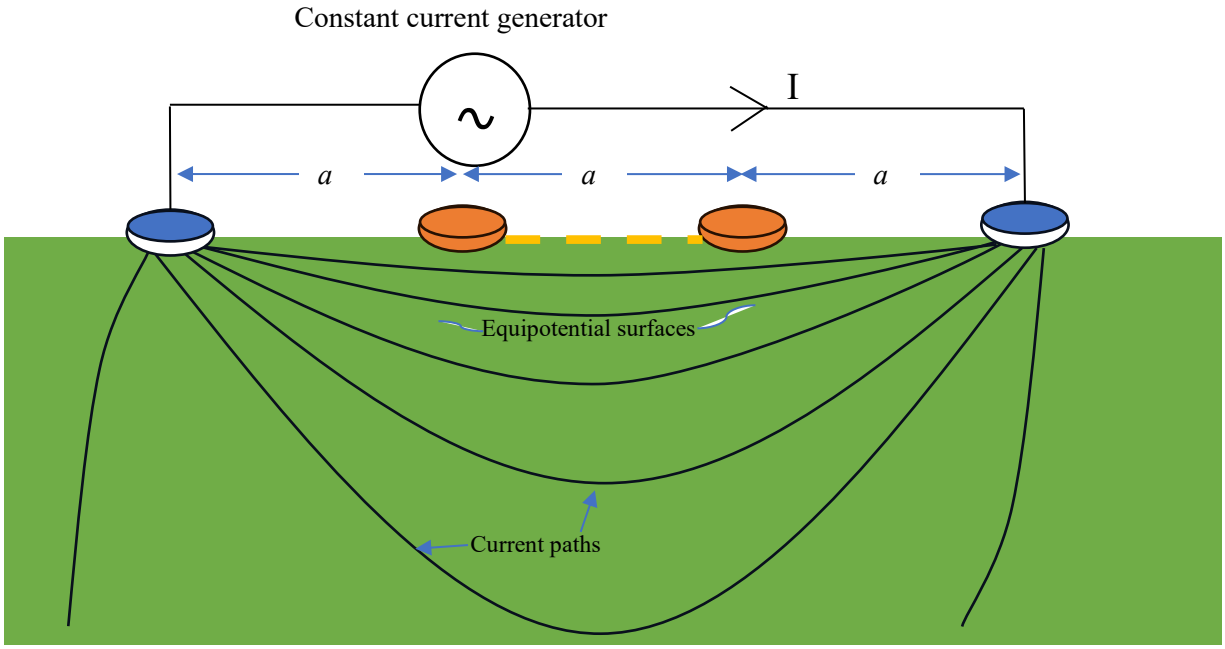

Figure 2-4 The soil volume measured with the Wenner test is bounded within the dotted yellow lines. The current paths and equipotential surfaces are indicative only.

Suppose all probes are in semi-spherical shape or the depth of the probe is less than ten times the probe spacing [22]. V_1 is the voltage measured between Probes C1 and P1 in Figure 2-3, according to V_1 can be written in (2) as follows:

$$V_1 = \rho\, I \left(\frac{1}{2\pi a} - \frac{1}{2\pi(D-a)}\right)[V] \tag{2}$$

where,

D is the distance between Probes C1 and C2 (m),
I is the current injected (A),
ρ is the apparent soil resistivity (Ω-m).

The equation is rewritten in terms of a, given:

$$V_1 = \rho\, I \left(\frac{1}{2\pi a} - \frac{1}{4\pi a}\right)$$
$$V_1 = \rho\, I \left(\frac{1}{4\pi a}\right)$$

Similarly, for V_2,

$$V_1 = \rho\, I \left(\frac{1}{2\pi(2a)} - \frac{1}{2\pi(3a-2a)}\right)$$
$$V_2 = \rho\, I \left(-\frac{1}{4\pi a}\right)[V]$$

Therefore, the potential difference between two Probes, P1 and P2, is calculated to be expressed in (3):

$$V_{12} = \rho\, I \left(\frac{1}{2\pi a}\right)[V] \tag{3}$$

Since V_{12}/I is the apparent soil resistance, the equation for calculating soil resistivity using the Wenner test is expressed in (4) as follows:

$$\rho = 2\pi a R\ [\Omega.m] \tag{4}$$

where,

ρ is the apparent soil resistivity in ohm-metre (Ω-m)

a is the spacing between current electrodes (m)

R is the apparent soil resistance (Ω)

Due to the symmetric property of the test array, the Wenner test generally can obtain more accurate resistivity values than the Schlumberger test for shallow soil measurements [2, 23].

The soil resistivity is a main component to define the electrical performance and safety of earthing systems. The reliable measurement of soil resistivity is of paramount importance since it directly

impacts the magnitude of the earth potential rise on the earth's surface in the event of a fault condition. The safety and integrity of electrical systems are complexly linked to the property of earth potential rise, making it a critical factor in electrical engineering. The following section will describe the concept of earth potential rise and its implications for safety and system performance.

2.3 Earth Potential Rise

An earth potential rise (EPR) is defined as a measure of the voltage between the distant soil surface and remote earth potential (0 V), where remote earth is used to describe the resistance between a point in earth and a distant earth test point, beyond which measurement of the earth resistance will not decrease [22]. When a fault current enters the earth, the earth potential is the highest at the fault location. The magnitude of the earth potential is the highest during the fault. This highest EPR condition is applied to all the related studies as the worst case can maintain the conservatism of the hazardous voltage predictions.

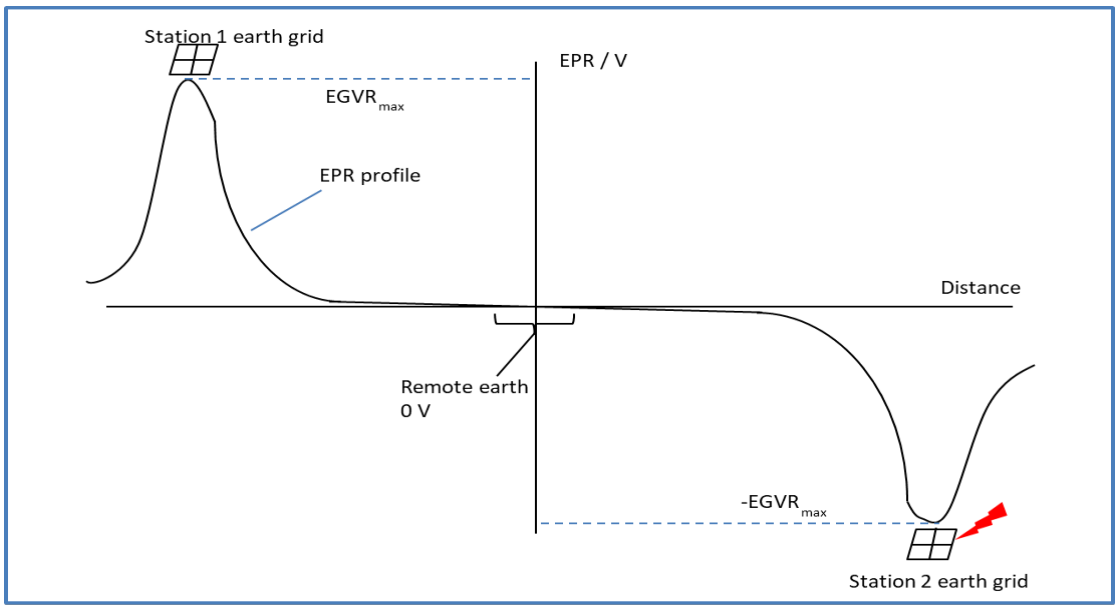

Figure 2-5 *Earth Grid Voltage Rise (EGVR) caused by an earth fault at Station 2. Earth Potential Rise (EPR) appeared immediately outside the earth grids.*

The fault location can be within the power system facility or a remote location such as a transmission tower. Nonetheless, EPR will not manifest outside the earthing system if the fault occurs within the earthing system of the source because the fault current remains confined within

the earthing system, circulating between the fault and the earthed star-point of the source. Thus, it does not extend beyond these boundaries. The EPR is measured in reference to a remote earth potential during an earth fault; as shown in Figure *2-5*, the electrical potential is observed to have the highest magnitude at the earth grid of the fault location, Station 2. As the observation moves away from the earth grid of Station 2, the earth potential falls until the observer measures a zero potential. Beyond this zero potential point, the EPR increases again as the observation approaches the source, Station 1. This pattern illustrates how the EPR varies with distance from the fault location to the source. Since the appearance of this EPR curve only lasts until the circuit breaker is tripped, it is impossible to measure the actual fall-of-potential [2] during a fault. The declining potential gradient can be measured by injecting a continuous constant current to simulate a miniature earth fault.

The fall-of-potential measuring result for an undisclosed substation is shown in Figure 2-6 for reference. A constant 2 A, 58 Hz test signal current was injected between the substation earth grid and a remote location according to the test method of IEEE Std 81 [22]. The earthing system impedance was calculated to be 0.75 Ω based on the potential difference between the current probe and the current injected. Therefore, the calculated earth grid voltage rise for the worst-case fault current of 2 kA is 1,500 V. The potential gradient on the fall-of-potential curve indicates the EPR measured at 1 m from the edge of the substation's earth grid was 1,341 V. If the perimeter fence of the switchyard was bonded to the earth grid of the substation, the potential difference in this contact scenario is 159 V. To determine whether this electric shock scenario can be sustained safely by a human being, the hazard identification is needed, and it is discussed later in this section.

Additionally, Figure 2-6 shows that the 430 V EPR contour was located at 75 m from the edge of the earthing system. This 430 V is a typical value, was recommended by the International Telecommunication Union (ITU) Standard, formerly CCITT directive, that set the limiting value to define hot zone limits for human safety related to coupling into telecommunications systems from AC electric power and AC electrified railway installations in fault conditions [24, 25]. The value of 430 V is defined based on experience that 430 V with 0.1 s duration and 300 V for a

duration up to 1.0 s could result in severe situations for humans. Therefore, if a metallic lamp post were installed on the 430 EPR contour, a maximum of 430 V could appear on the lamp post during a fault condition.

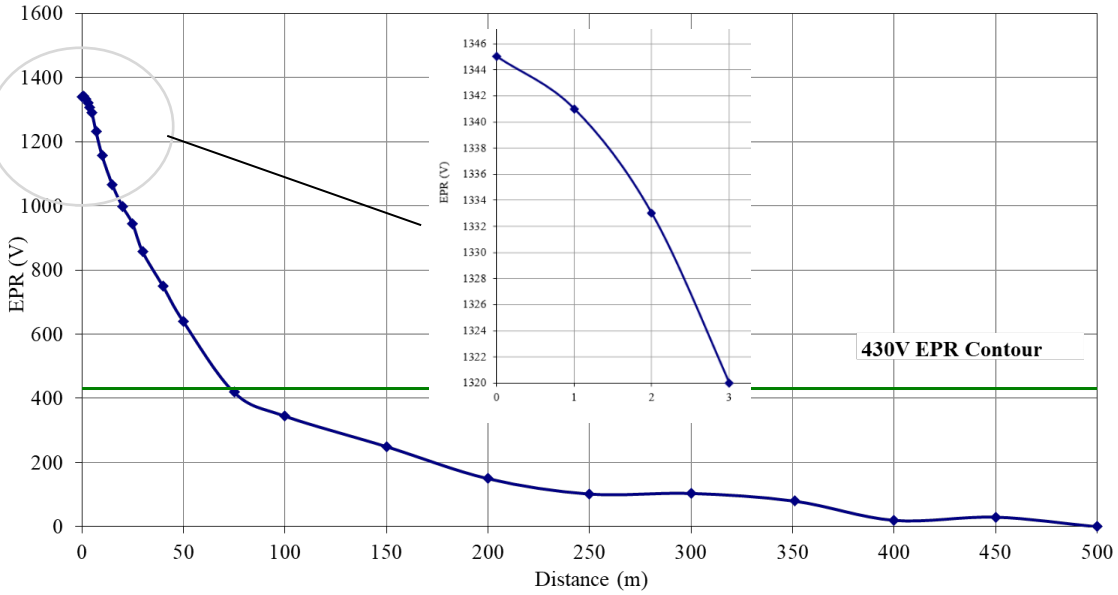

Figure 2-6 The plot of a scaled-up fall-of-potential measurement and EPR contour of an undisclosed substation during an injection test with a continuous test signal of 2 A @ 58 Hz. (Scaling factor = 1,000 to simulate a 2 kA earth fault)

2.3.1 Human Safety during Fault Conditions

There are two main safety requirements for an earthing system: the conduction of earth current will not exceed the designed thermal limits to any physical structure of the earthing system, and the earth current will not create any danger to humans or animals along the conduction path [5].

The earthing system must be designed to manage fault currents without exceeding the thermal limits of any physical structure in the system. When a fault occurs, a significant amount of current flows through the earth, and this fault current must be safely dissipated without causing overheating or damage to any metallic components, conductors, or grounding electrodes. Therefore, adequately sized and designed conductors, grounding electrodes, and connections are

essential to ensure the earthing system can handle the current conditions during the fault conditions.

The earthing system must also prevent the creation of any danger to humans or animals in the vicinity along the conduction path of the earth current. The steep potential gradient on the earth's surface means the potential difference between two points a person might come into contact with is high. By Ohm's law, the current that can flow through the person's body can be high enough to cause damage to the living tissue. Therefore, electrical standards and codes [5, 26] provide guidelines and requirements to ensure that the earthing system meets these safety criteria. Regular inspection, testing, and maintenance of the earthing system are required to verify its effectiveness against the safety standards.

A significant amount of current flows into the earth when a fault occurs within an electrical installation. This current flow can have a range of negative consequences, affecting equipment and human safety. One of the concerns during a fault is the potential damage to electrical equipment, including components like the rectifier circuit of cathodic protection systems for high-pressure metallic pipelines or penstocks for hydroelectric power stations, which are connected directly to the soil and serve a critical role in preventing metal corrosion. High fault currents can disrupt or damage these components, rendering them ineffective in safeguarding the infrastructure from corrosion.

Other than equipment damage, the consequences of a fault can extend to create hazards to living beings near the fault site or in the earth return path. Dangerous arcs and sparks can be generated when the fault potential is sufficiently high to ionize the air along the path of the fault current. These can have severe implications, potentially igniting flammable materials in the vicinity and leading to fires or explosions, especially if combustible materials or gases are present.

While high fault currents and voltages pose risks to equipment and can cause catastrophic events, even relatively lower levels of current and voltage can be hazardous to human safety under specific hazardous exposure conditions. An example is when a person inadvertently becomes a part of the electrical circuit during a fault. The hazardous scenario is when someone touches two

objects with different electrical potentials, such as the surface of the ground and a conductive object, and the fault current can pass through the person's body, resulting in an electric shock. This dangerous scenario can lead to severe injury or even death. To address these concerns and ensure the safety of personnel in the vicinity of electrical systems, standards and guidelines have been developed to mitigate the hazards. One widely adopted standard is the IEEE Std 80 [2], which offers comprehensive guidance on the design of earthing systems for AC power systems. It provides methods for evaluating and managing the hazards associated with electric shocks to humans during fault conditions.

The following sections will describe two commonly used methods for calculating the limits of touch and step voltages to which a person can be exposed without the risk of harmful electric shock. These calculations are critical for designing effective and safe earthing systems in electrical installations.

2.3.2 Dalziel Equation

Charles Dalziel, who invented the miniature differential current breaker [27], significantly contributed to electrical safety and protection against electric shock. Later, his invention was modified by various groups and marketed as the ground circuit fault interrupter (GFCI) in the USA and the residual current device (RCD) in Europe and Australasia today. Dalziel's other research performed and documented the quantitative effects of electric current on men, women, and other animals of similar size to average humans [28]. The human participants, 134 men and 29 women, were volunteers to determine the let-go currents. Since determining non-lethal electric shock could still potentially be dangerous to human lives, Dalziel continued the electric shock test on animals, including sheep, dogs, pigs, and calves, in determining the safety limit for ventricular fibrillation or heart fibrillation. Dalziel concluded that moderately small currents caused ventricular fibrillation that could produce overstimulation to the heart's muscles rather than damage to the heart. His research discovered that the hearts of some smaller animals could recover from ventricular fibrillation more likely than larger animals. However, prompt application of cardiopulmonary resuscitation or an automated external defibrillator could significantly increase the chances of survival in cases where ventricular fibrillation occurred [6]. The Dalziel

equation in IEEE Std 80 [2] is adopted to determine the permissible fault current limits as a function of human body mass and protection time for a high-speed fault-clearing power system. The tolerable body current, l_b, in (5) below is calculated based on the constant, k, in (6) and the duration, t, of shock and is given by [2, 29]:

$$l_b = \frac{k}{\sqrt{t}} \quad [A] \tag{5}$$

where,

$$k = \sqrt{(S_b)} \quad [A \cdot s^{\frac{1}{2}}] \tag{6}$$

and S_b is the empirical constant related to the electric shock energy that can cause ventricular fibrillation in a given weight group of the human population. In the 2013 revision of IEEE Std 80 [2], $S_b = 0.0135$ for the shock energy that can be survived by 99.5% of persons weighing approximately 50 kg is used for public access areas assessment. For the controlled or restricted access area, such as within a substation boundary, the average body weights of the workers are assumed to be 70 kg with $S_b = 0.0247$. This value means that workers can tolerate higher shock energy without risking ventricular fibrillation. Therefore, there are different threshold body current limits for public and restricted areas, with the (7) and (8) given by [25]:

for a 50 kg body weight

$$I_b = \frac{0.116}{\sqrt{t}} \quad [A] \tag{7}$$

for a 70 kg body weight

$$I_b = \frac{0.157}{\sqrt{t}} \quad [A] \tag{8}$$

2.3.3 Biegelmeier Z-Curves

IEEE Std 80 has also introduced the Biegelmeier Z-curve to provide an alternative method for determining tolerable body currents. In addition, other standards and guidelines also refer to the Biegelmeier Z-curve to identify tolerable body current limits [1, 5, 18]. Biegelmeier experiments were conducted in the 1960s to expose pigs of various sizes to different electric current levels to study the effects on their bodies. The plot of the body current against the shock duration where ventricular fibrillation occurred to the test subjects formed a Z-shaped distribution, as shown in

Figure 2-7. In recent years, there has been a growing recognition of the importance of ethical considerations in animal research, and many countries have implemented regulations to ensure that only animals are used when necessary and that animal welfare is protected. Conducting experiments on live animals can cause suffering and pain, and therefore, both the experiments of Dalziel and Biegelmeier are unlikely to be repeated due to ethical concerns.

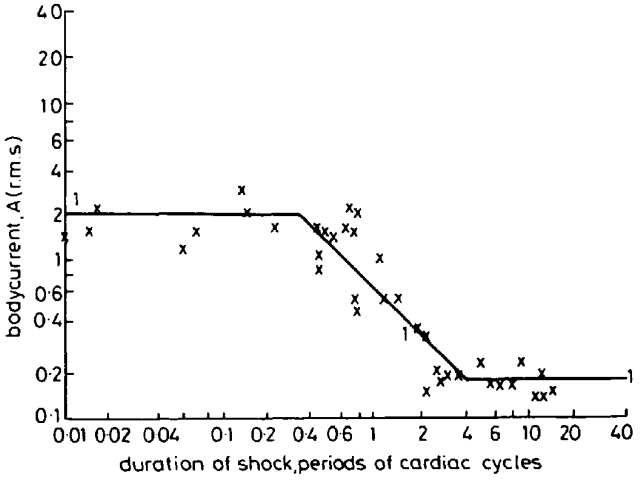

Figure 2-7 Biegelmeier Z curve of ventricular fibrillation for pigs

(Extracted from Figure 12 *[4]*)

2.3.4 The Comparison of Dalziel Equations and Biegelmeier Z Curve

Both the Biegelmeier Z-curves and the Dalziel equations, as presented in [2], have limitations in their applicability. Specifically, they are valid for faults with clearing times falling within the range of 0.03 to 3.0 seconds [5].

Since the Biegelmeier Z-curve has three distinct zones, the body currents are constant if the shock time is less than 0.3 s and more than 2 s. Within 0.3 and 2 s, the tolerable body current curve is similar to the Dalziel equation but with a steeper slope. The choice between the Dalziel equation and the Biegelmeier Z-curve depends on the specific safety requirements and the level of conservatism needed for a given power system. The Biegelmeier Z-curve is more detailed and offers a steeper slope within the 0.3 to 2 s range. However, the Dalziel equation provides a widely accepted conservative estimate for broader applications. Engineers and safety experts should carefully consider these factors when selecting the appropriate safety measure for a particular electrical system.

Figure 2-8 provides a visual comparison, displaying that the Dalziel equations tend to be more conservative in terms of tolerable body current for protection times ranging from 0.05 seconds to 0.8 seconds in public access areas and from 0.1 seconds to 0.4 seconds in restricted access areas. To illustrate this with an example, if the primary protection time setting for a transmission class system is 0.2 seconds, employing the Dalziel equations would result in a lower permissible body current for the transmission system.

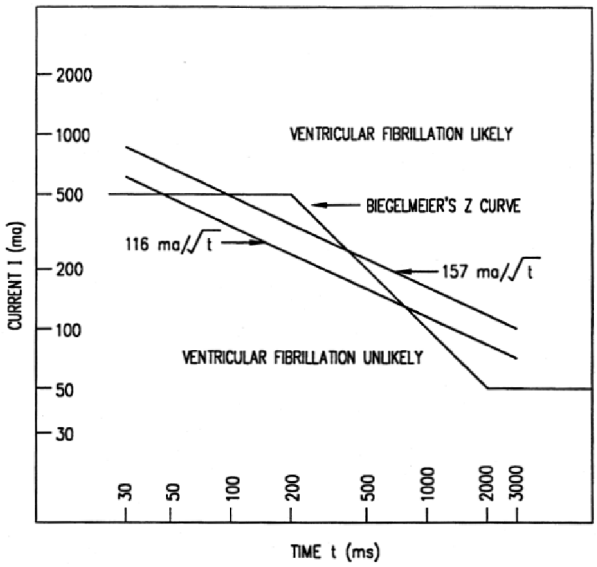

Figure 5—Body current versus time

Figure 2-8 The plot of body current versus time (Dalziel equation and Biegelmeier Z curve) [25]

The distribution networks are designed to serve a wide range of consumers, including residential, commercial, and industrial. These consumers are more sensitive to fluctuations in load demand [30]. Rapid tripping or protection settings in a distribution system can lead to frequent and unnecessary power interruptions to the consumers. Therefore, protection settings are often set to be more tolerant of momentary disturbances and are slower than transmission systems. In scenarios where a substation comprises transmission and distribution equipment, each with distinct protection time settings, the selection of tolerable body current must be made judiciously and subject to the specific application requirements and the regulations in the particular country or region. In essence, the choice between Dalziel equations and Biegelmeier Z-curves must align with the system's protective standards and operational demands.

In the context of this research, the focus is on EPR hazards affecting the pipeline within the transmission corridor. Therefore, the utilisation of the Dalziel equation represents a rational and conservative approach, particularly when assessing safety in connection to the transmission system. This decision ensures that the research upholds a high degree of realism and remains in accordance with the specific requirements of the transmission line operation and protection standards.

2.4 Tolerable Touch and Step Voltages

The tolerable body currents were determined for the 50 and 75 kg population groups in Subsection 2.3.2. According to Ohm's law, calculating tolerable touch and step voltages required understanding the impedance within the accidental shock circuit. This circuit incorporates various components, such as the resistance of the human body, the resistance introduced by boots, and the earth contact resistance.

The resistance of the human body is subject to variability, contingent on several factors, including the moisture level of the skin, the contact area, and the specific path taken by the electrical current through the body. Dry human skin typically exhibits poor conductivity, yielding a resistance of approximately 100,000 Ω. However, when the skin is wet or damaged, this resistance can decrease significantly, reaching approximately 1,000 Ω [3]. Hence, to determine the voltage limit for ventricular fibrillation, a conservative estimate of 1,000 Ω is utilised to account for the worst-case scenario regarding human body resistance.

2.4.1 Touch Voltage Limit

When a person comes into contact with an energised object, a potential earth gradient is created between the point of contact and the ground. The left hand is considered the worst case of touch voltage because the conduction path is closest to the heart, the critical organ in the body and can be interfered with by external electrical energy from the fault. In severe cases, the fault current flowing through the body and into the heart can result in cardiac arrhythmias or life-threatening ventricular fibrillation.

Therefore, the worst case of human body resistance of 1,000 Ω is commonly used to represent the total body resistance and the total resistance of the accidental circuit for touch voltage is given as in (9) [2]:

$$R_{touch} = 1000 + R_{glove} + 0.5\, R_{boot} + 1.5 C_s \rho_s \ [\Omega] \tag{9}$$

where C_s in (9) is obtained from the empirical equation given by (1)

$$C_s = 1 - \left(\frac{0.09(1 - \frac{\rho}{\rho_s})}{2h_s + 0.09} \right) \tag{10}$$

where,

C_S is the surface layer derating factor,
ρ_s is the surface material resistivity in [Ω-m],
ρ is the resistivity of the earth beneath the surface (second layer soil) material in [Ω-m],
h_s is the thickness of the surface material in [m]

The insulation breakdown potential of a shoe is the ability of the shoe to provide electrical insulation between the wearer's foot and the ground. The shoes are classified into six different classes. Each class should pass its corresponding voltage tests. The insulation can be compromised if the voltage between the human foot and the ground exceeds the shoe's maximum AC-proof test voltage [31]. Therefore, if the calculated touch voltage limit is higher than the AC-proof test voltage, the touch and step voltage limits are calculated using the AC-proof test voltage. Since AC-proof test voltage is not the insulation breakdown voltage, there is a 10 kV conservative margin for class 1 to 4 shoes according to the expected to withstand test limits. Also, the insulation can degrade and become less effective due to aging. In the controlled and restricted areas of electrical installation, management can control this variable to ensure that personal protective equipment (PPE) is in place and is updated as planned. However, it is difficult to accurately predict personal exposure voltage limits in publicly accessible areas, as personal protective equipment may be substandard or unused. Therefore, it is essential to consider a conservative

estimate of the touch voltage limit that considers possible changes in the breakdown potential of shoes and gloves to ensure the safety of individuals working in electrical shock-hazard environments. However, controlling all the uncontrollable factors to meet the designed situation is difficult and complex. Therefore, the calculation of touch voltage limits is usually based on the assumption that the individual is not wearing shoes and gloves throughout the electrical installation and the derating factor C_S in (10) is conservatively assumed to be 1.

The tolerable touch voltages for the body weights of 50 and 70 kg can be calculated using Ohm's law with the resistance of touch voltage circuit (9) and the body current (7) and (8), respectively, and expressed in (11) and (12) as below:

$$E_{touch50} = \frac{(1000 + 1.5C_S\rho_s) \times 0.116}{\sqrt{t_s}} \quad [V] \tag{11}$$

$$E_{touch70} = \frac{(1000 + 1.5C_S\rho_s) \times 0.157}{\sqrt{t_s}} \quad [V] \tag{12}$$

where,

$E_{touch50}$ and $E_{touch70}$ are the touch voltage limits for the body weight of 50 and 70 kg, respectively.

2.4.2 Step Voltage Limit

The other hazardous contact scenario is the potential difference between one foot and the other, known as the step voltage. Usually, a hazardous step voltage only appears immediately outside the earth grid or at the corner of the earth-bonded perimeter fence of a substation, where the earth current density may be the highest during an earth fault. A step voltage is a person standing two feet 1 m apart simultaneously on two different earth potentials [25]. Usually, the barefoot step voltages will be applied for safety assessment. The resistance of the step voltage resistance is shown in (23) [25]:

$$R_{step} = 1000 + R_{boot} + 6C_s\rho_s \ [\Omega] \tag{13}$$

Therefore, the step voltage limits for body weights of 50 and 70 kg can be evaluated using (13) and the body current (7) and (8), respectively and can be written as (14) [25]:

$$E_{step50} = \frac{(1000 + 6C_S\rho_s) \times 0.116}{\sqrt{t_s}} \quad [V] \tag{14}$$

$$E_{step70} = \frac{(1000 + 6C_S\rho_s) \times 0.157}{\sqrt{t_s}} \quad [V] \tag{15}$$

where,

E_{step50} and E_{step70} are the step voltage limits for the body weight of 50 and 70 kg, respectively.

2.4.3 Metal-to-Metal Touch Voltage Limit

Metal-to-metal touch voltage is also known as reach touch voltage. It can occur when a person simultaneously touches two surfaces with different electrical potentials. This touch scenario can create a conduction path through the person's body, leading to electrical shock hazards. Metal-to-metal touch voltage is unrelated to soil resistivity because the victim does not need to contact the ground or earth. Therefore, the metal-to-metal touch voltage limits are not related to the soil resistivity and are calculated by assuming the body resistance is 1,000 Ω as expressed in (16) and (17) as follows:

$$E_{metal-metal\ touch50} = \frac{1000 \times 0.116}{\sqrt{t_s}} \quad [V] \tag{16}$$

$$E_{metal-metal\ touch70} = \frac{1000 \times 0.157}{\sqrt{t_s}} \quad [V] \tag{17}$$

2.5 EPR Hazard Identification and Mitigation Methods

Periodic inspection and testing of the earthing system are essential to ensure the earthing system is in good working order and meets the required safety standards. The interval between the inspections will depend on the applicable regulations or standards [26]. The method to test the integrity of the earthing system includes injecting a constant off-frequency current (48 Hz for 50 Hz system and 58 Hz for 60 Hz system) between the main earth of the electrical installation and a remote earth location to create a miniature earth fault [22]. The off-frequency current allows the frequency-tuned voltmeter to differentiate the test signal from the nominal frequency of the power system. Sometimes, the miniature earth fault can be created by injecting a test current through a power line between two substations under a planned outage. When one end of the de-energised power line is connected to the earthing system of a substation, the off-frequency current can be

injected through the other substation's power line and the earthing system. During the miniature earth fault is created, the touch and step voltages and EPR contours can be measured with a frequency-tuned voltmeter with the methods specified in IEEE Std 81 [22].

In Figure 2-9, an engineer was taking touch voltage measurement (left) and step voltage measurement (right) according to the recommendation of IEEE Std 80 [2]. At the same time, a constant current was injected from the substation earthing system to a remote location.

Figure 2-9 Measuring the touch voltage on wet concrete ground (left) and step voltage on crushed rocks (right) in a transmission class substation using the IEEE Std 80 recommended current injection method. The photos were taken by the author in 2014.

As the impedance of the earth is predominantly resistive [2, 5], determining the actual touch and step voltages involves multiplying them by a scaling factor. This scaling factor is the ratio of the worst-case fault current to the constant test current injected. Any hazard can be realised by comparing the measured voltages to their corresponding voltage limits calculated based on the contact scenarios and soil resistivity. The notable change in touch or step voltage from the previous inspection can signal potential defects or deficiencies in the earthing system. Consequently, when EPR hazards are identified, mitigation measures must be considered. These mitigation options include various methods to reduce body current to a safe level during a fault, with the choice of technique depending on the specific circumstances. The subsequent section provides descriptions of commonly used techniques.

2.5.1 Crushed Rocks

Crushed rocks with irregular shapes are a low-cost, effective way to reduce touch and step voltages. The clean crushed rocks with an average resistivity value of 5,000 Ω-m can provide sufficient insulation properties to reduce the body current to flow during a fault [5, 32]. However, the irregular shape of crushed rocks can create voids and air pockets that trap moisture, soil and organic substances that can promote vegetation growth, reducing the insulation properties of the layer. Therefore, the industrial standards [2, 5], have defined that if using the crushed rocks to replace the surface soil layer, the crushed rock layer must have a minimum thickness and the average size of each crushed rock [1, 32]. Additionally, all installed crushed rock material must be screened to periodically remove dust, soil, and vegetation. The new crushed rock is isolated from river-run gravel or quarried aggregate and free from friable stone, wood, clay, or other material [2]. Although the drawback of using crushed rocks is that periodical maintenance is required to avoid vegetation growth, crushed rocks are still a low-cost EPR hazard mitigation method commonly used as a standard design feature of outdoor substations.

2.5.2 Gradient Control Conductors

The design incorporating a gradient control conductor typically involves using a sufficient-sized continuous copper strip placed around and bonded to the affected structure. The primary purpose of the gradient control conductor is to establish a gradual voltage gradient between the structure and the adjacent soil. By burying this conductor, the contact surface area with the soil is significantly increased. This increase, in turn, leads to a reduction in the current density surrounding the affected structure. Consequently, the potential difference between the surface that a person may touch and the immediate ground where they stand can be lowered to a safer level.

Industrial practices recommend that a gradient control conductor be securely connected to the earth point of the affected structure and buried to a depth of 0.5 m while extending 1 m around the structure, as detailed in [2]. Gradient control conductors are included as standard design components for all structures constructed within or close to high-voltage installations [2, 5, 17][2][5][18]. The gradient control conductor can physically reduce the electrical potential that appears on the earth's surface; therefore, it is the most effective and reliable method for reducing

body currents and exhibiting resilience to disturbances in specific uncontrolled environments, such as those prone to vegetation growth.

2.5.3 Non-Conductive Coating

Applying a non-conductive coating layer on concrete posts, metallic posts, and pipelines can help to create an insulating layer between the person and the structure, thereby minimising exposure to touch voltage hazards during an earth fault [2]. However, it is important to note that non-conductive coatings should not be used if the touch voltage on the affected structure is greater than the specified breakdown voltage of the coating. In such cases, the coating may not be able to provide adequate insulation, which could result in touch voltage hazards.

When non-conductive coating is used to mitigate touch voltages, only certain product brands and models can be selected for the task. In addition, non-conductive coating applications must follow the manufacturer's recommended procedure, industrial standards, and guidelines to ensure that the coating provides adequate insulation and protection against voltage hazards.

On the other hand, the non-conductive coatings can be degraded over time, are subject to common wear and tear, and are unsuitable for mitigating touch voltage hazards in a populated area where contact frequency is high.

In the context of high-pressure metallic pipelines, holidays are small gaps or voids that develop in pipeline insulation coatings due to various factors, such as improper application or damage to the coating during handling, transportation, or installation. These holidays can compromise the integrity of the insulation coating; besides the touch voltage hazards, holidays allow corrosive agents to penetrate the surface and attack the metal substrate, leading to corrosion and other damage. Therefore, the insulation coating is one of the items of pipeline periodical inspection [12].

2.6 Probabilistic Risk Analysis

Certain touch voltages resulting from electrical earth faults can be difficult or expensive to eliminate, particularly on long-distance infrastructure where these hazardous touch voltages can

extend over several to tens of kilometres. As mentioned in Section 1.4, some countries accept the application of statistical analysis to demonstrate that the residual risk, which refers to the level of risk that remains after risk mitigation measures have been applied, can be deemed acceptable under specific, well-documented criteria, such as the "As Low As Reasonably Practicable" (ALARP) principle [5, 7, 12]. The current risk assessment guidelines [1, 5] propose that touch voltage risk arises from the collision of two events: the occurrence of an earth fault and human contact with the hazardous spot identified through the current injection test.

2.6.1 Calculating Touch Voltage Risk with Poisson Distribution

For the collision of two independent events, two separate scenarios can contribute to a touch voltage risk. The first scenario, X_A, is human contact on a hazardous part while an earth fault event is already in progress, and the second scenario, X_B, is human contact on an accessible and hazardous part before and during an earth fault event. These two scenarios can be approximated as the Poisson processes, assuming that earth faults and human contacts are equally likely to occur, are independent of season or time of day, and that the average time between events within a fixed period is known. However, the exact timings of events are random. Therefore, the probability of the Poisson process $P(X = \zeta)$ can be evaluated using the probability density function equation [13] and is expressed in (18).

$$P(X = \zeta) = \frac{(\lambda T)^{\zeta} e^{-\lambda T}}{\zeta!} \tag{18}$$

where, λ is the arrival rate of Scenario X, and $P(X = \zeta)$ is the probability of Scenario X within the observation period, T (year), with zeta-ζ occurrence counts. If the occurrence of Scenario X is 0 within the observation period T, then using (19), the zero-probability equation is given by (19) as follows:

$$P(X = 0) = e^{-\lambda T} \tag{19}$$

where,

λ is the arrival rate of the occurrence of Scenario X.

The λ of each process is calculated based on whether X_A or X_B applies. For X_A, λ_A is given by (20) as follows:

$$\lambda_A = u_A \sum_{i=1}^{n} t_i u_B = u_A u_B t_B \tag{20}$$

where,

within T, u_A is the occurrence of a fault (count/year),
u_B is the number of human contacts (count/year), and
t_B is the mean duration of each human contact (year).

Similarly, for the arrival rate of the occurrence of X_B, λ_B can be written as (21).

$$\lambda_B = u_B \sum_{i=1}^{n} t_i u_A = u_A u_B t_A \tag{21}$$

where,

t_A is the mean duration of each fault (year) within the T.

Therefore, by substituting (20) and (21) into (19) for each scenario, the zero probability equations of both scenarios can be written as (22) and (23):

$$P(X_A = 0) = e^{-u_A u_B t_B T} \tag{22}$$

$$P(X_B = 0) = e^{-u_A u_B t_A T} \tag{23}$$

The coincidence probability P_{conc} of scenarios X_A and X_B within T can be written in terms of (22) and (23) as (24) as follows:

$$P_{conc} = 1 - (e^{-u_A u_B t_B T})(e^{-u_A u_B t_A T}) \tag{24}$$

The coincidence probability in (24) can further be simplified by applying the approximation as expressed in (25):

$$(e^{-n}) \approx 1 - n \tag{25}$$

For n < 0.287, the estimation error is less than +5%. Since both processes' duration and arrival rate are small compared to an observation period, T, of one year, only a tiny amount of conservative error will be added using the approximation (25). The coincidence probability P_{conc} in (24) can be simplified as (26) as follows:

$$P_{conc} = u_A u_B t_B T + u_A u_B t_A T \tag{26}$$

To evaluate the annualised coincidence probability [2]. In this case, and because T = 1 year, the equation can be written as (27).

$$P_{conc} = u_A u_B (t_A + t_B) \quad (27)$$

where, P_{conc} is the annualised occurrence probability of fatality of an individual from a touch voltage. (27) does not consider that touch voltage hazards that result in ventricular fibrillation may not occur daily with the observation period T due to the soil resistivity variations.

2.6.2 As Low As Reasonably Practicable

"As Low As Reasonably Practicable" (ALARP) is a risk management principle that aims to provide a guideline to reduce the risks to a level that is as low as possible while still being practicable to achieve [1, 5, 8, 12]. It is often used in high-risk industries such as aviation, chemical manufacturing, and energy storage and delivery. In practice, the ALARP principle involves a risk assessment process to evaluate the likelihood of the hazards based on the set consequence, such as the probability of fatalities, serious injuries, direct economic loss, environmental pollution, or other irreversible events.

The consideration of the ALARP principle requires organisations to take all reasonable steps to identify and reduce risks to the lowest possible level. This practice means that risks should be reduced as far as practicable, taking into account factors such as cost and the availability of resources. Some of the risks may not be eliminated and are called residual risks [12]. However, risk mitigation is practical, or its cost is grossly disproportionate to the improvement gained; therefore, the organisation can implement safety procedures into the tasks related to the identified hazards, introduce additional personal protective equipment, and provide periodic competent training and assessment for the staff to make the risks acceptable. The risk acceptance criteria can vary with time and geography but are mainly dependent on culture, government policy and the weighting of the cost of risk mitigation in proportion to the benefits.

For instance, in New Zealand, the ALARP limit for a societal risk of 10 fatalities is defined as an acceptable risk range between 10^{-6} and 10^{-4} per year [5]. Therefore, any probability of fatality calculated below the upper limit of 10^{-4} is considered acceptable. If the calculated risk falls below the lower limit of ALARP, it may be omitted due to its insignificance. However, the decision to

omit a risk should be made following a comprehensive risk assessment while considering potential consequences.

Adhering to the ALARP principle does not imply that all risks can be entirely mitigated to a safety level. There will always be some residual risk that must be managed. However, the ALARP represents the point at which the risk is reduced to the lowest possible and cannot be reduced further, or the cost for further risk reduction is disproportionate to the benefit gain. The following example is not an electrical engineering case. However, it is a good example of how overachieving risk mitigation and disregarding the ALARP principle could produce more adverse effects than benefits.

Two independent cases were considered for the ALARP example. The first one was that the New Zealand Government decided to reduce the fatality on the road to zero by rolling out a speed limit reduction throughout the country. However, the campaign failed as the road toll increased by 6.8% compared to 350 in 2019 and 374 in 2022 [33], which is one year after the reduction of the speed limit was introduced. Disregard the incurred economic loss due to unnecessary traffic congestion from higher traffic density and the cost of changing the road signs. A thirty-million-dollar budget will be allocated to reverse this failed risk mitigation attempt by the next elected Government [34].

The second case was a fire that broke out in Wellington, the capital city of New Zealand, on 16 May 2023. Firefighters arrived at the scene with a smaller ladder firefighting appliance that could not directly reach the top floor. The firefighters improvised tactical approaches to transport equipment to the top floor manually. Where multiple rooms were already on fire, making the situation appear un-survivable. Meanwhile, the firefighting appliance outside experienced difficulties with water pumping. As a result, ten people lost their lives in the fire. A senior officer of the fire department informed the media after this tragedy that the firefighter union had been raising concerns for years about the urgent need for the additional 32 m ladder trucks and maintenance or replacement of the existing aging equipment that would enable firefighters to

access multi storey buildings more safely and efficiently [35]. Regrettably, none of these requests had been addressed.

According to the road safety and traffic data provided by the International Transport Forum Road safety data- New Zealand, the number of deaths due to traffic accidents per billion vehicle kilometres was 7.2 in 2019 [36]. Assume the average range of a vehicle was 8000 km in 2019 [33]. The calculated risk was 1.1×10^{-6} and this result indicated that the risk was nearly negligible according to the societal risk range of 10^{-6} to 10^{-4}under ALARP [12]. Furthermore, the International Transport Forum only recommended that the risk mitigation was to reduce the speed limit on the highest-risk roads where there are high numbers of active users, such as around schools. However, the government disregarded the recommendation and rolled out a risk mitigation campaign to reduce the overall speed limits throughout the country. More than 30 million dollars was spent on this overdone campaign. If a part of this budget had been allocated for the upgrade and maintenance of firefighting equipment, ten lives could have been saved in the Wellington fire incident. This example highlights the importance of minimising risk to an as low as reasonably practicable extent without imposing grossly disproportionate costs, resources, and sacrifices.

2.7 Summary

The current injection method is a common and effective technique to determine the actual touch and step voltage hazards during the prospective earth fault condition. Engineers can calculate the actual touch and step voltages during an earth fault condition by analysing the test data obtained from the current injection test. However, the engineers usually summarise a conservative soil resistivity model based on conducting multiple soil resistivity tests in different locations around the test site to cover the effect of the variability of soil resistivity. The conservatism added to the touch and step voltages assessment allows the engineers to pinpoint the hazardous touch and step voltages confidently. If the touch voltage is overestimated due to conservative assumptions or inaccurate measurements, the resulting risk assessment may be overly pessimistic and lead to unnecessary or ineffective hazards mitigation measures.

For gas pipeline systems, however, the situation differs. Unlike high-voltage installations, pipelines typically span long distances, often across varied terrains and environments. Applying a gradient control conductor along the entire length of the pipeline is not feasible due to the long stretches of pipeline and the varied soil resistivity. Furthermore, gas pipeline maintenance often involves workers being exposed to touch voltage hazards at multiple points along the pipeline during activities like Cathodic Protection (CP) maintenance. During these maintenance activities, the pipeline's decouplers are temporarily disconnected from the earth [12], and temporary earthing cannot be used for accurate CP measurements. Workers are therefore required to work under the threat of touch voltage hazards during such measurements. While these hazards are present, the associated risks can still be managed through appropriate safety measures and practices designed for the specific maintenance activities, even though the worker remains exposed to potential danger throughout the operation.

Moreover, the drawback of being overly conservative in probabilistic risk analysis can lead to unrealistic results and may not help meet the ALARP criteria. Therefore, soil resistivity monitoring near the hazardous site can help accurately identify the touch and step voltage hazards. Eventually, an improved version of probabilistic risk analysis can be developed.

Chapter 3 - Literature Review

3.1 Introduction

In the previous Chapter, the background knowledge of how soil resistivity can affect touch and step voltages and mitigation techniques to overcome issues related to hazards incurred from touch and step voltages were also described. Since the soil resistivity can vary in different seasons subjected to weather conditions, the hazards can also vary. The present industrial practices, however, consider soil resistivity a constant quantity. Sometimes, the single conservative soil resistivity model can falsely indicate non-existent hazards and incur unnecessary expenses in hazard mitigations. Therefore, it is necessary to use statistical data to improve the accuracy and appropriateness of the parameters of soil resistivity with the season or specific periods within a year. Accordingly, a literature review on the soil resistivity variations was undertaken. This Chapter reviews the literature on probabilistic risk analysis, soil resistivity data collection, characterisation, modelling, and simulation.

3.2 Review Methodology

Primarily, the knowledge gaps in probabilistic risk analysis are explored through pinpointing areas where present methods might be lacking. In this way, a clear understanding of the limitations and gaps in the present risk analysis method in electrical and non-electrical installations such as pipelines must be established through a thorough review of the previous research and the existing standards.

The secondary objective of this literature review is to support the originality and innovation of the proposed method in addressing the improvement in probabilistic risk analysis. Through a comprehensive review of existing literature, this survey seeks to establish that no previous research has proposed or implemented any similar method that lines up with the novel approach this thesis is proposing. By identifying the absence of comparable methodologies and techniques in the reviewed literature, the goal is to emphasize the uniqueness of the proposed method, which can contribute to the advancement in accuracy and practicality of the EPR hazard probabilistic

risk analysis for pipelines. The absence of prior implementations will further reinforce the significance of this research and highlight the need for its consideration.

Since the research intents to develop a statistical model of touch voltage profile deduced from the seasonal soil resistivity data, the third objective is to assess the quality and methodologies of previous research for soil resistivity data collection and selecting a suitable method in terms of site selection, data size, post-processing of the soil resistivity data, electrical system modelling and simulation. This systematic approach allows the contribution to advancing risk analysis methodologies and their broader applicability across various fields.

3.3 Inclusion and Exclusion Criteria

In the 1990s, significant advancements in earthing system technology were facilitated by breakthroughs in computer technology. The exponential increase in computational power had a great impact on the development and application of simulation software used in electrical engineering. One key example is MALT (Module for the Analysis of Lightning Transients), a component of the CDEGS (Current Distribution, Electromagnetic Fields, Grounding and Soil Structure) [17] software suite. Although MALT was established in 1972, its practical utility was initially constrained by the limited computational resources available at that time. Early computers were not powerful enough to handle the complex calculations required for accurate simulations of grounding systems, which involved numerous variables and intricate electromagnetic interactions. With the technological advancements of the 1990s, including the development of faster processors and more sophisticated algorithms, the limitations imposed by computational power were significantly reduced. This allowed simulation tools like MALT to fully realize their potential. Engineers could now perform more detailed and accurate simulations, leading to improved design and analysis of grounding systems. This enhancement in software capabilities contributed to better safety and performance in electrical systems, marking a substantial advancement in earthing technology.

Thus, IEEE Std 80 [25] underwent a significant revision in the year 2000, incorporating simulation results into its guidelines. Since then, it has been widely used and referenced internationally, incorporating all the important research on earthing systems. IEEE Std 80 was revised in 2013 [2] with minor wording corrections from the previous revision. This review considers previous research in soil resistivity variations related to power systems, and therefore the article search time frame was set from 1990, ten years before the release year of [25]. The article search was undertaken using the IEEE Xplore® database and Google Scholar with the search terms “soil resistivity”, “seasonal soil resistivity variation”, and “probabilistic risk analysis for touch voltages”. The exclusion criteria are based on the research focus's justification and the available data collection budget.

The review explicitly identified electrical safety concerns related to earth return currents. As such, the focus is on low-frequency studies involving frequencies up to 200 Hz. This frequency range is optimal for investigating phenomena relevant to earth return currents. This review particularly omits high-frequency considerations, as these are more relevant to lightning protection investigations, and the human safety risk due to lightning events can easily be eliminated by the rain radar weather forecast [37].

The research focuses on long-term soil resistivity monitoring. Therefore, the data collection equipment should meet the available budget and security against theft on site. For the soil resistivity measurement, equipment selection is guided by the need for effectiveness and feasibility. While electrical resistivity tomography (ERT) methods using GPR, as described in Section 2.2.1, particularly in 2D or 3D configurations, hold promise for obtaining comprehensive data, their adoption was restricted by spatial requirements and the considerable financial investment required for procuring specialized equipment. Consequently, due to practical considerations, studies employing these sophisticated techniques are purposefully excluded from the current research.

3.4 Review Discussions

On July 19, 2023, a search yielded 320 articles. This result comprised 153 articles from IEEE Xplore® and 167 from Google Scholar. Subsequent evaluation of the full-text articles led to identifying 276 articles that were either redundant or unrelated to seasonal variations in soil resistivity. After this filtering process, 44 articles remained and underwent thorough examination for inclusion in the study.

As a result, 32 articles met the criteria and were deemed eligible for inclusion in the literature review. These selected articles are summarized in Table 3-1. The research materials containing pertinent information concerning the impact of seasonal effects on EPR safety and pipelines were categorized into various topics for further analysis.

Table 3-1: A summary of the eligible articles for the literature review

Year	Research Group	Measurement	Software	# Site	Test Period/month	Sample/site	Wenner Spacing/m	Ref
2013	A. Amin	N/A	CDEGS	N/A	Unspecified	Unspecified	Unspecified	[38]
2022	A. Madikizela	Wenner	CDEGS	1	12	12	50	[39]
2014	C. Prabhakar	Wenner	N/A	2	12	2	2	[40]
2020	C. Wang	N/A	CDEGS	N/A	Unspecified	Unspecified	Unspecified	[41]
2017	Christy Thomas	Wenner	CDEGS	2	24	24	50	[42]
2010	F. E. Asimakopoulou	Wenner	ANN	1	12	365	10	[43]
2011	F. E. Asimakopoulou	Wenner	ANN	1	12	365	10	[44]
2011	F. E. Asimakopoulou	Wenner	ANN	1	12	365	10	[45]
2013	F. E. Asimakopoulou	Wenner	ANN	1	12	365	10	[46]
2015	F. E. Asimakopoulou	Wenner	ANN	1	12	365	10	[47]
2011	Fraser King	Wenner	N/A	1	10	1	3	[48]
2003	Jinliang He	Wenner	CDEGS	1	Unspecified	2	Unspecified	[49]
2005	Jinliang He	Wenner	CDEGS	1	Unspecified	1	1.2	[50]
2005	Jinliang He	Wenner	CDEGS	1	Unspecified	2	1	[51]
2005	Jinliang He	Resistance measurement	N/A	1	Unspecified	1	N/A	[52]
2010	JT Afa	Wenner	N/A	18	10	5	1.2	[53]
2017	K. K. M. Rezende	Resistance measurement	N/A	4	11	1	N/A	[54]
2000	Lin Li	Resistance measurement	CDEGS	1	Unspecified	1	N/A	[55]
2013	M.G. Unde	Step and Touch voltages	Autogrid	3	12	12	N/A	[56]
2006	P. J. Lagace	Resistance measurement	N/A	1	Unspecified	1	N/A	[57]
2017	Q. Louw	Wenner	DIgSilent	10	Unspecified	1	3	[58]
1990	R.J. Gustafon	Wenner	N/A	3	15	15	48	[59]
2001	Seiichi Sakamoto	Wenner	N/A	7	12	12	0.1	[60]
2001	Seiichi Sakamoto	Wenner	N/A	1	Unspecified	Unspecified	2	[61]
2018	T. A. Papadopoulos	Wenner	N/A	3	12	12	10	[62]
2014	V. P. Androvitsaneas	Wenner	ANN	1	12	365	10	[63]
2014	V. P. Androvitsaneas	Fall-of-potential	ANN	1	48	365	N/A	[64]
2015	V. P. Androvitsaneas	Wenner Fall-of-potential	N/A	1	48	1460	8	[65]
2018	V. P. Androvitsaneas	Fall-of-potential	ANN	5	Unspecified	2	N/A	[66]
2018	Wolfgang Fieltsch	Resistance measurement	N/A	1	Unspecified	1	N/A	[67]
2012	Xun Long	Step and Touch voltages	N/A	1	Unspecified	1	N/A	[68]
2011	Noradlina Abdullah	Wenner Fall-of-potential	CDEGS	1	18	18	18	[15]

In Table 3-1, 32 references are included, some exceeding 10 years in age. While recent studies offer valuable insights, older references remain highly relevant for several reasons. Foundational research from the 1990s and early 2000s continues to provide the theoretical and methodological basis for modern studies, with key principles and models established during this period still influencing current research on soil resistivity and earthing systems. For example, in 1990, R.J. Gustafson [59] used the Wenner test to address seasonal variations in grounding resistance, laying the foundation for understanding the temporal behaviour of soil resistivity. Additionally, in 2000, Lin Li [55] demonstrated the use of software to analyse the influence of earthing system resistance, a key contribution that still shapes current simulation approaches. Many of these older references were published in high-impact journals and frequently cited at the time, playing a pivotal role in the development of earthing system standards, such as IEEE publications.

Moreover, older studies offer long-term perspectives on issues like soil resistivity variation, providing a valuable basis for comparing newer data. Some of these older works have also been revisited and validated by more recent research, further confirming their ongoing relevance. Thus, retaining these references adds depth to the review, illustrating the evolution of knowledge in the field of soil resistivity and earthing systems.

3.4.1 Horizontal Multi Layer Soil Resistivity Model

A horizontal multilayer soil resistivity model represents the subsurface soil structure that assumes the soil can be divided into distinct horizontal layers; each layer is assumed to have uniform resistivity throughout its thickness [57]. This soil resistivity representation is commonly used in electrical engineering, particularly for analysing earthing systems [22]. The literature review has identified seven publications that have used CDEGS [17] for earthing system analysis. Additionally, one early article utilized AutoGrid [17], an early software product developed by the same company of CDEGS, specifically for processing soil resistivity data. Furthermore, seven other publications have focused on using artificial neural networks (ANNs) in the context of earthing system-related studies, particularly in methodologies for resistivity data collection. ANNs are a machine learning technique commonly applied to model complex systems, including earthing systems, although they are not a primary focus within this literature review.

The accuracy of the model is based on the quality and quantity of data used and the sophistication of the data inversion algorithms utilized [57]. Widely recognized computer software such as RESAP within the CDEGS suite has been utilised in seven different research groups and has found extensive application in converting apparent soil resistivity data from methods like the Wenner test or Schlumberger method into comprehensive multilayer soil resistivity models. Moreover, the benchmark cases in the annexe of IEEE Std 80 [2] showed that other software like ETAP [69], SGW [70], and SDWorkstation [71] could only handle the soil resistivity model up to two layers. Hence, the use of reputable industrial software CDEGS can ensure the accuracy and excellence of research outcomes.

For instance, rough estimations of soil resistivity, such as assuming a homogeneous soil structure during the earthing system's design phase, often yield undesirable results in the performance of power systems. This undesirable outcome arises due to the seasonal variations in soil resistivity, which can introduce substantial errors in earthing system parameters [12]. Particularly, errors in estimating earth grid resistance constitute the primary source of inaccuracy in defining step and touch voltage limits because the prospective fault current used to evaluate these limits is contingent upon the earth grid resistance [67]. Thus, overly simplified soil resistivity models or inaccurate representations of the soil can give rise to deficiencies and challenges in earthing system design. Simplified soil resistivity models may not realistically reflect the actual soil conditions, leading to design outcomes that significantly diverge from real-world performance. Furthermore, these models may fail to capture the details that influence system performance, ultimately resulting in suboptimal designs that fall short of established safety and performance standards.

3.4.2 Seasonal Soil Resistivity Variation

The survey's key findings have substantiated the presence of seasonal variations in soil resistivity, which directly impact touch voltages and the acceptable safety thresholds for humans. These variations in soil resistivity affect the parameters within the multilayer soil resistivity model that may involve alterations in layer resistivity, thickness, or both.

The survey's results have identified 29 distinct studies investigating various issues arising from seasonal changes in soil resistivity. These issues comprise concerns related to touch voltage hazards, AC corrosion, and the resistance of earthing systems. Among these studies, twenty-one have reported using the Wenner test method for collecting soil resistivity data. Four studies [15, 63, 64, 65] have directly measured the earthing system resistance using the fall-of-potential method [22], and five studies [52, 54, 55, 57, 67] did not specify the measurement method.

An eighteen-month substation safety study [15] in Malaysia demonstrated that soil resistivity variation could yield a 100 V difference in touch voltage limits across seasons, with hazardous touch and step voltages only occurring during particular months. The study was based on a

twelve-month data collection interval of approximately 30 days [16]. The three-layered soil resistivity model demonstrated that the middle and bottom soil resistivity layers were stable throughout the data collection period. The research pointed out that the top resistivity layer could not be predicted by simply referring to the particular season or month but was closely related to the variation of soil moisture level. In other similar research based on monthly soil data, the computer simulation results have shown that soil resistivity changes with the season could lead to variation in transmission tower footing impedance, affecting the correct operation of high-speed protection equipment of the transmission system [41].

The seasonal change of the top layer soil resistivity is mainly due to temperature and water content changes in most soil types [63, 64, 65, 66]. In raining and freezing seasons, the top layer soil resistivity can change to very low and very high, respectively and in both cases, the touch voltages can rise significantly [50]. Therefore, the time and weather conditions under which soil resistivity tests are taken can substantially influence the performance of the earthing system if the seasonal effects on soil resistivity are not taken into account. The industrial standards recommend that the earthing system designers adjust the soil resistivity model according to the seasonal effects [2, 5]. However, the absence of a systematic method for making these adjustments can present challenges for earthing system designers. Different designers may adjust in varying ways without clear guidelines, leading to inconsistent approaches in earthing system designs. Designers may lack confidence in their adjustments, potentially resulting in either over-design (leading to unnecessary costs) or under-design (posing safety risks). Effective risk management relies on accurate and consistent adjustments to account for seasonal variations in soil resistivity. Without a systematic approach, risk assessment and mitigation may be compromised.

3.4.3 Data Collection and Sample Size

In reference to Table 3-1, most past research was based on one-year soil monitoring. Some studies have focused on the short-term effects of soil resistivity variation. In contrast, others may require long-term monitoring to capture seasonal soil resistivity variations to address the earthing system-related problems. The quality of research depends on the appropriate alignment of data collection methods and data size with the research objectives and questions.

The Greece research group F.E. Asimakopoulou et al. conducted a year-long daily fall-of-potential measurement on estimating earthing resistance using artificial neural networks [43, 44, 45, 46, 47]. Factors such as rainfall, soil moisture level and soil resistivity are the predictors for the prediction of earthing system resistance.

The most extensive scale study was conducted by V.P. Androvitsaneas et al. in Greek. The pilot studies [63] and [64] were published in 2014 using the Wenner test for daily soil resistivity and driven rod resistance measurements. The experiment was extended to four years, involving the collection of 1,460 sets [65] of daily soil resistivity data with Wenner spacing of up to 8 m and earthing resistance of three vertical driven rods. This collected data was used for estimating and validating earthing system resistance using inductive machine learning. The researchers have used the collected data, developed similar models, and fine-tuned the proposed methods for estimating grounding system performance [66].

Jinliang He et al.'s work addressed the challenge of earthing system resistance variation [50] in China. Jinliang He et al. pointed out that with the electricity demand's rapid expansion, the prospective fault current setting needed to be increased to cope with the safe operation of the power system. The group reported that the seasonal variations of earthing system resistance that increase the EPR to a high level could create a risk of preventing the normal operation of the protection system. The damage to the control equipment of the power system incurred by high EPR is quite common in small-scale substations or substations built on high-resistivity soil in China. The vast economic loss has also been reported. To encounter this challenge, the research group proposed installing the bonded vertical electrodes in a deep well to reach the underground water to lower the earthing system resistance could eliminate the seasonal influence created by the soil resistivity change in different seasons. In Jinliang He’s other deep-driven earthing electrode research emphasised the importance of low earthing system resistance design can eliminate the hazards created by seasonal soil resistivity variations and also pointed out that applying the overly simplified seasonal factor to the measured soil resistivity could not satisfy the actual condition of the surface soil layer which could be highly sensitivity to the environment in China [49].

Christy Thomas et al. conducted the soil measurement with the most extended Wenner spacing of 50 m to study the soil in the Gauteng area of South Africa. The data collection was carried out with a monthly interval over twenty-four months in 2015 [42]. The result was used to evaluate the soil resistivity correction factors for the earth grid design. The goal of the correction factor is to ensure the design is up to the worst case. A recent conference paper was written based on Christy Thomas et al.'s study [42] for optimal substation earth grid design in the Eastern Cape region, South Africa [39]. The group concluded that the developed soil resistivity correction factor was a suitable guideline for all grid designs within the Eastern Cape region.

Nonetheless, soil resistivity is subject to substantial variability driven by diverse factors involving soil composition, moisture levels, temperature fluctuations, and geological attributes. Furthermore, regional distinctions can exert a significant influence on soil behaviour. The differences observed in the outcomes of various studies underscore the complicated nature of soil resistivity and its complexity interplay with the design of earthing systems.

Hence, it is reasonable to establish that the findings of Christy Thomas et al. and Jinliang He et al. remain valid within the context of their specific investigations. Scientific research frequently involves ongoing exploration and inquiry, and it is not uncommon for different studies to yield divergent results. This diversity of findings contributes to an enhanced comprehension of soil resistivity variations. Importantly, it emphasizes the importance of considering a multitude of factors, including the methods used for soil resistivity measurement, data processing techniques, and interpretation practices in real-world applications.

3.4.4 Soil Resistivity Variation on the Earthing System

The deeper soil resistivity layers can significantly affect the earth resistance of an earth grid [59]; however, they exhibit less sensitivity to seasonal effects [49, 50, 53, 58]. A study by R. J. Gustafson et al. found in a simulated case study that a +30 % error in earth grid resistance incurred by an inaccurate soil resistivity model could yield a +110 % error in step and touch voltages calculations [59]. Deep vertical earth electrodes, or multiple vertical electrodes that are driven in

the deeper low resistivity layers, could reduce the seasonal influence on the large-scale earthing system resistance [47, 50, 51, 60, 61].

However, the seasonal water table level fluctuation affects the performance of smaller-scale earthing systems, such as those for pylons or power poles [62]. Further, a recent study [72] on evaluating microgrid earth grid design under different soil conditions showed that the touch voltage, step voltage and tolerable limits are sensitive to the resistivity and thickness of each layer of the soil resistivity model. The magnitudes of the touch and step voltages are affected by the parameters of the middle and the bottom layers depending on the earth grid's burial depth. Therefore, it is apparent that accurate soil resistivity models are required to correctly determine touch and step voltages and, thus, risk levels. Moreover, reliably monitoring soil resistivity and exposure under extreme seasonal conditions is necessary for the earthing system [50, 63, 65]. The above publications indicated that the monitoring of such seasonal effects was carried out manually.

Since the pipeline's earthing system is also considered small-scale and is highly susceptible to electrical hazards, the seasonal variation in the soil resistivity around the pipeline route could significantly affect the determination of electrical safety.

3.4.5 Effect of soil resistivity variation on underground pipelines

Three underground pipeline studies in the literature review have considered the seasonal variation of soil resistivity effect, and two are related to corrosion protection. K. B. Adedeji et al. assumed in the study that the apparent soil resistivity could vary seasonally from 10 to 200 Ω-m [73]. Using these resistivity values and for a fault with a duration of 0.5 s sourced from a nearby transmission system, the tolerable touch voltages could vary from 167 to 213 V. Therefore, the maximum error in calculated touch voltage could be significant without considering the seasonal influence. In 2018, W. Fieltsch et al. [67] pointed out that although it is standard practice in the electrical industry to consider seasonal variations in soil resistivity when modelling earthing facilities for substations and generating stations, this is often not considered in AC interference studies related to pipelines.

Research on seasonal soil variations concerning pipelines has been undertaken [48], with results from Canada showing that soil resistivity affecting the pipeline understudy in the winter could be nine times higher than measurements in the spring and summer. Although the research focused on the performance of the pipeline cathodic protection (CP) system, this significant change in soil resistivity indicates the extent to which seasonal variations in touch voltage are possible. In [41], a comparison between the induced voltages due to inductive coupling between a parallel pipeline and a transmission line showed that a 2% difference could exist, depending on whether two-layer or homogeneous soil resistivity models are used. A pipeline corrosion case study [74] summarised the soil resistivity model in a two-layer soil resistivity model for evaluating the induced current and voltages using HIFREQ of CDEGS [17]. The study highlighted how modern simulation approaches could be used to analyse a wide range of practical pipeline scenarios.

3.4.6 Probabilistic Risk Analysis

In the designated literature search period, the search results yielded only one article related to probabilistic risk analysis. Subsequently, the search period was extended by another ten years, covering the period from 1980 to the present. An additional article published in 1983 was discovered during this expanded search. This article proposed using probabilistic risk analysis to determine the risk of step and touch potentials near transmission line structures [75]. The overall evaluation of risks was based on the exposure to step and touch voltages, and when the applied voltage exceeded the tolerable threshold, it indicated a potentially fatal accident. The introduction of this concept was subsequently developed and incorporated into standards and guidelines [1, 5, 12], as discussed in Section 2.5.

Moreover, another conference paper was published in 2013, focusing on safety in transmission substations. A. Amin et al. [38] used CDEGS to simulate EPR in various substation areas. The substation was then divided into risk zones based on the levels of EPR. The risk acceptance criteria adhered to the ALARP principle.

3.5 Review Summary

In this comprehensive review of soil resistivity and its effects on various aspects of electrical systems, the choice of soil resistivity model significantly influences the performance and safety of power systems. The multilayer soil resistivity model, commonly used in electrical engineering for earthing system analysis, divides the soil into horizontal layers with uniform resistivity. The accuracy of the multilayer soil resistivity model depends on data quality, quantity, and sophisticated data inversion algorithms. Particularly, computer software like RESAP of the CDEGS has industrial reputations in converting apparent soil resistivity data into multilayer soil resistivity models, ensuring research accuracy.

Seasonal variations in soil resistivity have been identified as a critical factor affecting human touch voltages and safety thresholds. Numerous studies have investigated the impact of seasonal changes, with the Wenner test being a popular choice for collecting soil resistivity data. However, the complexity of soil resistivity and its sensitivity to various factors, including temperature, moisture, and geological attributes, underscores the challenges in accurately modelling and designing earthing systems. These seasonal variations significantly affect earthing system resistance, particularly in smaller-scale systems like pylons or power poles. Accurate soil resistivity models are essential for determining touch and step voltages and their tolerable limits. However, the drawback of employing the Wenner test is that all probes in the Wenner array are required to be repositioned for the subsequent Wenner spacing measurement. This labouring effort required additional persons to assist with the measurement. Since the human safety related to the earthing system is greatly affected by the shallow layers in EPR hazard identification [23], the superior accuracy for shallow layer measurement made the Wenner test a commonly chosen method used in soil resistivity data collection.

Two different research groups demonstrated disagreement in the use of seasonal factors for soil resistivity studies. The diverse findings from their studies underscore the complexity of soil resistivity and its complicated relationship with various aspects of electrical systems. It is clear that the accurate measurement and modelling of soil resistivity are vital for designing safe and

reliable electrical systems, with a need for more research and systematic approaches to address the seasonal variability of soil resistivity.

Since soil resistivity is not a fixed quantity, it can vary in time and geographical location. By understanding the seasonal variations in soil resistivity, engineers can improve the design of the pipeline infrastructure and implement mitigation measures according to the worst case of EPR hazards. However, not all identified hazardous spots can be easily or practically mitigated, and some hazards have appeared after the power system was upgraded to the increasing demand. In order to address these challenges, the utility industries allow the use of probabilistic risk assessment methods based on specific well-documented criteria [1, 5, 12]. This approach involves quantifying the probability of an EPR event and evaluating its potential consequences. Stakeholders can understand the risks involved by considering both the probability and potential impact of an EPR event.

Despite the importance of the use of probabilistic risk analysis in evaluating step and touch potentials near transmission line structures, only a limited number of publications have explored this topic. One early article [75] laid the foundation for using probabilistic risk analysis to assess the risk associated with step and touch potentials, eventually influencing the development of standards and guidelines that incorporate this approach. For over 40 years, only a conference paper [38] applied computer simulation [17] to simulate electric potential risk during a fault condition in substations, emphasizing adherence to the ALARP principle for risk management. The extended gap between these two publications suggests that the method of probabilistic risk analysis had been somewhat overlooked for an extended period.

Recently, government and engineers have increasingly emphasized the concepts of safety by design and safety in design [76, 77, 78]. Nevertheless, accepting residual risk may carry potential legal liabilities. These factors have contributed to the reduced favourability of research on probabilistic risk analysis. However, fault levels of the transmission circuits have increased significantly with the rapid surge in electricity demands, driven by the electrification of transportation and the growth of renewable energy. This situation, in turn, has made the mitigation

of touch voltage hazards more challenging, particularly in certain industrial sectors like gas pipelines.

3.6 Identification of Research Gaps

Over 40 years, only two articles addressing probabilistic risk analysis in the context of touch voltages have been identified. The probabilistic risk analysis, along with the ALARP principle, has been integrated into both the gas pipeline [12] and power infrastructure sectors [1]. The literature review draws attention to substantial unexplored research opportunities in the field of probabilistic risk, emphasising a significant knowledge gap related to enhancing the existing probabilistic risk methodologies.

Several deficiencies need to be acknowledged to address this knowledge gap. The literature review has confirmed the presence of seasonal variations in soil resistivity and their impact on touch voltage hazards in previous research. However, a critical gap exists concerning how this impact can be observed and predicted through actual soil data. This gap is particularly significant for smaller-scale earthing systems, such as underground pipelines, which exhibit high sensitivity to soil resistivity variations. The pipelines occasionally require temporary isolation from the earthing system for essential testing procedures. In order to gain a comprehensive understanding of the impact of soil resistivity variations on earthing system safety, there is a critical necessity for statistical data about the variability in soil resistivity.

On the other hand, earthing system design commonly relies on a representative soil resistivity model that incorporates a conservative margin to accommodate variations in soil resistivity model parameters. The literature revealed that the variation in soil resistivity affects touch voltage levels and tolerable touch voltage limits. Consequently, touch voltages may not remain uniform under power system fault conditions. Leveraging this touch voltage variability as an innovative probability reduction factor provides an opportunity to enhance the accuracy of the existing probabilistic risk analysis approach outlined in [12], aligning it more closely with the risks encountered in real-world applications.

3.7 Research Scope

In pursuing a comprehensive understanding of the 40-year gap in probabilistic risk analysis for electricity and long-distance pipeline infrastructures, it is essential to delineate the specific focus areas to answer the research questions and rationale for this research gap. The scope of this research was defined and focused on the following key aspects:

3.7.1 Test Site Selection and Data Collection Method

The area for data collection was confined to the Great Auckland region, with a preference for locations within or near the corridor of the transmission class gas pipeline and power line system. This geographical limitation established the boundaries for data collection. The literature review found that the Wenner test was the preferred data collection method due to its reliability in gathering shallow data, aligning with the requirements of the gas pipeline study. Consequently, the decision was to employ manual Wenner tests for data collection.

3.7.2 Transmission System Fault Analysis

Given the primary focus on power system earth faults, the root mean square (rms) value of zero-sequence current was under different load conditions. The worst-case fault condition was assumed to be a scenario where the rms symmetrical fault current would be three times the zero-sequence current, remaining relatively constant for approximately 0.25 seconds [2]. DIgSILENT PowerFactory [79] calculated the prospective fault current at the nearest substation affecting the pipeline.

3.7.3 Soil Resistivity Analysis

The collected soil resistivity data would be mathematically inverted into multi-layer soil resistivity models using RESAP of CDEGS [17]. The research drew upon existing literature [15], which used soil temperature and cumulative rainfall data to investigate the effects of soil resistivity variation. Monitoring these variables facilitated an examination of the correlation between soil temperature, rainfall patterns, and changes in soil resistivity over time. Consequently, soil temperature and rainfall data were recorded for further numerical analysis.

3.7.4 Pipeline and Transmission Line System Model

The characterization of the pipeline and transmission line system model relied on information from the transmission system operator and an undisclosed source. Additionally, the software HiFreq of CDEGS [17] was used to simulate the system model. The simulation results were the touch voltages. It was expected to see the variation of the touch voltages as the soil resistivity varied.

3.7.5 Developing an Improved Statistical Model for Probabilistic Risk Analysis

The touch voltage profile was used in determining the probability reduction factor through statistical methods. This factor enhanced the accuracy of the existing probabilistic risk analysis and provided the hazard control points for risk management.

3.8 Research Plan

The research plan outlines the approach and methodology used in this study to investigate soil resistivity characteristics and their implications for risk assessment, particularly regarding touch voltage hazards. The Wenner test method is preferred for data collection because it can provide higher accuracy in estimating the resistivity of shallow soil layers. Parameters for the pipeline and transmission line system model, used to identify touch voltage hazards, are determined based on factors such as the transmission system's target protection time, prospective fault levels in the transmission line, and hypothetical cathodic protection systems for the pipeline. The specialist computer software RESAP of CDEGS is utilised to convert collected apparent soil resistivity data obtained through the Wenner test into multilayer soil resistivity models. These models construct a soil resistivity profile for the pipeline and transmission line system. This profile aids in identifying potential occurrences of touch and step voltage hazards. By analysing the soil resistivity profile, the research determines the number of hazardous days, contributing to calculating the adjusted probability of heart fibrillation. This step aims to enhance risk assessment practices. The research methodology follows a quantitative approach supported by mathematical statistics. The research adopts a practical action research framework to statistically address soil

resistivity variation and improve risk assessment, recognising the challenges in generalising and maintaining accuracy in soil resistivity variation.

In summary, the research was organized into five distinct stages, each serving a specific purpose. These stages included:

1. In the first stage, the careful selection of test sites was carried out, with a preference for locations within or near the corridor of the transmission class gas pipeline and power line system. Land with a flat platform, undeveloped, and free from non-uniform soil structures such as vertical fault lines was considered ideal for soil monitoring.
2. A twelve-month data collection using the Wenner test was conducted. The collected data was then inverted to a multilayered soil resistivity model using RESAP of CDEGS to investigate seasonal soil resistivity variations further.
3. The worst-case scenario of the earth return current associated with the nearby transmission line was determined using the DIgSILENT Power Factory model downloaded from the Electricity Authority of New Zealand Government's public domain [64].
4. The pipeline and transmission line shared corridor were modelled based on the information above in the Hi-Freq of CDEGS. The model was rerun with different soil resistivity models derived from the twelve-month data collection. The system model's outcome provided the magnitude of touch voltages and the corresponding touch voltage limits.
5. Statistical calculations apply the system modelling results to develop a probability reduction factor that improves the accuracy of the current probabilistic risk analysis.

Chapter 4 - Soil Resistivity data collection and modelling

4.1 Site Selection

The selected test site is at the fringe of a major city, Auckland, New Zealand. The location used for this case study was chosen based on information available to the public [80, 81]. Aerial photographs [82] show the undeveloped test site for soil resistivity data collection. Records show that no building or underground infrastructure has existed since record-keeping in 1939. The site is underlain by the Colville Formation of the Waitemata Volcanic region, comprising alternating lithic volcanic sandstone, limestone, and mudstone [83]. The lithic volcanic sandstone is rich in calcium carbonate, which reacts with rainwater to form a conductive calcium bicarbonate solution [84]. The mudstones of fine-grained quartz, mica and feldspar can create a barrier to slow down moisture diffusion to deeper ground. An image of the site is shown in Figure 4-1. The transmission line shown is approximately 190 km long, operates at 220 kV AC and terminates at a transmission class substation approximately 8 km from the test site. The section of the transmission line entering the populated area converts to an underground cable approximately 0.5 km from the test site. According to public information [80], a transmission-class high-pressure gas pipeline converges near the test site and is close to the transmission line for a length of approximately 500 m. The average distance between the two transmission system paths is about 20 m along this length, forming a transmission corridor-sharing situation. These conditions make it a suitable test site; however, since the pipeline system model is a hypothetical case study, they may or may not influence the experiment's outcome. While the earth current converges to the earthing system of the cable transition station, and nearby transmission towers and underground infrastructure are susceptible to most of EPR events along the transmission line, the simulation model for this research did not explicitly include the 0.5 km underground cable. The primary focus of the research was to evaluate the impact of seasonal variations in soil resistivity on touch voltages, using a hypothetical pipeline model for risk assessment. The presence of the underground cable, while acknowledged, was not included in the simulation model, as the focus was on assessing the impact of soil resistivity variations rather than the full infrastructure of the transmission system.

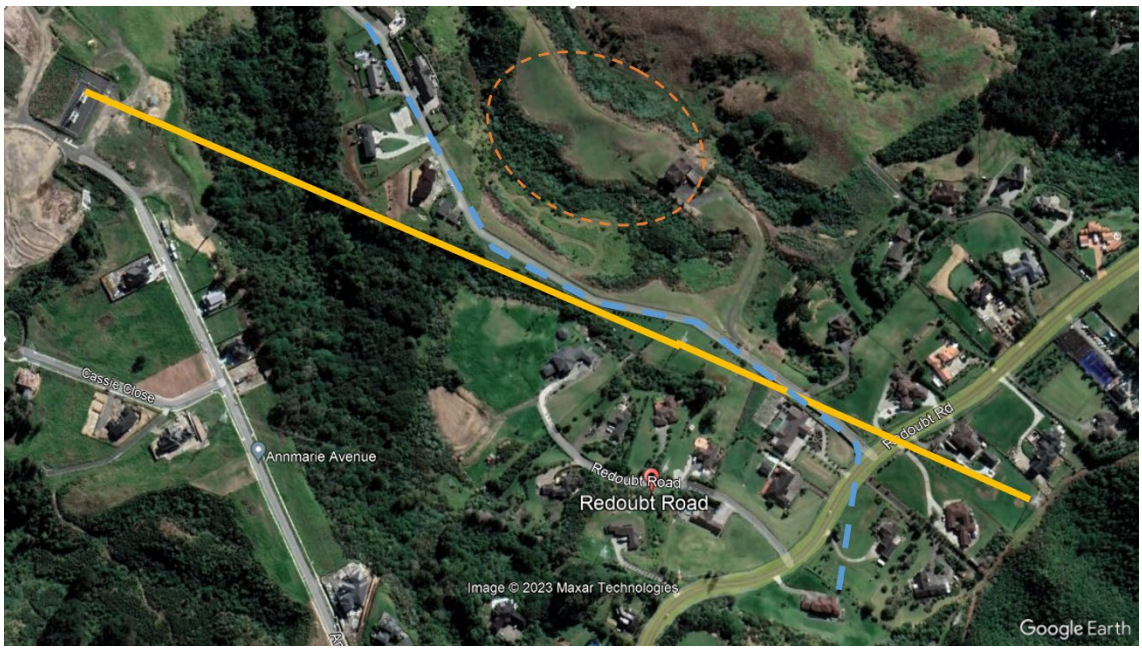

Figure 4-1 The proposed test site and the transmission corridor in Google Earth image. The selected test site (orange dotted lines), 220kV transmission lines (yellow), and transmission class high-pressure gas pipeline (blue dotted lines). Information from Transpower (NZ) Limited [85] and FirstGas [80].

4.2 Initial Test Site Assessment

The primary objectives of the initial test site assessment were to identify a representative Wenner test traverse for local soil resistivity. Hence, multiple Wenner test traverses were measured for comparison, and one representative test traverse was selected from the initial analysis, as shown in Figure 4 2. Any potential future difficulties would be discovered and resolved before the twelve-month soil resistivity monitoring commenced.

Additionally, two low-cost earth testers were selected during the initial assessment to determine which provided the most reliable results compared to the sponsor's calibrated earth tester. The selected candidate would be used for the 12-month data collection.

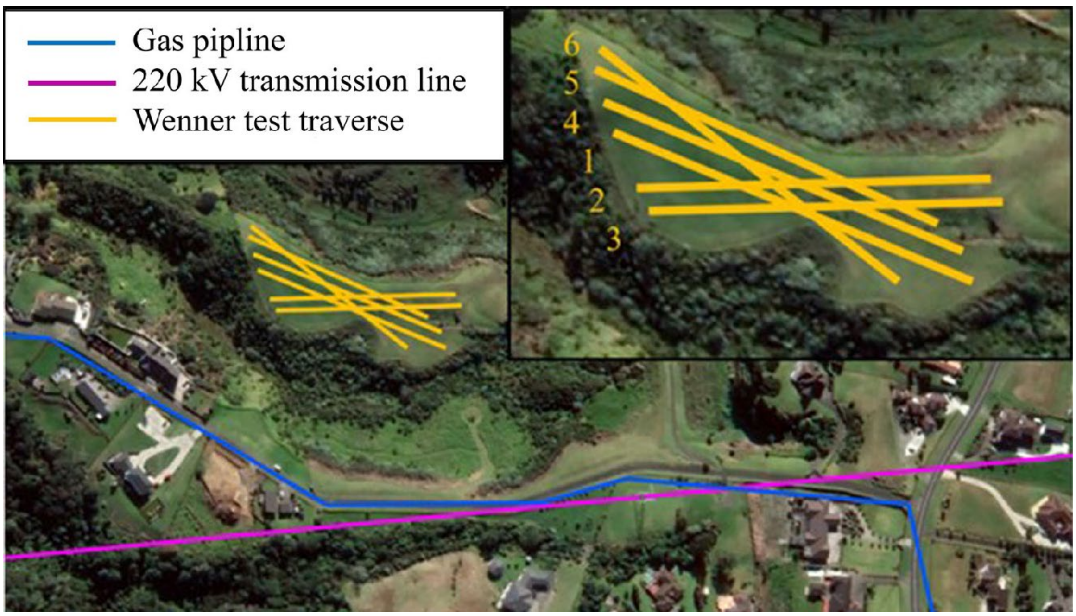

Figure 4-2 Wenner test traverse for initial soil resistivity assessment before the twelve-month data collection

The test setup commenced with driving a plastic rod or marker into the ground at the centre of the test traverse, marking the midpoint between the current and potential electrodes. Two fibreglass measuring tapes were then extended from this central point to each end of the test traverse, ensuring they were kept taut and aligned with the measurement line. These measuring tapes were utilized as guides for the placement of the electrodes.

Next, the earth resistance tester was positioned at the marked centre point. One end of each connecting wire with a banana jack was securely plugged into the corresponding tester port. In contrast, the other end of each connecting wire was clamped to the electrode to establish secure connections.

The location of each electrode for the initial analysis was determined according to a table showing the locations of the current and potential electrodes from the centre point of the traverse. Ideally, two individuals were designated to carry out the electrode placement. Each individual handles the potential electrodes P1 and P2, then proceeds to the positions for driving the current electrodes C1 and C2 into the ground. The depth to which these electrodes were driven does not exceed $a/10$ for the Wenner spacing is small.

The Wenner spacings for the initial soil assessment were 0.5, 1, 2, 3, 4, 5, 10, 20, 30, 40. The locations of electrodes for each Wenner spacing measured from the mid-point are shown in Table 4-1 below. The setup of the Wenner array during the initial site assessment for Traverse-5 is shown in Figure 4-3.

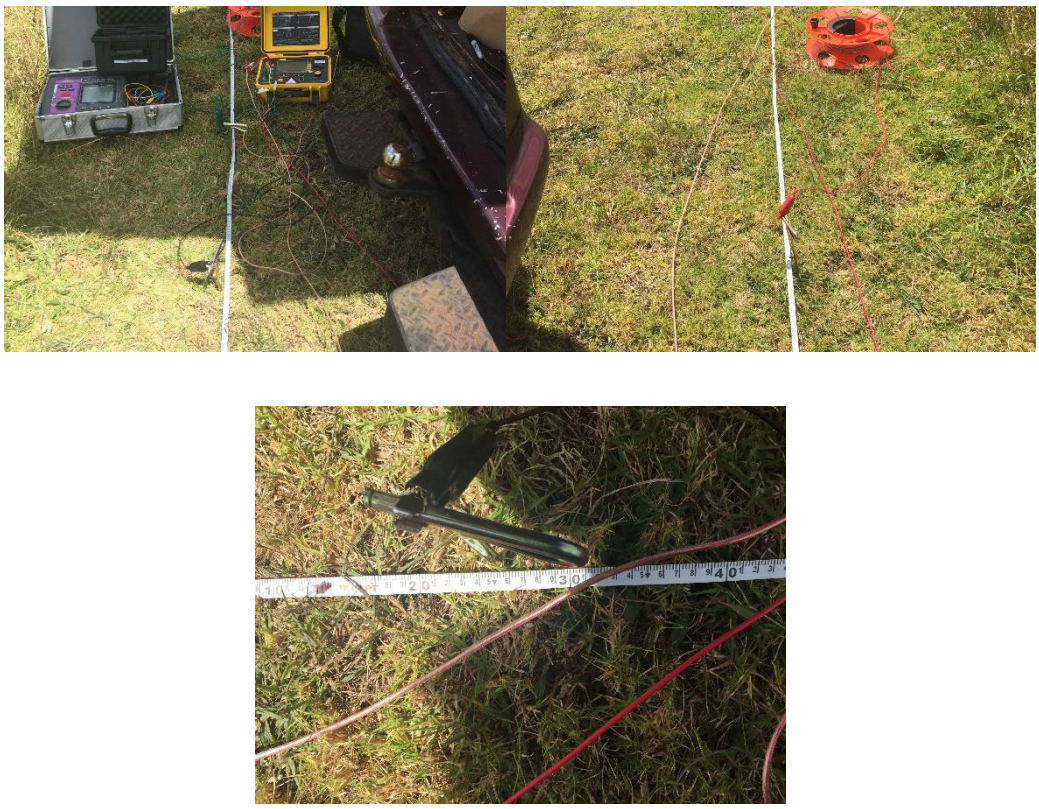

Figure 4-3 The setup for Traverse-5 measurement during the initial site survey. Taking readings using AEMC 6471 (top-right); current probe location (top-left); voltage probe location (bottom)

Table 4-1 Electrode locations showing on the fibreglass tape measures for each Wenner spacing for initial site assessment.

Wenner Spacing	Probe location from the mid-point (m)	
a (m)	Potential	Current
0.5	0.25	0.75
1	0.5	1.5
2	1	3
3	1.5	4.5
4	2	6
5	2.5	7.5
10	5	15
20	10	30
30	15	45
40	20	60

4.2.1 Selection of the test traverse for the twelve-month soil resistivity monitoring

Six test traverses were measured using the Wenner test method. Each traverse underwent measurements with three different earth resistance testers: two were the candidates for the twelve-month soil resistivity monitoring, while the third was a calibrated instrument-grade earth resistance tester. The measurement results from each test traverse with these various earth resistance testers are summarized in Table 4-2.

To identify the most suitable Wenner test traverse for the twelve-month soil resistivity monitoring, a Two-Way Mixed-Effects Analysis was conducted to evaluate its reliability. The analysis showed a statistically significant difference in soil resistivity measurements among the Wenner test traverses at the $p < 0.05$ level, with $F(5,45) = 2.595$ and $p = 0.038$. Consequently, the null hypothesis, positing that the mean of each Wenner spacing measurement is equal, was rejected.

Table 4-2 The Wenner test measurement for six traverses with different earth resistance testers. (The errors of measurement are shown in red).

Wenner Spacing(m)	Soil resistance(Ω) Traverse					
DY4300B	1	2	3	4	5	6
0.5	22.58	21.32	24.16	21.22	19.22	23.18
1	12.27	11.11	12.42	11.43	11.78	11.82
2	7.73	6.87	7.69	7.19	6.64	7.31
3	6.13	5.29	6.09	5.76	5.35	5.95
4	5.10	4.49	5.11	4.85	4.53	5.05
5	4.35	3.51	4.38	4.24	3.95	3.89
10	2.28	2.18	1.32	2.28	2.02	2.29
20	1.06	1.13	1.13	1.11	1.08	1.01
30	0.72	0.73	0.74	0.72	0.72	0.73
40	0.53	0.52	0.55	0.54	0.55	0.54
AEMC 6471						
0.5	23.18	21.26	24.53	21.28	19.5	22.52
1	12.33	11.54	12.36	11.37	10.59	11.22
2	8.99	4.61	7.56	8.07	6.51	6.05
3	5.98	5.10	6.09	6.14	5.54	5.76
4	4.35	4.49	4.28	5.10	5.11	5.30
5	3.97	4.14	3.88	3.93	4.18	4.20
10	1.97	2.18	2.01	2.20	1.40	2.35
20	1.01	1.00	1.05	1.10	1.10	1.09
30	0.74	0.71	0.77	0.78	0.69	0.66
40	0.53	0.52	0.61	0.50	0.57	0.54
ST4106						
0.5	21.76	21.01	20.04	20.84	23.85	22.99
1	10.39	12.99	11.28	9.67	12.29	12.45
2	7.54	6.68	5.51	6.25	6.94	7.12
3	6.13	4.28	4.85	4.75	5.84	4.94
4	4.47	3.55	4.22	4.54	4.48	4.74
5	3.6	2.94	3.2	3.93	4.32	3.01
10	1.84	2.15	1.28	1.98	0.69	2.98
20	1.03	1.93	0	1.53	0	1.54
30	0.87	0.12	0.89	0.33	0.13	0.13
40	0	0.1	0.1	0	0	0

Despite achieving statistical significance, the observed mean differences between the Wenner test traverses were relatively small, with an effect size of 0.022. As previous research indicates, this effect size suggests a gradual change between the test traverses [35].

Furthermore, the 95% confidence interval of the resulting Intraclass Correlation Coefficient (ICC) value of 0.99 suggested that any of the Wenner test traverses could reliably represent the soil resistivity of the test site. Therefore, Traverse-5 was selected for the twelve-month soil resistivity monitoring, aligning with an agreement reached with the landowners.

Before the twelve-month soil resistivity data collection, deciding the sample size according to the available budget for travelling to the site and minimum data sets for the statistical analysis was essential. Multiple regression with three predictors was planned to be included in the research to find the equation to estimate the touch voltage on site. Therefore, a minimum sample size of 90 was required to detect the alpha level at 0.05 for three predictors and the F statistic effect size of 0.39 with a precision of 6 digits. The calculated test power of 0.87 for 90 samples would be acceptable because if there was a relation in the population for multiple regression, the conventional threshold of 0.80 for random samples from the same population would be significant [90]. In other words, the data should be collected twice a week with a fixed interval to ensure the data meets the minimum statistical analysis requirement.

4.2.2 Selection of Earth resistance tester

The research sponsor, BECA (NZ) Limited, generously loaned the calibrated AEMC 6471 earth tester [86], as shown in Figure 4-4, for a short period. Due to the high demand for the AEMC 6471, its long-term use was impractical. As an alternative, two affordable earth resistance testers were compared to the AEMC 6471 to evaluate their suitability for the twelve-month data collection. The Wenner test data collected during the initial site assessment were used to assess the reliability and accuracy of the low-cost testers, as precise earth resistance measurements were crucial for the quality of the soil resistivity model.

The objective of this analysis was to determine whether there was a statistically significant difference between the measurements obtained from the two earth resistance testers. An alpha level of 0.05 was set to determine statistical significance [88].

The remaining tester, the DY4300B, successfully completed all measurements. As shown in Table 4-2, the ST4106 earth resistance tester consistently failed to produce valid readings when

the Wenner spacing was increased to 20 m. Consequently, the ST4106 tester was deemed unsuitable for further statistical analysis and was excluded from consideration.

(a) (b)

(c)

Figure 4-4 The earth resistance testers for Wenner Test. (a) Unbranded ST4106, (b) DUOYI DY4300B [87], and (c) AEMC 6471

The normality test for the paired data of the DY4300B and AEMC 6471 was conducted through a visual inspection of the histogram illustrating the differences between the measurements of the two testers. The distribution of these differences was centred around zero, indicating a good level of normality, as shown in Figure 4-5.

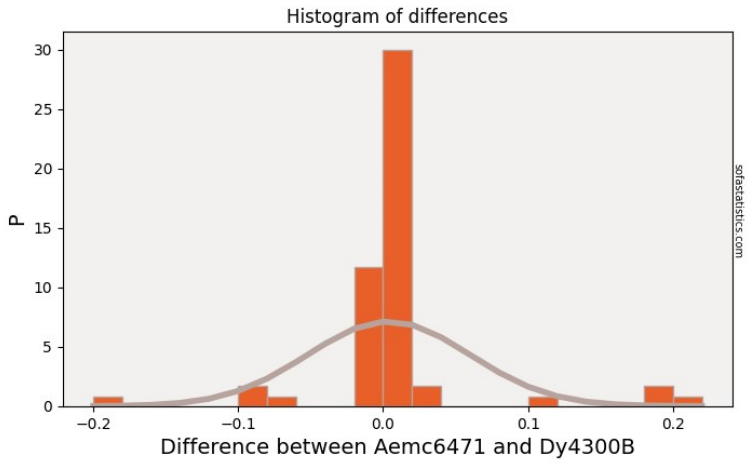

Figure 4-5 The normality test for the paired data of AEMC6471 and DY4300B earth resistance tester. The y-axis is the number of paired samples. The unit for the difference between AEMC6471 and DY4300B is in (Ω).

A paired-sample t-test was performed between the DY4300B and AEMC 6471 using data from six Wenner test traverses, consisting of 60 paired measurements. Table 4-3 summarizes the dataset characteristics used for the t-test.

Table 4-3 The characteristics of the dataset of DY4300B and AEMC 6471

	Earth resistance tester	
	DY4300 B	AEMC6471
Mean (Ω)	5.99	5.95
Standard deviation (Ω)	6.35	6.36
Standard error mean (Ω)	0.82	0.82
Number of samples	60	60

The analysis yielded a t-value of 0.61 and a two-tailed p-value of 0.54. This p-value exceeds the significance threshold of 0.05, which means the Null Hypothesis (H0)—stating no significant difference between the two testers—could not be rejected. Typically, failing to reject H0 suggests insufficient evidence to claim a statistical difference, often attributed to a Type II error (false negative). However, given the substantial sample size of 60 and the normal distribution of the mean difference, as shown in Figure 4-5, the risk of a Type II error affecting the conclusion is minimal. The mean difference (DY4300B – AEMC 6471) was 0.04 Ω, with a 95% confidence interval ranging from -0.088 to 0.166 Ω. The t-value of 0.61 indicated a relatively small observed difference between the measurements.

In summary, the analysis showed that the measurements obtained from both testers were statistically comparable. The absence of significant statistical differences suggests that the DY4300B provided measurements consistent with the more precise AEMC 6471 tester. Both testers, equipped with the FFT DSP technique, demonstrated that the FFT method improved measurement capability, particularly when the signal-to-noise ratio was high due to increased Wenner spacing. Therefore, the DY4300B was deemed suitable for use in the twelve-month soil resistivity data collection.

4.2.3 Determination of Wenner Test Traverse

With the testing equipment validated, the next challenge was to determine the most representative Wenner test traverse for the twelve-month monitoring period. Statistical analysis played a key role in identifying the best traverse in Table 4-2 by assessing the alignment between multiple test traverses and selecting the one that best represented the overall soil conditions at the site.

The statistical analysis of a two-way mixed-effect analysis resulted in an F(5, 45) value of 2.60 and a p-value of 0.038. Additionally, an effect size of 0.022 was calculated. These results indicate statistically significant differences between all six test traverses. However, the small effect size suggests that these differences are practically insignificant, implying that the observed variation among the traverses was relatively minor.

The two-way mixed-effect analysis discovered the statistically significant differences between the traverses. However, the soil structure can exhibit gradual geographical variations [22], and the small effect size indicated that the variations across traverses were relatively minor, which allowed for the selection of Traverse-5 in Figure 4-2 as the most suitable test traverse. This decision, backed by statistical analysis and landowner preference, ensured that the data collected over the monitoring period was representative and consistent.

4.2.4 Inverting Soil Resistivity into a Multi-layer Soil Resistivity Model

The collected apparent soil resistivity data set is input into RESAP to obtain the multilayer soil structure. An example of that detailed setup for RESAP is shown in **Error! Reference source not found.**. Since the electrode depth is controlled to be less than a /10 [22], the electrode depth

is considered negligible. The plot of the apparent soil resistivity values against the corresponding Wenner spacing is often plotted on a logarithmic scale, with soil resistivity values on the y-axis and Wenner spacing on the x-axis. The best-fit curve on the plot is known as a Wenner curve and is shown in Figure 4-6.

The mathematical data inversion performs based on the best fit of the Wenner curve obtained from the actual earth testing, aiming to identify the number of soil layers, the resistivity value, and the thickness of each layer. The bottom layer of the soil resistivity model has an infinite depth. The shape of the curve, including any turning point or change in slope, indicates the location of boundaries between layers. The multi-layer soil resistivity model in Figure 4-6 demonstrates a three-layer soil resistivity model, with the surface soil layer with a resistivity of 31.22 Ω-m and a thickness of 0.41 m. Beneath it lies a middle layer with a resistivity of 7.57 Ω-m and a thickness of 3.36 m. Finally, as mentioned earlier, the bottom layer demonstrates a resistivity of 0.66 Ω-m with infinite depth.

For ease of reference and convenience, this soil resistivity model can be concisely represented as follows: (31.22 Ω-m, 0.41 m; 7.57 Ω-m, 3.36 m; 0.66 Ω-m, ∞).

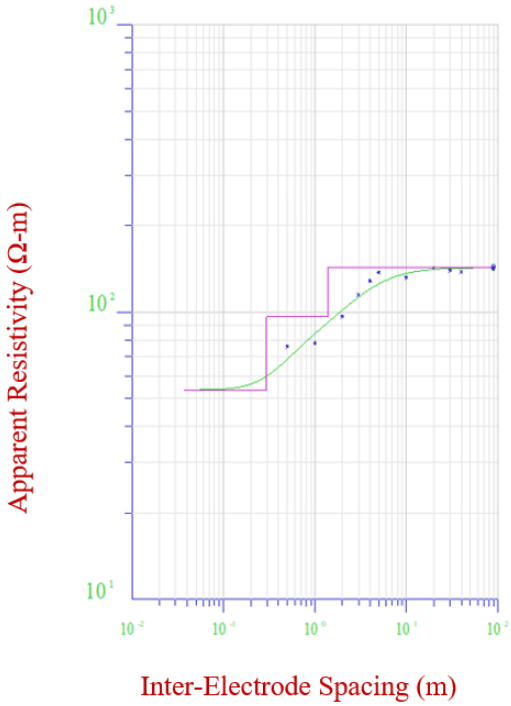

LEGEND

x Measured Data

Computed Result Curve

Soil Model

Measurement Method : Wenner

RMS error : 5.71%

Layer #	Resistivity (Ω-m)	Thickness (m)
Air	Infinite	Infinite
2	53.61	0.29
3	96.38	1.1
4	142.94	Infinite

Figure 4-6 The soil resistivity inversion result shows a three-layer model.

4.2.5 Additional Wenner Spacings for Shallow Resistivity Layer Estimation.

During the initial assessment of the collected data, the Wenner test traverse initially began with a 0.5 m spacing. However, a data entry mistake occurred while using the RESAP software to model Traverse-1, and this error had a significant impact on the accuracy of the surface layer estimation. The additional Wenner spacings of 0.1 and 0.2 m for each traverse were measured on the same day to ensure the accuracy of determining tolerable touch voltages. By introducing these additional Wenner spacings, a comprehensive analysis of the differences in all six test traverses was conducted, which is summarized in Table 4-4. The most substantial difference was observed in Traverse-6, with a significant 16.1% variance between the Wenner spacing starting at 0.1 and 0.5 m. In contrast, the least difference was found in Traverse-5, where only a minor 1.1% difference in surface soil resistivity estimation was recorded. The soil resistivity modelling results for both cases of Traverse-5 are shown in Figure 4-7 and Figure 4-8.

Table 4-4 The surface soil estimation affected by the initial Wenner spacing.

	Test Traverse											
	1		2		3		4		5		6	
Initial Wenner spacing (m)	0.1	0.5	0.1	0.5	0.1	0.5	0.1	0.5	0.1	0.5	0.1	0.5
Estimated surface soil resistivity (Ω-m)	61.3	69.4	60.0	65.6	61.5	74.8	62.0	64.1	53.0	53.6	62.1	72.1
Difference (%)	13.1%		9.3%		21.7%		3.4%		1.1%		16.1%	

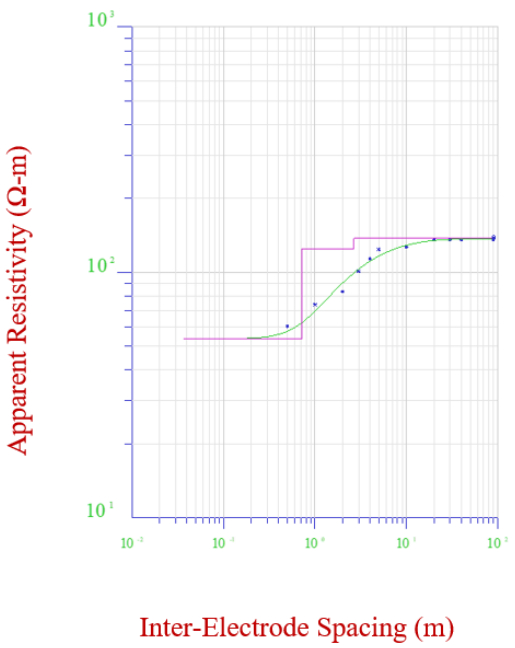

Measurement Method : Wenner

RMS error : 4.25%

Layer #	Resistivity (Ω-m)	Thickness (m)
Air	Infinite	Infinite
2	53.61	0.72
3	124.44	1.95
4	137.55	Infinite

Figure 4-7 The soil resistivity modelling for Traverse-5 with the initial Wenner spacing of 0.5 m.

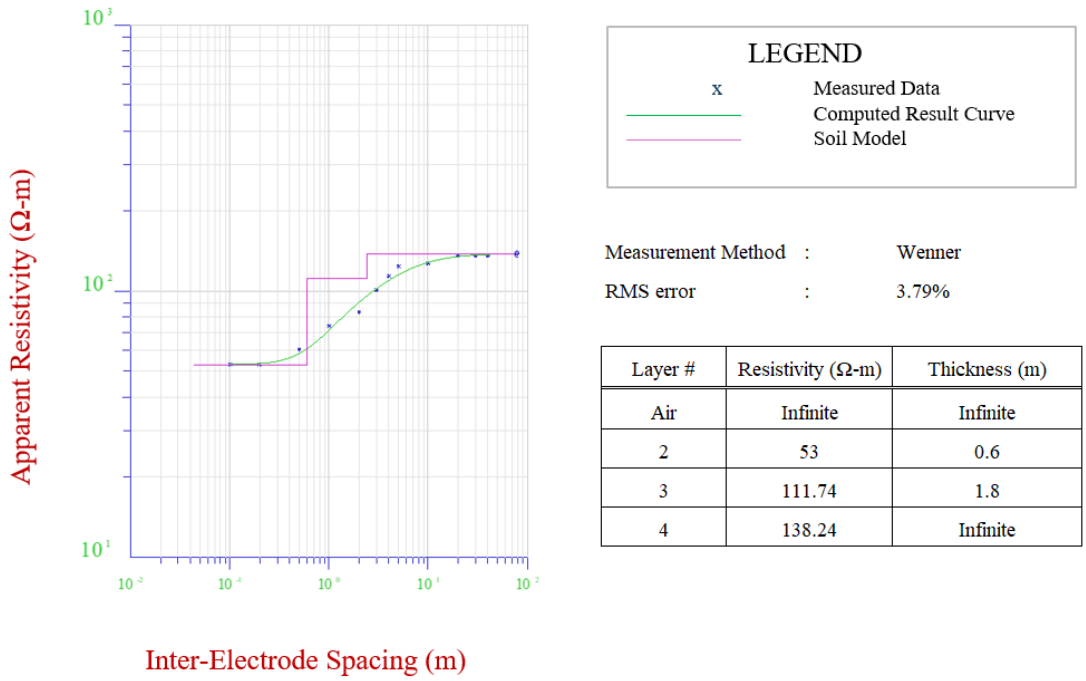

Layer #	Resistivity (Ω-m)	Thickness (m)
Air	Infinite	Infinite
2	53	0.6
3	111.74	1.8
4	138.24	Infinite

Figure 4-8 The soil resistivity modelling for Traverse-5 with the initial Wenner spacing of 0.1 m.

4.2.6 Wenner Spacing Reduction Strategy

The determination of the Wenner test traverse for the twelve-month soil resistivity monitoring was primarily based on the quality of the results obtained during the initial site assessment. Recognising that the manual Wenner test is a labour-intensive task, especially when conducted over an extended period and under challenging weather conditions, efforts were made to enhance the efficiency of the task.

For example, assuming the Wenner test in the initial test site assessment was carried out by only one person, measuring a test traverse with maximum Wenner spacing of 40 m would require walking 767 m. Given the task's laborious nature, for a person to measure soil resistivity down to a depth of 40 meters alone, this measurement process can be physically demanding to a substantial distance on foot. Therefore, the shortest test traverse is crucial in optimising the efficiency of data collection and minimising the physical demands on the personnel conducting the measurements. This efficiency becomes especially important when the Wenner test is conducted over an extended period or in challenging environmental conditions.

In order to reduce the length of the Wenner test traverse for the data collection process, soil resistivity modelling was revisited with a focus on eliminating the large Wenner spacings while preserving the quality of the soil resistivity model. The complete Wenner array results were converted using the mathematical data inversion software to generate a baseline soil resistivity model. The test soil resistivity model was obtained from a reduced Wenner spacing configuration. Subsequent test soil resistivity models were iteratively generated with shorter Wenner spacing until the best-fit curve deviated from the baseline soil resistivity model. The optimal final Wenner spacing for soil monitoring was determined as the maximum one that maintained an undistorted model before the deviation occurred. This reduction strategy aimed to determine the shortest possible array that would not compromise the quality of the soil resistivity modelling.

The data collected for Traverse6 in Figure 4-2 was used to illustrate the Wenner spacing reduction strategy. The initial data collection involved using the complete Wenner array with a maximum Wenner spacing of 40 m. This initial data resulted in a baseline soil resistivity model with three soil layers characterized by resistivity values of (73.05 Ω-m, 1.31 m; 180.49 Ω-m, 2.69 m; 136.74 Ω-m, ∞). Subsequent iterations and refinements of the soil resistivity model are shown in Appendix A and summarised in Table 4-5.

Table 4-5 The Wenner spacing reduction for Traverse-6. The figures shown in red indicate a significant soil structure change.

	Layer 1		Layer 2		Bottom Layer	
Max a(m)	Resistivity (Ω-m)	Depth (m)	Resistivity (Ω-m)	Depth (m)	Resistivity (Ω-m)	Depth (m)
40.00	73.05	1.31	180.49	2.69	136.74	∞
30.00	72.93	1.31	183.32	2.45	136.71	∞
20.00	72.65	1.28	182.42	2.39	135.79	∞
10.00	74.83	1.44	258.22	0.85	136.26	∞

This case study determined that the optimal Wenner spacing that reached a balance between reducing the number of measurements and maintaining an accurate soil resistivity model is 20 m. The relatively small differences between the baseline resistivity values of each soil layer made

this spacing choice effective. This 20-m spacing allowed for a substantial reduction in data collection efforts without significantly compromising the quality of the soil resistivity modelling. The deviation from the baseline model with a maximum spacing of 40 m remained within acceptable limits, ensuring that the resulting soil resistivity model was efficient and accurate.

Furthermore, the Wenner spacings of 0.1 and 0.2 m were added in the test traverse for the twelve-month soil resistivity monitoring. These additional Wenner spacings are intended to assist the mathematical data inversion in accurately modelling the resistivities of the surface soil layer. This finer granularity in measurements can provide more detailed information about soil resistivity variations, especially in areas where substantial resistivity variations are expected.

4.3 Twelve-Month Soil Resistivity Monitoring

In expectation of the twelve-month soil resistivity monitoring, detailed preparations were undertaken to establish a robust foundation for accurate and reliable soil data collection. The selection of a test traverse is positioned as the foundation of soil resistivity monitoring and is a critical element in the research. Therefore, the accuracy of the collected data can directly impact the quality and reliability of the research. Every aspect of the preparations, from traverse selection to data collection methodologies, is designed to achieve the highest data accuracy and dependability standards.

4.3.1 Sample Size Calculation

The research investigated the complex relationship between data collection, accuracy, and reliability, with the aim of explaining the reliability's design and its link to statistical methodologies. Reliability is an essential concern. Achieving a high level of reliability in the research design required a systematic and methodical approach. To establish the reliability of the proposed methods in this research, pair-t-tests and statistical power calculations were carefully utilised. These tools allowed for a thorough statistical examination of the consistency and dependability of the data and contributed to the determination of the quantity of data required to maintain the overall robustness of the research.

Within the research scope, the prediction of touch voltage is one of the focused topics. To realize this objective effectively, a key factor was the determination of an adequate sample size with fixed intervals. This step was of paramount importance, involving the knowledge which was not present during the research planning. Therefore, conservative assumptions on standard deviation number predictors were used to calculate the statistical power prior to the minimum sample size being calculated.

With three predictors and considering a medium effect size of 0.39 [88], a precision of 6 digits, and a minimum sample size of 90, the calculated test power was determined to be 0.87 using IBM SPSS [89]. This level of test power is considered acceptable, as it exceeds the conventional threshold of 80% for statistical power in multiple regression. This threshold is often used as a minimum acceptable level of power, ensuring that if there is a true relationship in the population, 80% of random samples from the same population would find significance [90].

A substantial dataset comprising 90 continuous data sets was specially allocated for the development of the regression equations. Subsequently, the remaining 14 data sets were reserved for the equation validation, assuring that the touch voltage equations not only provided accurate predictions but also demonstrated a high degree of consistency and reliability.

In preparation for the twelve-month soil resistivity study, it was crucial to determine the appropriate sample size based on budget constraints and the minimum data required for statistical analysis. The research sought to integrate a multiple regression model featuring three predictors to formulate an equation for estimating on-site touch voltage. A significance level of 0.05 was established to ensure the statistical validity of the outcomes.

In practical terms, data collection needed to be carried out twice a week, at fixed intervals, to ensure that the dataset met the minimum requirements for robust statistical analysis.

4.4 Soil Resistivity Modelling

At the end of the twelve-month soil monitoring period, the Wenner measurements were inverted into the soil resistivity models using RESAP using the method described in the previous chapter,

as shown in Figure 4-13. The initial identified that the local soil possessed a three-layer structure at the measurement time. Preliminary observation discovered that the top layer demonstrated a property sensitivity to the moisture level and soil temperature, as shown in Figure 4-13 (b).

4.4.1 Soil Resistivity in Rainy Seasons

The soil resistivity model exhibited a significant degree of stability during the rainy season from early June to late September 2020, with sufficient moisture content maintaining consistent soil resistivity models throughout the winter months. The mean resistivity values for the top, middle, and bottom layers were as follows: 64.99 Ω·m (σ = 2.93 Ω·m), 174.56 Ω·m (σ = 28.80 Ω·m), and 105.41 Ω·m (σ = 8.09 Ω·m), respectively. Hence, the resistivity variations observed in the top and bottom layers were minimal, suggesting that soil resistivity did not undergo significant changes during the rainy seasons.

4.4.2 Mitigating False System Changes in Soil Resistivity Modelling Using Warm-Starting

In late October 2020, low precipitation was experienced at the test site. This dry condition led to inaccuracies in the three-layer soil resistivity model, making it impossible to interpret soil resistivity variations correctly. The soil resistivity modelling results of 24/10/2023, shown in Figure 4-9 and detailed in Table 4-6, showed a significant increase in the resistivity of the top layer, which reached 262.50 Ω·m with a thickness of 0.23 m. In comparison, the previous surface soil resistivity on 21/10/2023 was 69.92 Ω·m. Moreover, the lower resistivity layers were indicated to commence at a depth of 0.60 m. These variations significantly differed from the average depth of the lower layer observed in the preceding 30 days, which started at a depth of 2.12 m (σ = 0.48 m). This inconsistency suggested a potentially misleading representation of changes in the soil system compared to the previous soil resistivity models.

Table 4-6 The comparison of soil resistivity models for the presence of the surface high resistivity layer (measured on 25/10/2020).

Soil resistivity model	Layer-1 resistivity(Ω·m) / thickness (m)	Layer-2 resistivity resistivity(Ω·m)/ thickness (m)	Layer-3 resistivity resistivity(Ω·m)/ thickness (m)	Bottom layer resistivity (Ω·m)	Bottom layer depth (m)
3-layer	262.50/0.23	42.48/0.37	NA/NA	115.74	0.60 to ∞
4-layer w/o initial values	262.50/0.24	33.25/0.39	288.07/0.31	111.91	0.94 to ∞
4-layer with initial values	300.02/0.21	49.98/0.71	186.37/1.41	104.90	2.33 to ∞
Initial values: 21/10/2020	69.92/0.80	193.23/1.38	NA/NA	100.51	2.18 to ∞

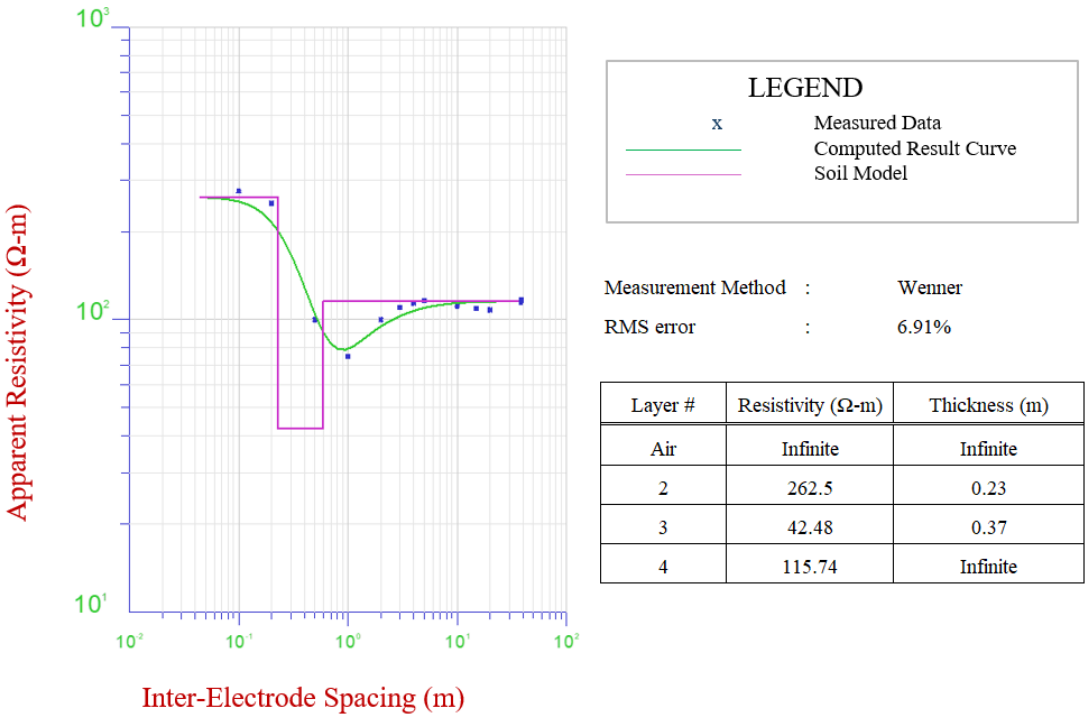

Figure 4-9: The 3-layer model led to a false system change in soil (25/10/2020).

An additional high-resistivity layer was added at the surface to reflect the soil conditions during the low precipitation period to address the false system change in soil resistivity modelling. However, the 4-layer soil resistivity model showed that the bottom layer's depth had shifted by approximately 1 m closer to the surface, as shown in Figure 4-10. Increasing the number of layers in the soil resistivity model introduced more degrees of freedom for data inversion. The increase in the degree of freedom could make the mathematical inversion sensitive to initial conditions for soil resistivity model estimation and result in an unrealistic soil resistivity model from one of many possible solutions. Therefore, a warm-starting approach was implemented to improve the stability of the soil resistivity model estimation. Instead of allowing the inversion algorithm to begin from arbitrary initial conditions, the solution from a previous well-converged model was used as a starting point for subsequent estimations. This method helped constrain the degrees of freedom introduced by the additional soil layers, reducing sensitivity to variations in initial conditions. By guiding the inversion process toward physically meaningful solutions, warm-starting mitigated erratic behaviour and improved the reliability of the soil resistivity model.

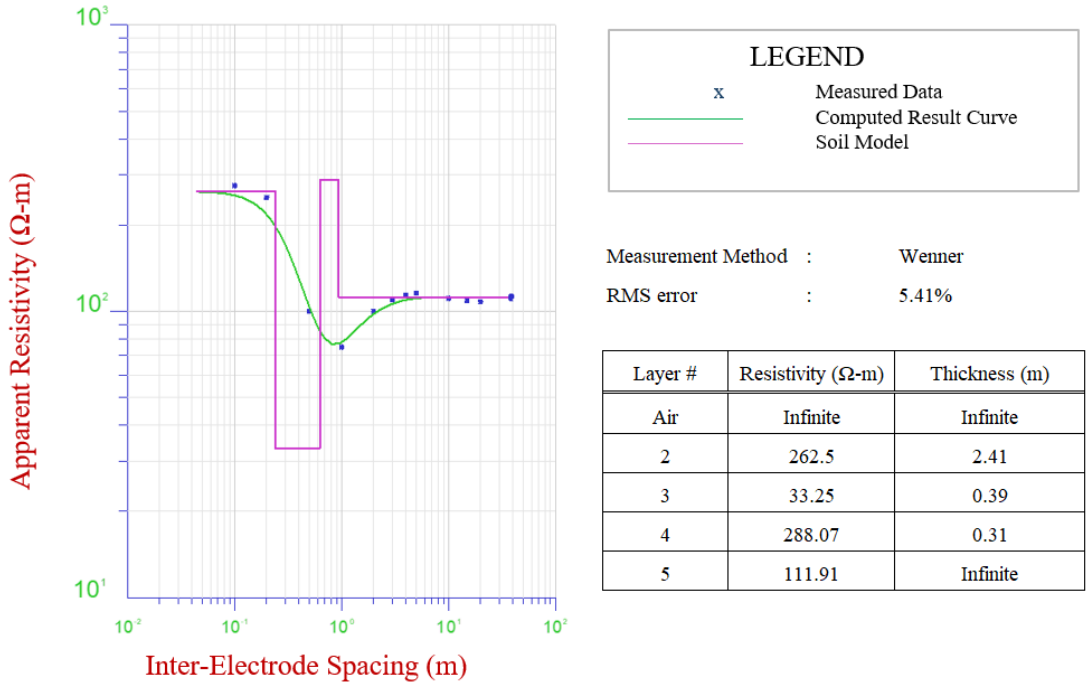

Layer #	Resistivity (Ω-m)	Thickness (m)
Air	Infinite	Infinite
2	262.5	2.41
3	33.25	0.39
4	288.07	0.31
5	111.91	Infinite

Figure 4-10 RESAP inverted the 4-layer model without defining the initial values (25/10/2020).

The previous soil resistivity model for 21/10/2020 was used as the initial condition for the data inversion to maintain a rational continuity soil resistivity variation and avoid reaching local minima on the misfit curve of the mathematical inversion process [91]. This approach provided a "warm starting" was utilised to guide the iterative data inversion away from the misfit curve but towards a path that could yield a soil resistivity model inheriting the characteristics of the previous one, so the soil resistivity model could accurately represent the soil resistivity of the site under study on the day the soil resistivity data was collected.

The parameters of the three-layer soil resistivity model on 21/10/2020 were as the followings: (69.92 Ω·m, 0.80 m; 193.23 Ω·m, 1.38 m; 100.51 Ω·m, ∞). These values were used as the initial values for Layer 2 to the Bottom layer, as shown in Figure 4-12. This warm starting approach narrowed the mathematical data inversion to converge on a soil resistivity model, with the bottom layer beginning at a depth of 2.33 m compared to the 30-day average depth of the bottom layer of 2.12 m.

The differences between the two distinct four-layer soil resistivity models are presented in Table 4-6. The soil resistivity modelling results in Figure 4-11 show that the best-fit RMS error was 2.5%, which was the lowest among the three-layer model with a 6.9% RMS error and the four-layer model without initial value setup, which had a lower RMS error of 5.4%. This low RMS error indicated that the estimated model was closer to the possible soil conditions, demonstrating the effectiveness of the warm starting approach in improving the accuracy of the soil resistivity model.

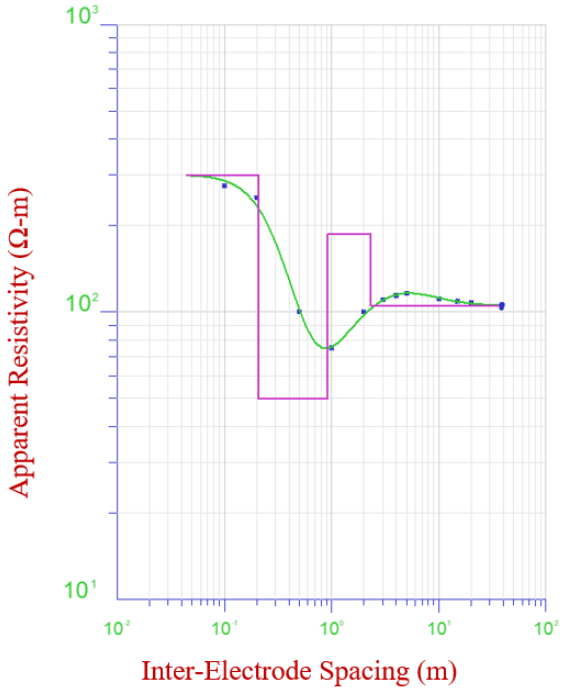

Layer #	Resistivity (Ω-m)	Thickness (m)
Air	Infinite	Infinite
2	300.03	0.21
3	49.98	0.71
4	186.37	1.41
5	104.9	Infinite

Figure 4-11 The 4-layer soil resistivity model (25/10/2020) carried the characteristics of the previous soil resistivity model (21/10/2020).

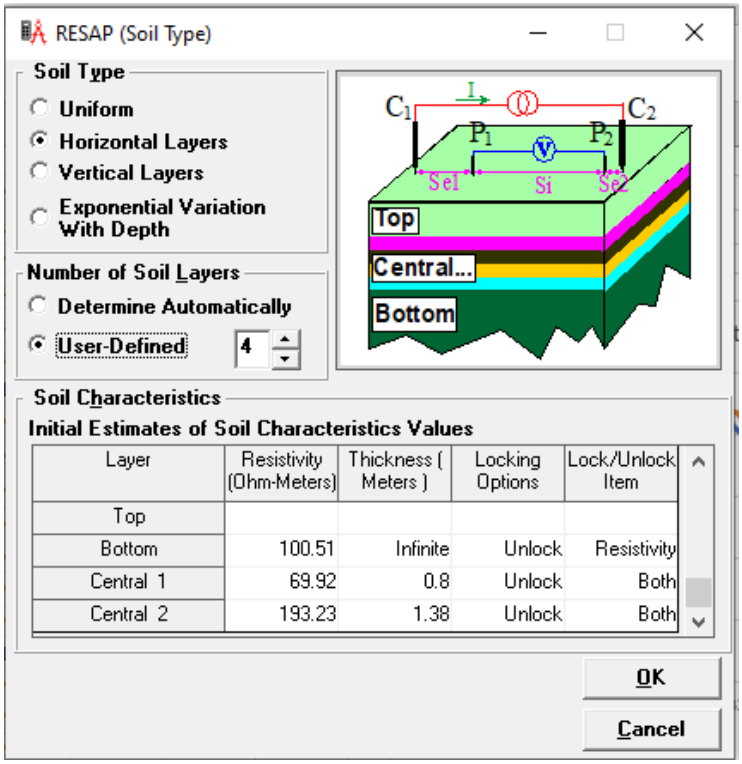

Figure 4-12 The setup of the initial condition for data inversion. The initial values are a three-layer soil resistivity model on 21/10/2020.

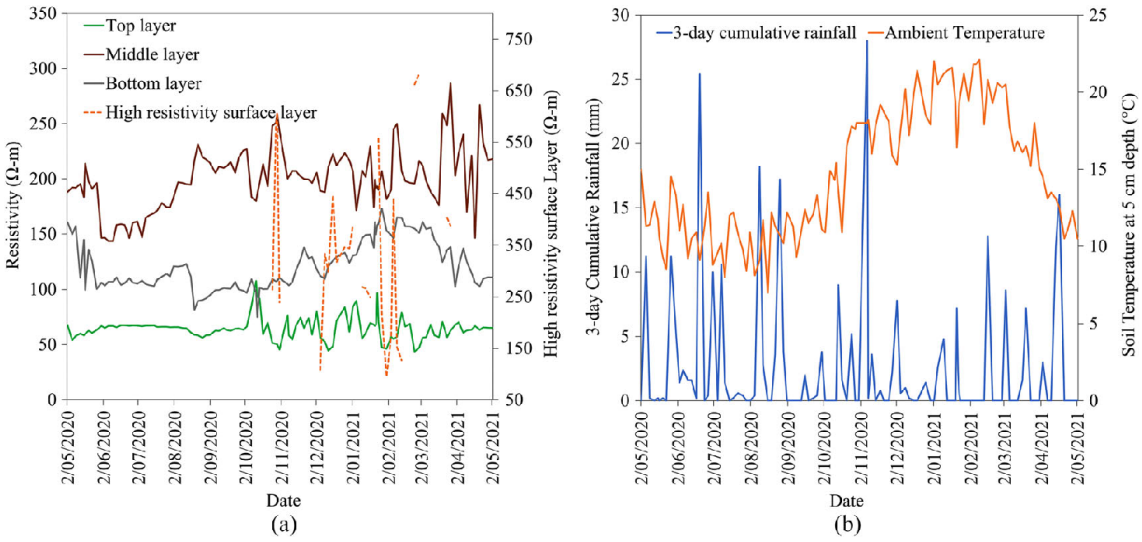

Figure 4-13 The Twelve-month soil resistivity model (a) and the 3-day cumulative rainfall and soil temperature measured at 10 cm below ground level(b).

4.4.3 Adjusted Soil Resistivity Model

The warm-starting soil resistivity modelling method has shown to be superior in enhancing the accuracy and representativeness of the models, as demonstrated in the previous section. Therefore, the soil resistivity model profile was reconfigured with controlled initial values to ensure reliable acquisition of touch voltages and their corresponding limits from the system modelling in Chapter 5.

The adjusted soil resistivity profile showed that the average depth of the bottom layer began at 2.07 m (σ = 0.46 m, a maximum depth of 3.20 m, and a minimum depth of 1.61 m). This result contrasted with the soil resistivity model in the initial run, which had an average depth of 2.07 m (σ = 0.83 m, a maximum depth of 6.32 m, and a minimum depth of 0.95 m). The reduced standard deviation and the narrower range of depths in the improved soil resistivity profile suggested that a more consistent and reliable representation of the soil's characteristics could be obtained using the warm-starting soil resistivity modelling method.

Furthermore, the data inversion's root mean square (RMS) errors also demonstrated that the modelling accuracy could be enhanced through the warm-starting soil resistivity modelling method. The average RMS errors were 4.68% (with σ = 3.0%, a maximum error of 13.5%, and a minimum error of 1.4%) for the uncontrolled method and 3.16% (with σ = 1.0%, a maximum error of 7.1%, and a minimum error of 0.5%) for the warm-starting method. This improvement in accuracy is crucial for ensuring the reliability of touch voltage assessments and safety considerations in the subsequent stages of the study.

4.4.4 High Resistivity Surface Layer

The twelve-month soil resistivity model profile showed that a part of the top resistivity layer of the soil resistivity model in the middle of October 2020 turned into a high resistivity layer with a maximum value of 606.77/0.38 Ω·m/m, as shown in Figure 4-13 (a). Additionally, Figure 4-13 (b) indicates that this high resistivity surface layer exhibited a high sensitivity to rainfall, particularly when the ambient temperature exceeded 18°C.

The Wenner measurement conducted on 31/10/2020, taken before the onset of rain, confirmed the presence of the high-resistivity surface layer. However, the subsequent measurement on 3/11/2020 found that the high-resistivity layer had diminished after a 7.2-mm rainfall event in 24 hours on 31/10/2020. This phenomenon recurred between January and February 2021.

The sudden change in the unstable high-resistivity top layer could significantly impact the safety of touch voltages, as the tolerable touch voltage decreased critically when the high-resistivity layer diminished. The following chapter will further investigate this safety concern using system model simulation.

4.5 Summary of the Twelve-month Soil Resistivity Monitoring

The successful identification of the test traverse laid the foundation for the creation of the soil resistivity model. However, the dynamic nature of soil resistivity over time presented challenges in constructing an accurate model. To address this, a warm-starting technique was applied to improve the data inversion process, ensuring that the soil resistivity model could maintain continuity and reflected realistic changes over the year.

The warm-starting technique leveraged parameters from previous soil resistivity models as starting points for subsequent inversions, providing a more accurate representation of the soil's electrical characteristics. This method allowed for the creation of a more reliable soil resistivity profile, which was critical in accurately predicting touch voltage hazards. Additionally, a four-layer model was adopted to account for the observed variations in soil resistivity during dry conditions, further improving the model's ability to simulate real-world conditions.

By refining the soil resistivity model in this manner, the study not only addressed the first research question but also set the stage for more accurate touch voltage hazard predictions, which are detailed in the following sections.

The comprehensive dataset, which includes soil resistivity measurements and the corresponding multilayer soil resistivity model, is thoroughly documented in Appendix B. These resources

provide a detailed explanation of soil resistivity's complex and dynamic behaviour throughout the year-long monitoring period.

Industrial practices, as referenced in [2, 5], often recommend using average values of soil resistivity and worst-case scenarios for different situations. This approach helps mitigate the impact of seasonal variations in soil resistivity by creating a conservative soil resistivity model representing the soil's characteristics across all seasons. However, this case study has demonstrated that long-term soil resistivity monitoring offers valuable insights into progressive changes in soil resistivity during specific seasons. For instance, it highlighted the critical change in soil resistivity models from a 3-layer to a 4-layer model during the hot summer.

Soil monitoring contributes to the knowledge needed to develop skills in handling continuously varying soil resistivity modelling. Furthermore, these findings have the potential to challenge the commonly recognized notion of a 'safe season' based on the assumption that surface soil resistivity is usually high during the summer.

In Chapter 5, the multilayer soil resistivity profile will be integrated into a pipeline-transmission line model simulation to calculate the touch voltage profile over the monitoring period. The system simulation results will identify the touch voltage hazards, and the existence of a "safe season" or its absence will be explored further.

Chapter 5 - Pipeline-Transmission Line System Modelling

5.1 The components of the system model

The system modelling used a pipeline-transmission line shared corridor situation similar to the data collection site to investigate the touch voltage hazards on a hypothetical cathodic protection (CP) system. The investigation focused on cases where pipeline maintenance and electrical fault events coincided within a pipeline and transmission-line corridor. While the system model was purely hypothetical, it was carefully designed to emulate the real-world conditions and challenges frequently encountered in environments where pipelines and electrical transmission lines intersect.

5.1.1 The Transmission Lines Understudy

The prospective fault current is the maximum current that could flow through a circuit in the event of a fault, whether it is a short circuit between phases or a single line to earth fault. This current level represents the highest possible magnitude under fault conditions and holds significant importance in designing an earth grid and the protection setting for a substation.

On the other hand, the configuration of the fault circuit determines how a fault can impact the electrical safety of the surrounding structures and facilities. For instance, if a single line-to-earth fault occurs within a Grid Injection Point (GIP) substation, the fault current will be confined to circulating between the substation's earth grid and the star point of the transformer that supplies power to the fault circuit. However, this changes if the fault circuit is supplied by more than one source, and one of these sources is located outside the GIP substation's earth grid. In such a case, a portion of the fault current supplied by the other source will flow into the earth and return to its source. Therefore, when calculating the prospective fault current, all possible fault sources need to be accurately assessed.

As per the information from the transmission system operator, two 220 kV circuits, OTA-WKM-1 and OTA-WKM-2, are located in close proximity to the test site. Each of these circuits was designed with a capacity to deliver a minimum of 426.78 MW per circuit, as specified in the

Transpower Excel spreadsheet [92]. They originate from Whakamaru (WKM) Substation B, which functions as a Grid Injection Point (GIP) substation located near the WKM Hydroelectric Power Station. These circuits extend all the way to Otahuhu (OTA) Substation, a major substation situated in Auckland. The electricity generated at the WKM Hydroelectric Power Station combines with ATI-WKM-1 at the WKM Substation and is then transmitted to Auckland through OTA-WKM-1, as shown in Figure 5-1. The distance between these two substations is approximately 190 km. This configuration provides an overview of the power transmission infrastructure in the area and its proximity to the test site.

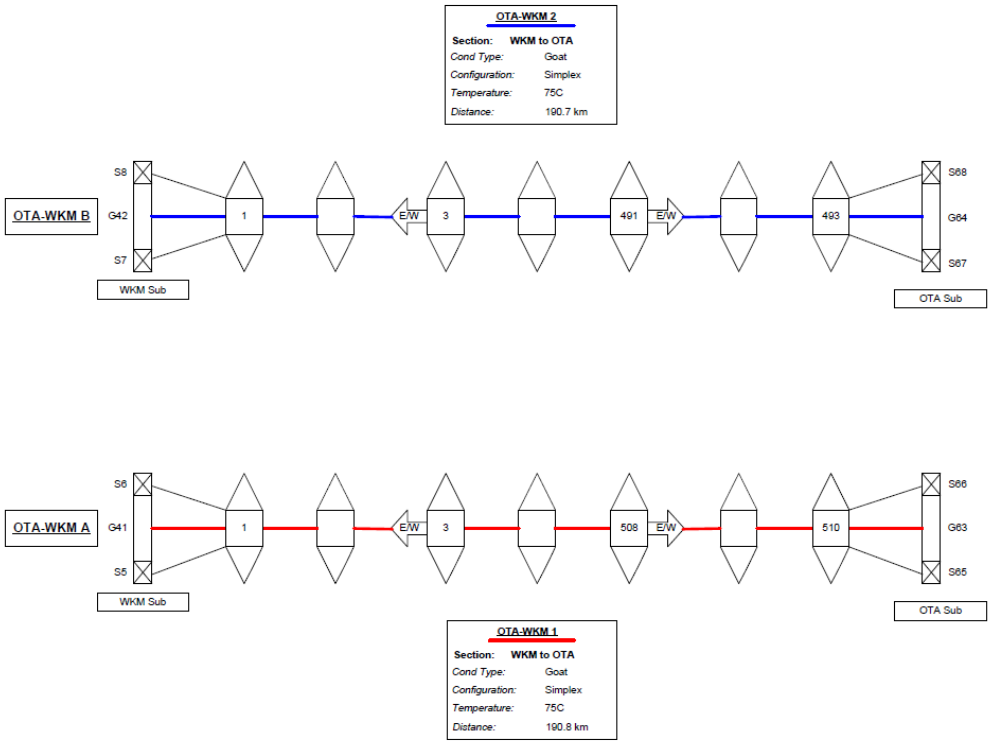

Figure 5-1 The line asset drawing was downloaded from the transmission system operator [93], showing the transmission lines situated near the test site.

5.1.2 The Prospective Fault Current

A line fault is a fault on a transmission tower outside the substation. In this case, a phase conductor is shorted to the transmission tower structure outside the substation's earth grid. The resulting fault current flows into the natural ground through the tower footings and then returns to the

substation where the source is. Since the footing resistance is much higher than the full-scale substation's earth system resistance, the fault location that will discharge the highest earth current is considered to be within the Grid Exit Point (GXP) substation's earth grid.

When a single line-to-earth OTA substation, the earth return current would pass through the test site, resulting in EPR and pose electrical safety concerns for the gas pipeline at the test site.

The prospective fault current resulting from a single line-to-earth fault appearing at the OTA Substation was simulated using the DIgSILENT PowerFactory with the transmission system model [85] provided by the Electricity Authority [94]. The single line-to-earth fault on the circuit OTA-WKM-1 at the OTA Substation was simulated to be 8.68 kA, as shown in Figure 5-2. This fault current represents a composite of electricity generated from both the Aratiatia (ATI) Power Station and the WKM Hydroelectric Power Station.

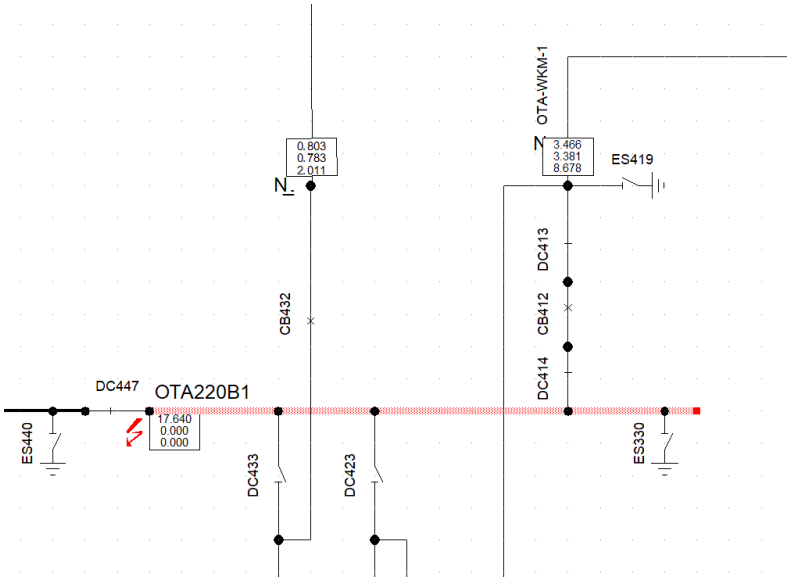

Figure 5-2 The simulation of a line-to-earth fault condition of the OTA-WKM-1 circuit at the OTA substation. Simulation of a single line-to-earth fault condition using the transmission system model [81].

5.1.3 Clarification on Layout Discrepancy

The layout shown in Figure 4-1, where the transmission line crosses over the gas pipeline, differs from the simulated model**.** This difference arises because the system model used in the study is hypothetical and was designed to demonstrate the effects of seasonal soil resistivity variations on touch voltage hazards, rather than to replicate a specific real-world site.

The sponsor provided a pipeline model for an undisclosed location, and at the time of simulation development, the exact site layout was not a primary consideration. The transmission line was positioned almost parallel to the pipeline in the model to facilitate a clear analysis of touch voltage risks under changing soil resistivity conditions throughout the year. Additionally, confirmation of the gas pipeline's presence at the actual site occurred late in the research, meaning the real-world layout could not be incorporated before simulations were conducted.

While differences in layout may affect certain proximity-related aspects, they do not impact the study's core objective: evaluating how seasonal soil resistivity variations influence touch voltage hazards. The hypothetical system model remains valid for illustrating these effects.

5.1.4 The Construction of the System Model

The system model was constructed using HiFreq of CDEGS [17] and comprised the following components:

- A 10-km-long 220 kV AC transmission line, with each phase suspended at 18 m above the ground and a 10 m separation between phases.
- A 500-m-long electrically insulated mild steel gas pipeline featuring an outer diameter of 1 m and a thickness of 1.5 cm. This gas pipeline is buried at a depth of 2 m and runs parallel to the transmission line, with a separation distance of 20 m.
- A hypothetical zinc anode bed has been buried at 30 m from the gas pipeline. This anode is connected to a cathodic protection (CP) rectifier via an insulated cable.

The fault scenario for the Hi-Freq simulation was assumed to have occurred at a substation located 5 km away from the CP rectifier, which is situated at the midpoint of the shared corridor. According to the previously calculated prospective single-phase-to-earth fault current for OTA-

WKM-1 of approximately 9 kA is injected into the ground from one end of the transmission line to simulate a fault current discharged into the ground.

5.1.5 Incorporating the Soil Resistivity Variation in the System Model

In order to evaluate how changes in soil conditions affect the pipeline and determine the touch voltages, the soil resistivity parameters based on the soil resistivity model profile obtained through the process discussed in the previous section are entered into the HIFREQ soil type interface, as shown in Figure 5-3. Based on the system model, simulation under these variable soil conditions allowed for the generation of both a touch voltage profile and a tolerable touch voltage profile. Therefore, both the soil resistivity model and the touch voltage profiles will serve as the basis for developing a statistical method to improve the accuracy of the risk assessment.

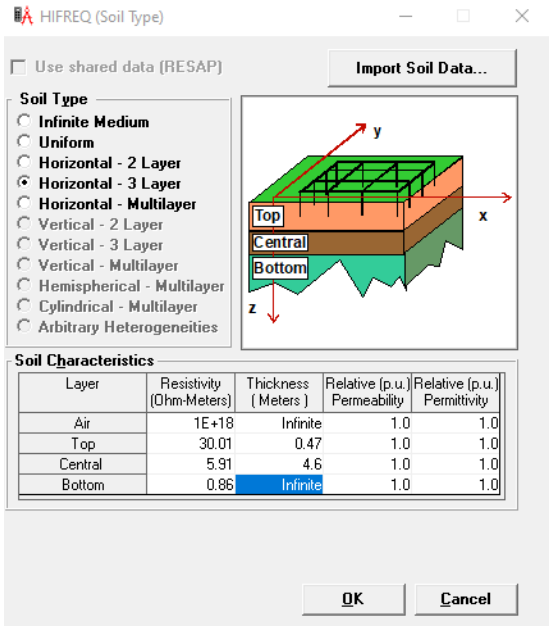

Figure 5-3 An example of soil resistivity input for HiFreq of CDEGS

5.2 Developing Touch Voltage Profile

The touch voltages could be computed and presented in a "Spot 2D" plot, which visually represents touch voltage distribution along the pipeline. An illustrative example of the touch voltage results, as shown in Figure 5-4, demonstrated that the highest touch voltage was observed at the location of the CP rectifier, reaching 257.06 V. On the other hand, the touch voltages at the

sacrificial Zinc anode bed were below 26.04 V. The touch voltages posed hazards if they exceeded the calculated limit using (12). In this example, a primary protection time was 0.2 s, a surface layer derating factor was conservatively set at 1, and a surface soil resistivity of 250 Ω-m was assumed. Given these parameters, the calculated tolerable touch voltage was determined to be 152.65 V. Therefore, the touch voltages observed at the CP rectifier as shown in Figure 5-4 are hazardous, with the touch voltage exceeding the limit by 104.41 V.

The touch voltage profiles can be obtained by repeating the same process using the soil resistivity models acquired from the twelve-month soil resistivity monitoring. Each simulation employs one of the soil resistivity models in the soil resistivity model profile to generate touch voltage profiles for various soil conditions corresponding to different times of the soil monitoring period. The touch voltage profiles, along with the tolerable touch voltage levels, constitute critical data inputs for developing a statistical method to enhance the accuracy of hazard identification and probabilistic risk analysis in the next section.

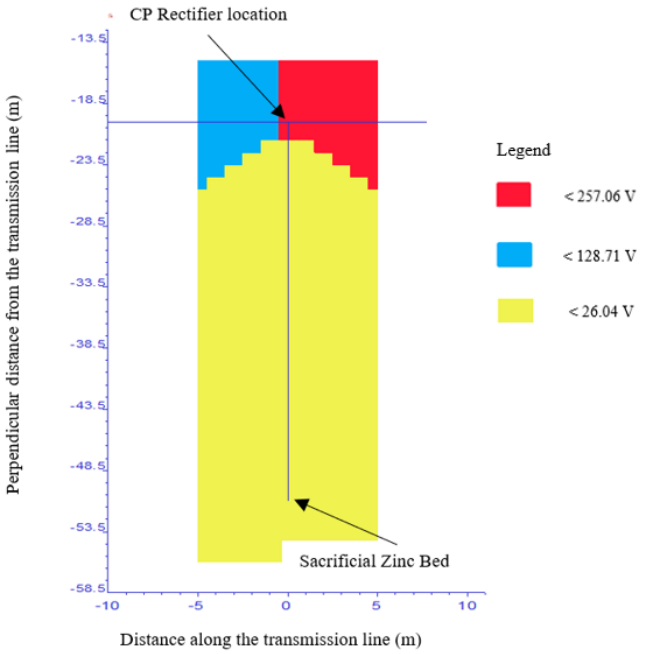

Figure 5-4 The simulation result of touch voltages around the pipeline and sacrificial Zinc anode bed

5.2.1 Touch Voltage Hazards Over the Monitoring Period

The twelve-month soil resistivity monitoring has revealed fluctuations in soil resistivity, indicating the dynamic response of touch voltages over time. This finding suggests that touch voltages can vary in response to changing soil conditions throughout the year. Another significant finding was that the evident time-varying nature of touch voltage magnitudes could only be shown with higher-resolution soil resistivity data over a long period of soil resistivity monitoring. This observation highlighted that the electrical properties of the earth, particularly soil resistivity, significantly influence the conditions that allow the touch voltage to become hazardous.

5.2.2 Touch Voltage Before and After the Decoupling of the Pipeline Earthing System

During normal operation, the pipeline is bonded to the earthing system to ensure the cathodic protection (CP) system functions correctly. However, when carrying out the performance test of the CP system, the pipeline must be decoupled from the earthing system to allow the measurement to be done correctly. This decoupling was hypothesised to cause an increase in touch voltage. Therefore, to confirm this phenomenon, the system model simulation conducted on 2/01/2021, with a fault level of 9 kA, resulted in the highest touch voltage of 288.38 has been revisited. A 2 m long copper rod was buried vertically into the ground where the pipeline was connected to the junction of the CP to resemble the normal pipeline operation, as shown in Figure 5-6. When the pipeline was bonded to the earth, the simulation showed a touch voltage of 63.04 V at the same location where the highest touch voltage was previously observed, as shown in Figure 5-5.

This substantial difference in touch voltage indicated that potentially hazardous situations could exist depending on factors such as the fault level magnitude and the resistivity of the surface soil. These concerns will be explored and discussed in more detail in the next section.

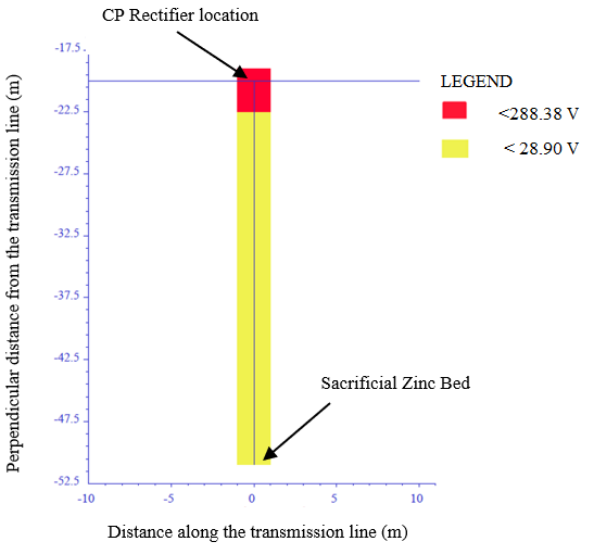

Figure 5-5 The system model simulation for the soil resistivity on 2/01/2021. The pipeline was decoupled from the 2 m long copper earth rod. The maximum touch voltage of 288.38 V was found in the CP connection to the pipeline.

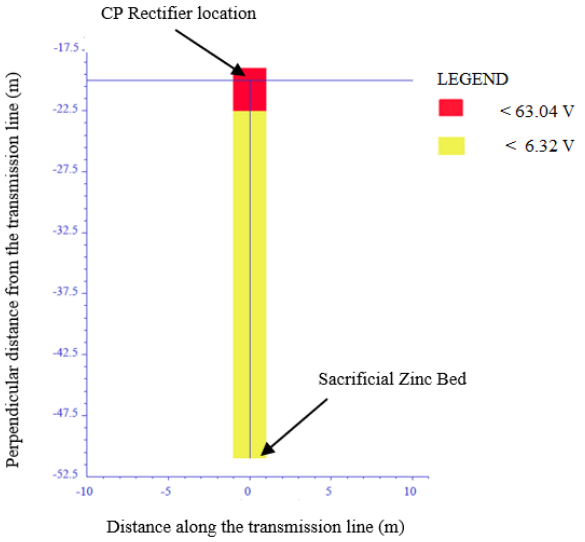

Figure 5-6 The system model simulation revisited for the soil resistivity on 2/01/2021. The pipeline was connected to the 2 m long copper earth rod. The maximum touch voltage of 63.04 V was found in the CP connection to the pipeline.

5.2.3 Simulation Results Under Different Fault Levels

Using the transmission system settings, a 9 kA fault was initially simulated. The results indicated no touch voltage hazards along the pipeline. To assess the impact of potential future upgrades in electricity demand, the fault level was increased. This adjustment demonstrated that the pipeline could remain free from touch voltage hazards even if the fault level were raised to 12.5 kA, as shown in Figure 5-7. The detailed simulation results, including touch voltage calculations under these fault levels, are presented in Table E-1.

The system model simulated the maximum touch voltages occurring on the gas pipeline. These touch voltages were found to exhibit correlations with both soil temperature and the resistivity of the bottom soil layer. The simulations indicated that touch voltage hazards were likely to occur during the summer when the fault level reached 13 kA. This phenomenon was primarily due to the high resistivity of the bottom soil layer, which resulted in more current conducted into the metallic pipeline, which is less resistive than the dry soil. It resulted in higher touch voltage magnitudes on the pipeline.

On the other hand, summer rain effectively reduced the resistivity of the surface soil and the tolerable touch voltage levels. Consequently, the likelihood of touch voltage hazards occurring in

the summer was high. This discovery challenges the common belief that touch voltage hazards were unlikely to manifest during seasons with low precipitation.

Of particular significance was the observation that once the fault level exceeded 13 kA, touch voltage hazards began to appear at the end of the summer season. This observation highlights that accommodating the increasing electricity demand required an adjustment to higher fault level settings, which, in turn, could introduce touch voltage hazards onto the pipeline that were not previously present. The conventional industrial practice of selecting a random day for soil resistivity measurement or conducting current injection tests, as outlined in IEEE Std 80 [2], may likely miss out on detecting touch voltage hazards.

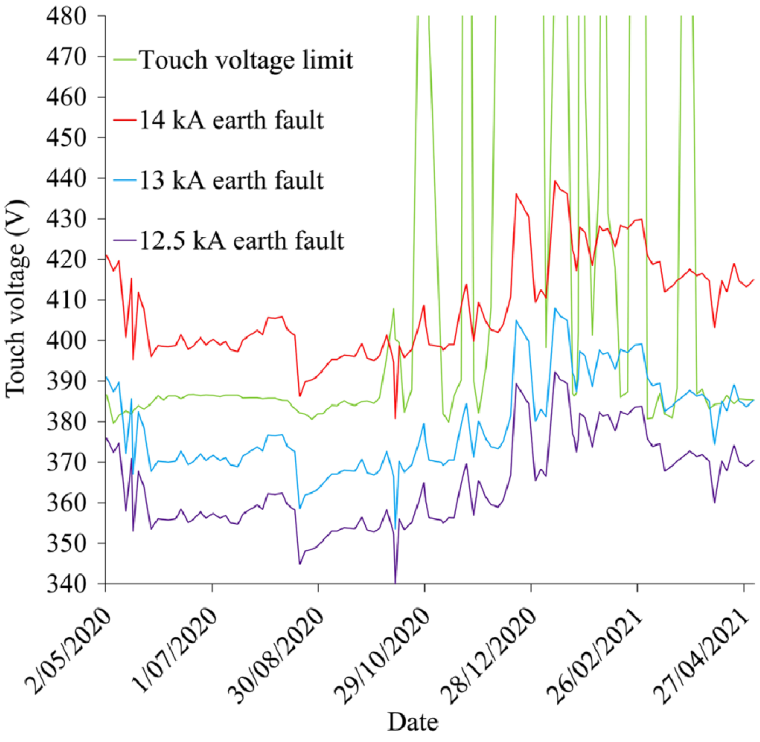

Figure 5-7 The pipeline-transmission line system model simulation in different earth fault levels is plotted. The fault level below 12.5 kA would not incur any hazardous touch voltage onto the pipeline. Note: the touch voltage limit profile is clipped to allow other variables to be clearly seen.

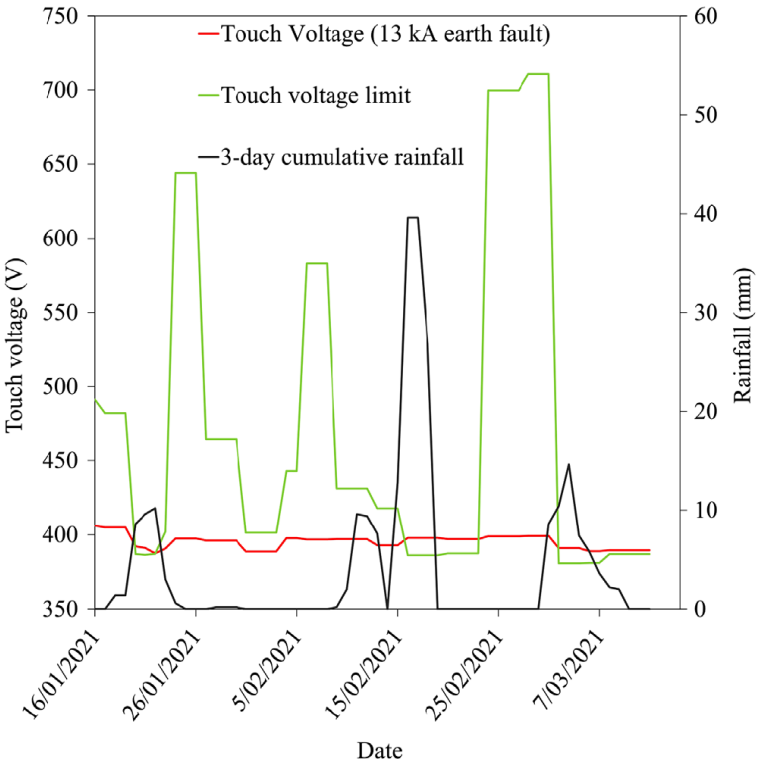

Figure 5-8 Hazardous touch voltages were identified after rain in the summer season.

The magnitude of the touch voltages between January and March 2021, as shown in the exploded view in Figure 5-8, demonstrated that the touch voltages were relatively stable. However, the hazards were closely linked to the sudden reduction in tolerable touch voltage limits due to rainfall.

Given that the local soil composition contains lithic volcanic sandstone rich in calcium carbonate [32], which reacts with rainwater to form a conductive calcium bicarbonate solution, it becomes evident that the high resistivity of the dried soil in the test site was highly sensitive to rainfall. Rainwater could quickly infiltrate the top layer of soil, dispersing the high resistivity layer and causing the tolerable touch voltage to drop critically. This circumstance gives rise to a scenario characterised by a high magnitude of touch voltage and a low tolerable touch voltage, typically occurring shortly after rainfall during the dry summer season. These coincidental factors implied that touch voltage hazards were more likely to occur during the dry summer, contrary to conventional expectations.

On the other hand, the average magnitude of the touch voltage in the summer remained relatively high because the pipeline became an alternative low-resistance path to conduct fault currents. When significant rainfall allowed moisture to penetrate deeper into the ground, the overall soil became more conductive. Therefore, less fault current would split into the pipeline to ease the touch voltage hazards concern. Therefore, the simulation showed no hazardous touch voltages during the rainy season for the earth fault of 13 kA.

The fault level for the touch voltage simulation was further increased to 14 kA to observe the impact of rainfall on touch voltages and its implications for electrical safety during pipeline maintenance. As shown in Figure 5-7, the touch voltages and the corresponding limits that affected the pipeline safety could be divided into two distinct periods. When the soil temperature was low and subjected to frequent rainfall was recorded in the winter from May to October 2020, the touch voltages were consistently higher than the corresponding touch voltage limit. The summer began from the middle of October 2020 to the end of March 2021. Both touch voltage and tolerable touch voltage were significantly higher in the summer than in winter. Table 6.1 provides greater clarity, indicating that the average tolerable touch voltage of 562.45 V was lower than the average touch voltage of 449.37 V. This observation seemed to align with the general industrial practice, which recognised that touch voltage hazards were less likely to occur during dry seasons. The rationale behind this assumption lay in forming a high resistivity layer developed near the surface during the dry summer period, which could effectively elevate the tolerable touch voltages, creating a safety buffer.

However, the standard deviation of the tolerable touch voltage of 417.27 V indicated a higher degree of variability or uncertainty in the tolerable touch voltage data. This outcome also suggested that relying solely on the average value can potentially lead to an underestimation of the hazards and may impact the interpretation and analysis of the data.

Table 5-1 The average touch voltage and the limit for two distinctive soil conditions of the test site with standard deviation σ.

Period	Average Touch voltage and σ (V, V)	Average tolerable touch voltage and σ (V, V)
2/05/2020 - 16/12/2020	421.53, 16.21	336.42, 103.30
17/12/2020 - 31/03/2021	449.73, 10.88	562.45, 417.27

5.2.4 Identifying the Number of Hazardous Days for Statistical Analysis

The previous sections established that touch voltage hazards arise under specific weather and fault conditions. To quantify the frequency of these hazards, a dataset has been generated based on simulated fault conditions. The number of hazardous days is identified by evaluating the touch voltage profile over a 12-month period while accounting for seasonal variations in soil resistivity.

To illustrate the relationship between earth fault levels and the occurrence of hazardous days, Table 5-2 presents the simulated earth fault levels, and the corresponding number of hazardous days recorded within a year. This dataset provides essential input for refining probabilistic risk assessment and improving risk quantification in the following chapter, helping to improve the accuracy of the existing probabilistic risk assessment approach.

Table 5-2 Simulated Earth Fault Levels and Corresponding Number of Hazardous Days per year.

Simulated earth fault level (kA)	Number of hazardous days *n* (day)
12.5	0
13.0	75
13.5	136
14.0	274
14.5	290
15.0	291
15.5	298
16.0	306
16.5	306

5.3 Summary of the System Modelling

Through the pipeline-transmission line system modelling, the twelve-month soil resistivity monitoring revealed the time-dependent nature of touch voltage magnitudes, highlighting the substantial influence of soil resistivity on touch voltage hazards. Ideally, daily data collection would have been conducted, but a twice-weekly data collection schedule was implemented to meet budget constraints. Consequently, when touch voltage hazards were identified through system model simulations, the days preceding the next measurement were treated as potentially hazardous. This level of data resolution is deemed sufficient for calculating the Probability Reduction Factor (*PRF*) in the following chapter and supports the concept of a pilot study.

Simulation results from the hypothetical case, under varying fault levels, provided further insights. At a 9 kA fault level, no touch voltage hazards were observed along the pipeline. At 12.5 kA, the pipeline remained hazard-free, while at 13 kA, touch voltage hazards were more likely to occur, particularly following rainfall events.

Soil composition and physical characteristics vary by location, so the findings of this study are specific to the local soil conditions within the shared corridor. Nonetheless, these results highlight the importance of regular soil resistivity monitoring to improve hazard identification, especially in areas with higher risks for pipelines or electrical infrastructure.

Additionally, this study introduced the new variable "hazardous days per year," which is sensitive to fault levels. This variable is critical in the next chapter, where it will be applied to develop the *PRF*.

Chapter 6 - A Novel Statistical Framework for Touch Voltage Risk Analysis

6.1 Introduction

Risk assessment in electrical safety, particularly for systems involving pipelines and transmission lines, requires a robust methodology that accounts for both deterministic and probabilistic approaches. Deterministic models effectively analyse worst-case scenarios but fail to capture real-world variability. Probabilistic risk assessment offers a more flexible approach by incorporating uncertainties, making it suitable for evaluating touch voltage risks during pipeline maintenance.

Existing risk assessment methods, as outlined in Section 3.4.6, primarily consider contact scenarios and fault duration but overlook environmental factors such as soil resistivity variations. These variations can influence touch voltage levels, potentially reducing risk below hazardous thresholds. A more refined approach is required to account for these dynamic factors and improve the accuracy of risk quantification.

To address this gap, a novel statistical framework based on the binomial distribution to model touch voltage hazards is introduced. A new metric, the probability reduction factor (*PRF*), is developed to incorporate the temporal distribution of hazards and refine probabilistic risk calculations. This approach ensures a more realistic assessment of risk, aligning with industry safety standards and the ALARP principle [12].

6.2 The Concept of Binomial Distribution

A binomial distribution describes the probability distribution of a discrete random variable with binary outcomes, such as true or false, present or absence, and head or tail [95]. The binomial distribution of a discrete random variable takes on values between 0 and 1, maps each possible binary outcome to its probability of occurrence and the sum of all the probabilities must equal 1. For example, an experiment is to map the outcomes of flipping a coin ten times. Assuming that the coin is fair (i.e., the probabilities of getting heads and tails from a fair coin flip are p = 0.5 and

1 – 0.5, respectively), the binomial distribution can be expressed using the probability mass function given by (28):

$$f(x,y) = (x\ y) \cdot p^{y} \cdot (1-p)^{(x-y)} \tag{28}$$

where,

x is the total number of independent coin flips,

y is the number of heads observed, taking values from 0 to x, and

$(x\ y)$ the binomial coefficient gives the number of ways to choose y heads from x flips.

The binomial coefficient can be expressed in mathematical form as (29).

$$(x\ y) = \frac{x!}{y!\,(x-y)!} \tag{29}$$

The binomial distribution can be computed using (29) for each possible value of y as follows:

$$f(10,0) = \frac{10!}{0!(10-0)!} \cdot 0.5^{0} \cdot (1-0.5)^{(10-0)} = 0.000977$$

$$f(10,1) = \frac{10!}{1!(10-1)!} \cdot 0.5^{1} \cdot (1-0.5)^{(10-1)} = 0.00977$$

$$f(10,2) = \frac{10!}{2!(10-2)!} \cdot 0.5^{2} \cdot (1-0.5)^{(10-2)} = 0.0439$$

$$\vdots$$

$$f(10,10) = 0.000977$$

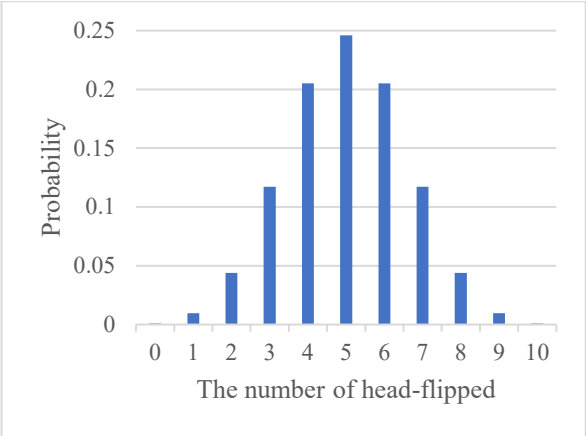

Figure 6-1 The binomial distribution of getting heads in ten fair coin flips.

The binomial distribution of getting head flipped in 10-coin flips is plotted in a bar chart in Figure 6-1. The shape of the plot is a symmetrical bell-shaped or Gaussian curve. The probability of getting 0 or 10 heads is the lowest among the other flipped heads.

6.3 Probability Reduction Factor

To transform the game of head and tail to study the daily probability of touch voltage hazards, suppose the "head" in the previous example is replaced by the "hazardous day" where the touch voltage hazards can occur. In that case, the calculation can be understood as the probability that the worker is exposed to the touch voltage hazard on a random day on-site or the probability of working on a hazardous day.

This probability represents an unfair chance of working on a hazardous day per visit and must be calculated before the binomial distribution is applied to the touch voltage hazard. Hence, it is hypothesised that touch voltage hazards may not exist daily. The system model simulation will prove that this hypothesis is sustained. Therefore, a soil resistivity field test must be conducted to identify when touch voltages can occur on various days of the year. Then, this historical information is used to compute the annualised probability Xi - ξ of a hazardous day based on the number of days identified as hazardous *n* as Expressed in (30).

$$\xi = \frac{n}{365} \tag{30}$$

Hence, the annualised probability ξ of a hazardous day in (30) represents the probability of an independent random single-day trip to work on-site under the threat of a hazardous touch voltage. Alternatively, the probability of working on a safe day is $1 - \xi$.

For an annual maintenance task that requires x days to complete, the probability of allocating the maintenance on all hazardous days is ξ^x. Any allocated day containing a touch voltage hazard contributes to the touch voltage risk in the job allocation. Therefore, the number of possible arrangements to observe y hazardous days on-site out of x days can be expressed by $C(x, y)$, given in (29), the probability of y hazardous days (given by ξ^y) and the probability of $x - y$ safe days (given by $(1 - \xi)^{x-y}$) can be re-written as (31).

$$f(x, y) = C(x, y)\, \xi^y\, (1 - \xi)^{x-y} \tag{31}$$

The risk of the maintenance plan is expressed in terms of the sum of the probability of each planned working day, which is calculated using (32). For the maintenance is required *x* days to complete, the binomial distribution function is expressed from *y = 1* to *y = x* and is shown below:

$$F(x, y) = f(x, y) + f(x, y - 1) + f(x, y - 2) + \cdots + f(x, 1)$$

$$F(x, y) = C(x, y)\, \xi^y + C(x, y - 1)\, \xi^{y-1}\, (1 - \xi) + C(x, y - 2)\, \xi^{y-2}\, (1 - \xi)^2 + \cdots + C(x, 1)\, \xi\, (1 - \xi)^{x-1}$$

$$F(x, y) = \sum_{y=1}^{x} C(x, y)\, \xi^y\, (1 - \xi)^{x-y} \tag{32}$$

Instead of summing all the probabilities of all the outcomes that can yield at least one hazardous day, alternatively, the total probability of working regardless on a safe or hazardous day is 1. Therefore, the complement rule can be applied to find the probability of working on multiple days with at least one day can surrogate the hazardous touch voltage. Firstly, the probability of working on all safe days is calculated and then subtracted that probability from 1 to get the probability of getting at least one hazardous day. In the context of assessing a maintenance work plan, $F(x, y)$ represents the probability of the planned maintenance that is hazardous. Since the sum of all the probabilities must equal 1, $F(x, y)$ can be re-written based on this property as below:

$$F(x,y) = 1 - f(x,0)$$

$$F(x,y) = 1 - (1 - \xi)^x$$

Since the binomial distribution is independent of y, it can be re-written as (33).

$$F(x) = 1 - (1 - \xi)^x \tag{33}$$

The outcome of (33) is used as a *PRF*, allowing for the seasonal variation of the soil resistivity. For a seven-day working plan at a touch voltage-affected site, the *PRF* can be evaluated according to the number of working days and the annualised probability ξ. By incorporating the *PRF*, the conservatism of the coincidence probabilistic assumptions in Subsection 2.5.1 can be reduced to levels close to reality.

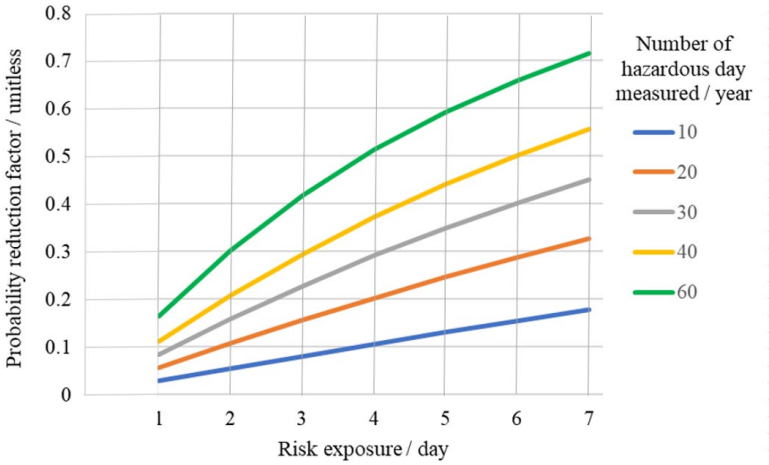

Figure 6-2 The plot of the probability reduction factor under the influence of the number of hazardous days measured per year and the risk exposure days.

6.4 Probabilistic Risk Calculation Using Touch Voltage Hazard Assessment

The present probabilistic risk is calculated based on the coincidence probability of fault and contact. The probability of heart fibrillation caused by touch voltages can be realised by conducting soil measurements for each day and evaluating the touch voltage profile through computer simulation. The binary outcomes of "safe" and "hazardous" within the observation period can dynamically quantify the probability of touch voltage hazards according to the job plan using the binomial distribution. By considering these probabilities together, $F(x)$ contains the information on the touch voltage hazard and can be used as a probability reduction factor to improve the accuracy of the existing probabilistic risk calculation. Therefore, the specific multiplication rule [95] of two independent probabilistic distributions, A and B, can be applied to calculate the joint probability of them written as (34) as follows:

$$P(A \,\&\, B) = P(A) \cdot P(B) \tag{34}$$

In this case, the coincidence probability P_{conc} and the binomial distribution of the touch voltage hazards in the job plan occurring together and the adjusted probability of fatality, P'_{conc} is given by (35).

$$P'_{conc} = F(x) \cdot P_{conc} \tag{35}$$

Since the *PRF* is not a constant value and is dependent on the number of working days x and operational conditions, such as the fault level, the binomial distribution $F(x)$ can be considered as a probability reduction factor that can help to adjust for these control parameters and provide a more accurate and dynamical prediction of the overall probability of hazards for the ALARP principle.

6.5 Validation of the Probability Reduction Factor (*PRF*)

This section presents the application of the *PRF* using the touch voltage profile derived from the hypothetical case study. The validation method relies on 12-month soil resistivity monitoring, previously described in Chapter 5 to develop the touch voltage profile.

6.5.1 Probabilistic Risk-based Model

The probabilistic risk-based model based on the Poisson distribution described in Section 2.5 was used to evaluate the fatality rate due to touch voltage hazards. The interaction of two contact scenarios contributing to the fatality risk is summarised in (*27*). The data required for the calculation are as follows:

- Occurrence of a fault u_A = 9 count/year
- Mean duration of each fault t_A = 0.2 s = 6.35 × 10^{-9} year
- Number of human contacts u_B = 10 count/year
- Mean duration of each human contact t_B = 60 s =1.90 × 10^{-6} year

$$P_{conc} = 9 \times 10\ (6.35\ \times\ 10^{-9} +\ 1.90\ \times 10^{-6})$$

$$P_{conc} =\ \ 1.72\ \times 10^{-4}$$

This probability was considered valid under the assumption that all feasible hazard mitigation measures had been implemented, available resources were optimally utilised to minimise risk, and no further improvements were viable at the time of assessment.

6.5.2 Probability Reduction Factor for Touch Voltage Hazards

The touch voltage results from system modelling, considering fault levels exceeding 12.5 kA, indicated that touch voltage hazards were present under certain conditions. This observation suggests that the actual coincidental probability of fatality should be lower than the previously calculated value in the earlier section.

The touch voltage profile enables the identification of the number of hazardous days within a year, which is a crucial factor in refining the risk assessment. The annualised probability ξ of hazardous days is calculated using (*30*) and presented in Table 6-1.

Table 6-1 Annualised Probability of a Hazardous Day Under Different Fault Levels.

Simulated earth fault level (kA)	Annualised Probability ξ
12.5	0
13	0.21
13.5	0.37
14	0.75
14.5	0.79
15	0.8
15.5	0.82
16	0.84
16.5	0.84

The annualised probabilities of hazardous days from Table 6.1, along with (*33*) were used to evaluate the *PRF* for different fault levels and exposure days. These results, presented in Table 6-2, enhance the accuracy of probabilistic risk assessment.

Table 6-2 Binomial distribution of different fault levels and number of planned working days within a year.

	Fault levels (kA)								
Number of workdays (day)	12.5	13.0	13.5	14.0	14.5	15.0	15.5	16.0	16.5
1	0.0	0.2	0.4	0.8	0.8	0.8	0.8	0.8	0.8
2	0.0	0.4	0.6	0.9	1.0	1.0	1.0	1.0	1.0
3	0.0	0.5	0.7	1.0	1.0	1.0	1.0	1.0	1.0
4	0.0	0.6	0.8	1.0	1.0	1.0	1.0	1.0	1.0
5	0.0	0.7	0.9	1.0	1.0	1.0	1.0	1.0	1.0
6	0.0	0.8	0.9	1.0	1.0	1.0	1.0	1.0	1.0
7	0.0	0.8	1.0	1.0	1.0	1.0	1.0	1.0	1.0
8	0.0	0.8	1.0	1.0	1.0	1.0	1.0	1.0	1.0
9	0.0	0.9	1.0	1.0	1.0	1.0	1.0	1.0	1.0
10	0.0	0.9	1.0	1.0	1.0	1.0	1.0	1.0	1.0

The *PRF* was organized as an array with indices representing fault levels and the number of workdays as shown in Table 6-2. In this case, the fault level of 12.5 kA served as the safety

boundary, yielding a *PRF* of 0.0, since system modeling indicated that the touch voltage on the pipeline did not reach hazardous levels.

The 3-D plot of the *PRF* in Figure 6-3 allows pipeline asset operators to identify a fault level threshold (e.g., 12.5 kA in this case) that ensures human safety during maintenance. For fault levels exceeding 14.5 kA, the *PRF* demonstrated a 20% reduction in the coincidental probability of fatality, provided maintenance tasks were completed within one day. If the work plan required more than one day, alternative safety measures would be necessary.

Thus, the ability to visualize risk boundaries is essential for coordinating maintenance operations with electricity grid operators. This coordination enables pipeline operators to request temporary reductions in fault current levels during maintenance, eliminating touch voltage hazards. The *PRF* provides pipeline operators with a clear understanding of safe operating boundaries, allowing them to take an active role in coordination meetings, make informed decisions, and negotiate risk mitigation strategies with power grid operators. This data-driven approach ensures that maintenance activities are conducted under the safest possible conditions.

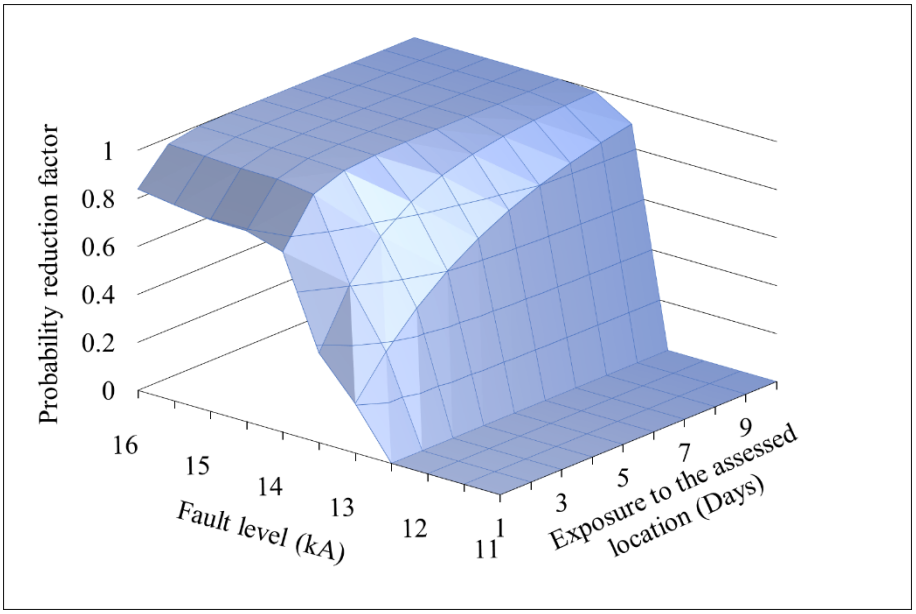

Figure 6-3 The profile of the probability reduction factor for touch voltage.

6.6 Adjusted Coincidental Probability of Fatality

If the fault level cannot be reduced due to operational constraints, the ALARP criteria must be applied to manage worker exposure to touch voltage hazards. Adjusting the fatality risk using the *PRF* results in an improved estimation of the coincidental probability of fatality, considering two key factors: the number of workdays in the pipeline maintenance plan and the prospective fault level of the transmission circuit.

In Figure 6-4, the blue area indicates that the individual fatality risk remains below 10^{-4}, which is considered an acceptable risk level. For fault levels exceeding 12.5 kA, the risk can be controlled to an acceptable level by limiting the number of maintenance visits per year. For instance, if the fault level is 13.5 kA, pipeline maintenance workers must complete all tasks within two days to ensure that risk exposure does not exceed the ALARP threshold. However, in this case study, the *PRF* had a limited impact on contact scenarios involving fault levels above 13.5 kA.

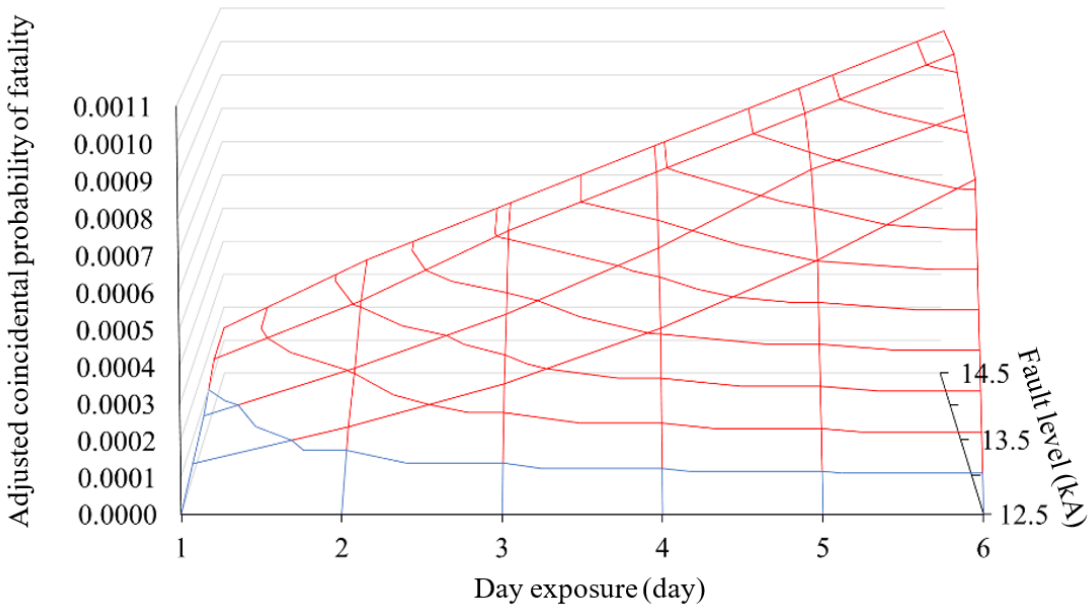

Figure 6-4 The adjusted coincidental probability of fatality. The blue region indicates that the risk level is below the ALARP upper limit of 10^{-4} and is considered acceptable.

6.6.1 Risk Management and ALARP Compliance

In situations where multiple transmission circuits can create hazardous touch voltages on a pipeline, reducing the fault level of each transmission circuit is not a feasible solution, as it could significantly disrupt the stability of the transmission network. Therefore, it becomes necessary to conduct a probabilistic risk analysis to ensure that the calculated coincidental probability of fatality falls within acceptable limits, in line with the criteria.

To accurately assess the adjusted coincidental probability of fatality for each transmission circuit, it is important to calculate these probabilities separately. Each transmission circuit possesses unique characteristics, such as varying fault levels, physical locations affecting pipelines, and the likelihood of generating hazardous touch voltages. Consequently, for each potential hazardous source, a dedicated probabilistic risk analysis framework must be established to compute the adjusted coincidental probability of fatality. This approach ensures a comprehensive and precise risk evaluation, taking into account the distinctive features of each potential hazardous source.

The summation of these adjusted individual coincidental probabilities of fatality is evaluated with respect to the ALARP criteria. If the calculated risk level falls within the boundaries of what is deemed "reasonably practicable" and does not pose a grossly disproportionate burden in terms of costs and sacrifices, it is considered acceptable. However, if the risk exceeds these boundaries and does not meet the ALARP criteria, further action may be required.

In such cases, potential actions may include implementing circuit outages or temporarily adjusting the protection level settings for specific transmission circuits. Subsequently, discussions with the transmission system operator may be necessary to identify a suitable solution that guarantees the safety of maintenance workers while also aligning with the ALARP principles.

The probabilistic analyses for touch voltage-related fatalities have long been standardized in various countries and regions [7, 12]. However, it has also uncovered a hesitancy among engineers to adopt risk acceptance under the ALARP criteria, largely discouraged by concerns surrounding legal liabilities and the need for more comprehensive risk information. This hesitation often led to a preference for physical hazard mitigation solutions, such as

recommendations for planned outages on affected transmission circuits or costly design variations.

The rationale for the preference for outage-based solutions, from the viewpoint of pipeline asset operators, is that circuit outages ensure zero harm from touch voltages, eliminating potential hazards and uncertainties related to electrical safety concerns. However, from the perspective of entities like transmission system operators responsible for the integrity and stability of the electricity network, the situation is distinct. Even though outages are carefully planned with the best intentions for human safety, they can introduce their own set of uncertainties and insecurities, posing risks to the overall reliability of the power grid.

In the context of these challenges, the innovative concept of the *PRF* serves as an innovative tool for enhancing risk assessment and management for pipeline asset operators in shared corridor situations. With the aid of the *PRF*, pipeline asset operators can efficiently identify crucial information, such as the safety threshold for the protection level setting of the transmission circuit, enabling them to effectively coordinate with the transmission system operator to reduce risks and mitigate hazards without the need of total outage on any transmission circuit.

By introducing the *PRF*, this research has effectively bridged the gap between traditional safety measures and the complex situation of legal liabilities. Serving as a structured and quantifiable approach, the *PRF* facilitates a more informed and confident understanding and management of risk. Beyond merely facilitating hazard mitigation, the *PRF* lays the foundation for future risk prediction, which will be instrumental in preparing for the anticipated surge in electricity demand resulting from the ongoing energy revolution in sustainable transportation.

Provided with the *PRF*, electrical engineers and pipeline asset operators possess a powerful instrument to navigate the complicated relationship of risk, safety, and liability. This approach exceeds ordinary risk mitigation, offering a complete decision-making framework that carefully balances the constraint of ensuring occupational safety with the operational integrity of critical infrastructure.

This comprehensive approach allows for a thorough risk assessment that not only accounts for probability but also considers the financial and operational aspects of risk mitigation. Consequently, it ensures the implementation of appropriate safety measures while meeting the acceptance criteria for ALARP.

6.6.2 Multiple Hazardous Sites in the Work Plan

When creating a work plan that covers multiple maintenance sites, it is essential to consider and summarise all potential fatality risks caused by touch voltage hazards as a single comprehensive risk. This final risk value is obtained by adding together the adjusted coincidental probability of fatality for each site under the threat of touch voltage hazards. The probabilistic risk analysis enables the pipeline operator to aggregate the adjusted coincidental probability of fatality associated with individual sections of the pipeline.

This approach to risk assessment across multiple sites holds significance in the context of ensuring safety throughout the entirety of a maintenance operation, particularly during the work planning phase. It gives a clear and full perspective on the cumulative risk posed by touch voltage hazards across multiple sites, thereby facilitating the efficient planning and management of safety measures. By adopting this comprehensive strategy, pipeline operators can enhance their ability to safeguard workers and mitigate risks during maintenance activities across diverse locations.

6.7 Application of *PRF* Considering Variable Line Rating

Electricity demand is growing at a high rate due to the phasing out of fossil fuels in transportation and the introduction of distributed renewable energy. However, this increase in demand is outpacing the development of transmission infrastructure [98]. Since transmission lines pose constraints on the operation of the electricity network, the traditional method for rating power lines assigns a fixed capacity based on conservative ambient temperature conditions. This approach often results in an underestimation of the actual capacity of transmission lines.

In response to this challenge, the transmission system has adopted variable line rating techniques to maximise the demand capacities of its assets [92]. However, this variable line rating approach can create a challenge when calculating an accurate *PRF* for assessing touch voltage risks. It

introduces variation in the prospective fault current instead of using a single maximum prospective fault current value. Nonetheless, this challenge also presents an opportunity to develop additional methods and strategies for applying *PRF* to manage touch voltage risks.

6.7.1 OTA-WKM-1 Line Ratings

Public information from the transmission system operator indicates that OTA WKM-1, which is located near the test site, operates under a variable line rating scheme [92]. As indicated by the table in Appendix C, the latest revision of the variable line rating for OTA-WKM-1 was made in 2018, as plotted on a 3D graph in Figure 6-5. The plot demonstrates that the prospective fault current settings were at their highest between 6 pm and 6 am and lowest around 10 am every day.

By strategically planning maintenance tasks to occur when the prospective fault current is at its lowest for the day, the exposure of maintenance workers to touch voltage hazards can be significantly reduced. This timing aligns with the period when the risk of high touch voltage is minimized, which can enhance safety measures for the maintenance personnel and reduce associated risks. However, in real-world situations, catching up in a small window of time in a day may not always be feasible. Therefore, this uncertainty could make this approach unfavourable to apply to pipeline hazard identification.

Strategically scheduling maintenance tasks during periods when fault currents are expected to be at daily minimums can be an approach that has not yet been applied to minimizing hazards from maintenance personnel's exposure to voltages. This timing coincides with the lowest risk window against touch voltages, thereby enhancing maintenance personnel safety measures and reducing associated risks.

However, in practical realities, capturing this small daily window may not always be feasible. Uncertainties, operational constraints, and various factors, such as traffic, can impose limitations on the feasibility of applying this approach to mitigate touch voltage hazards in pipelines. The dynamic and complex nature of real-world operations often presents challenges in consistently scheduling maintenance tasks to coincide with these small windows of the lowest expected fault current.

Therefore, where strict alignment of maintenance tasks with the minimum daily fault current cannot be achieved, a more flexible and adaptable approach may be required. Therefore, the touch voltage hazard identification needs to be revisited to develop a clear understanding of the actual hazard under these additional variable line ratings.

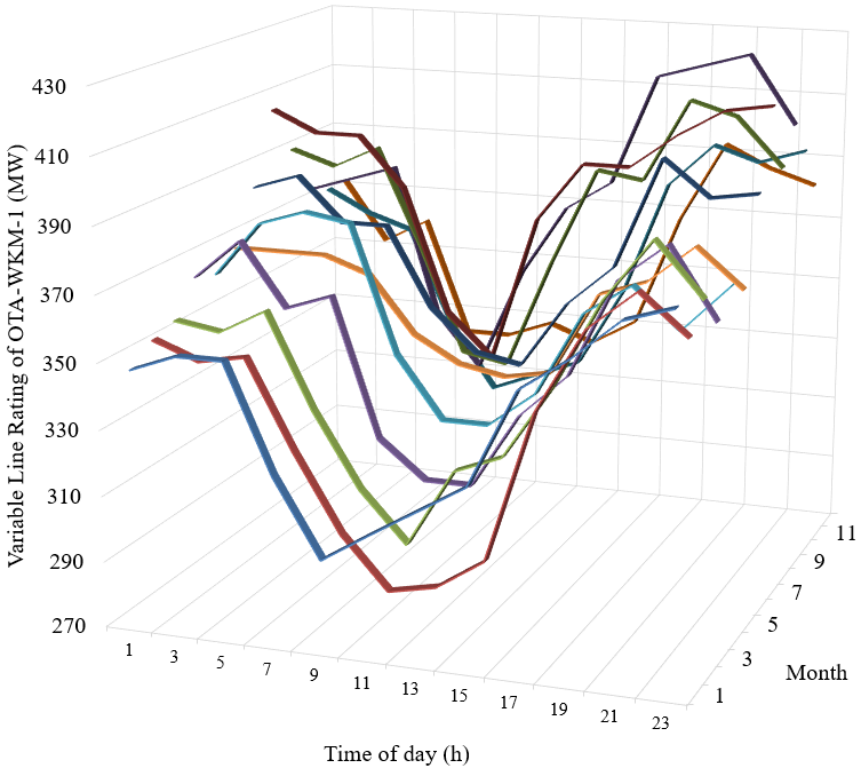

Figure 6-5 The variable line rating of OTA-WKM-1 in 2018 (Month 1 indicates January). The daylight-saving time has been converted into standard time.

6.7.2 Touch Voltage Hazard Identification with Variable Line Ratings

As per the variable line ratings displayed in Appendix C, supplied by the transmission system operator, the resolution of these ratings occurs at three-hour intervals. This level of detail exceeds that which is typically required for daily considerations. The highest daily protection setting value for fault level is utilised to represent the setting for the fault level to maintain a reasonable level of conservatism in hazard identification,

The variable protection settings are derived by min-max normalization the highest fault current for each month based on the highest fault current observed throughout the entire year. This

normalization process involves calculating the fault current ratio. This ratio is instrumental in assessing the impact of variable line ratings on touch voltages for different months, as shown in Figure 6-6.

For instance, the maximum fault current for October is 14 kA. The expected fault level is to scale 14 kA by a factor of 0.92, as shown in Figure 6-6, resulting in 12.88 kA for December. From January to June, the maximum fault current levels are significantly lower compared to the other months.

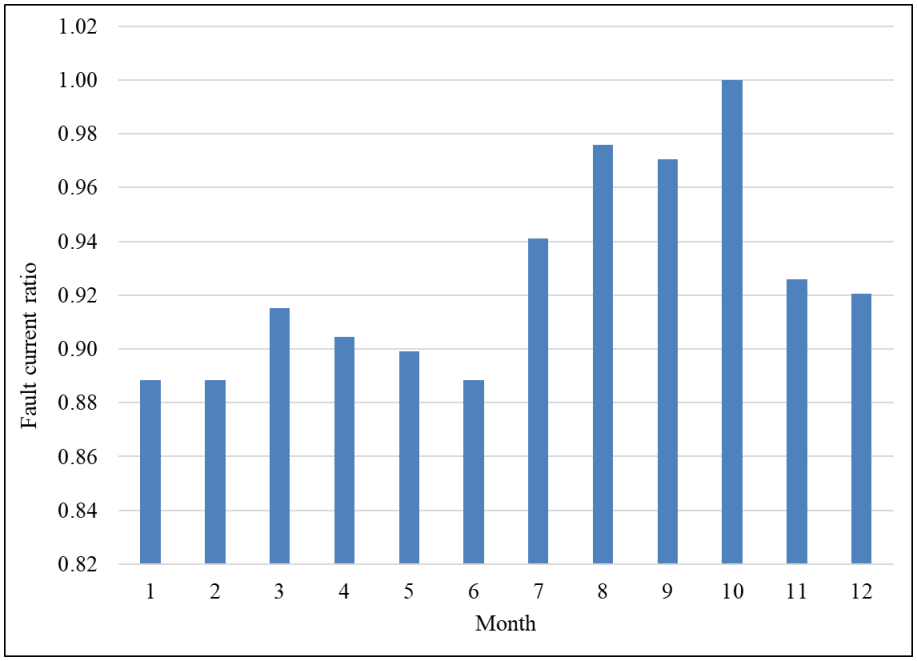

Figure 6-6 The fault current ratio for each month in 2018.

Using the maximum monthly fault current as input for the system model simulation can help in shaping the calculated touch voltages, as outlined in Section 5.2.3, in alignment with the actual potential fault scenarios. The accuracy of the touch voltage predictions can be further improved. This improvement is especially important in the context of risk assessment, where accurate touch voltage estimates are vital for evaluating the annualised probability of a hazardous day and further enhancing the reliability of the assessment of safety risks for the pipeline system.

The system model simulation results were re-calculated based on the monthly variation of protection level settings. If the maximum prospective fault current is 14 kA, only 16 days in a year can harbour the touch voltage hazardous between August to March.

6.7.3 Incorporating Variable Line Ratings into *PRF*

In the context of probabilistic risk analysis, the variable line ratings are not a random independent event. Therefore, it cannot be used as a probability distribution to incorporate into the *PRF* directly. This limitation arises from the fundamental requirement for the application of the general product rule of probability. Therefore, the variable line ratings were used in the last section to improve the accuracy of the touch voltage simulation. Using (30) and (33), the annualised probability of a hazardous day $\xi = 0.044$ and the $PRF = 1 - (1 - 0.044)^x$ are calculated, respectively. For the same contact scenario as described in Section 6.5.1, the unadjusted probability of coincidental fatality was 1.72×10^{-4}. Hence, the *PRFs* and the adjusted probability of coincidental fatality are calculated with the revised annualised probability of a hazardous day ξ and are shown in Table 6-3. The highest adjusted probability of coincidental fatality with the revised *PRF* is calculated to be 0.62×10^{-4}, which is an acceptable risk under the ALARP limit of 10^{-4}.

The number of days that were identified as hazardous was reduced from 274 to 16 days by taking the variable line settings into account. This significant improvement in the accuracy of the determination of the probability of coincidental fatality shows a significant reduction in that calculated risk that can confidently meet the ALARP criteria in the probabilistic risk analysis.

Table 6-3 The probability reduction factor and the adjusted probability of coincidental fatality with the distinctions between considering variable line ratings and fixed protection setting.

Day Exposure	*PRF*		P'_{conc} (10^{-4})	
	Variable	Fixed	Variable	Fixed
1	0.04	0.80	0.08	1.38
2	0.09	0.90	0.15	1.55
3	0.13	1.00	0.22	1.72
4	0.17	1.00	0.28	1.72
5	0.20	1.00	0.35	1.72
6	0.24	1.00	0.41	1.72
7	0.27	1.00	0.46	1.72
8	0.30	1.00	0.52	1.72
9	0.33	1.00	0.57	1.72
10	0.36	1.00	0.62	1.72

6.8 Summary

Touch voltage risk assessment for pipelines and transmission systems traditionally does not rely on deterministic models but only focus on worst-case scenarios. However, these models do not account for real-world variability, particularly in environmental conditions such as soil resistivity variations. To address this limitation, a novel probabilistic approach incorporating a binomial distribution is introduced to assess touch voltage risks during pipeline maintenance.

A key contribution is the development of the *PRF*, which refines existing probabilistic risk calculations by incorporating the temporal distribution of hazardous days. *PRF* is derived from annual soil resistivity monitoring and represents the likelihood of encountering hazardous touch voltage conditions over multiple working days. This factor improves risk estimation by reducing the conservatism in traditional coincidence probability models.

The *PRF* is validated using a hypothetical case study, where a 12-month soil resistivity dataset is employed to determine the number of hazardous days per year. The probabilistic risk model integrates *PRF* into the existing Poisson-based framework to adjust the probability of fatality due to touch voltage exposure. The findings demonstrate that fault levels influence the annualised probability of hazardous days, affecting the overall risk assessment.

By integrating *PRF* into ALARP assessments, pipeline operators can make informed decisions about risk mitigation strategies, such as planned outages or temporary fault level reductions. This novel framework enhances the accuracy of touch voltage risk analysis, aligning with industry safety standards while improving decision-making for maintenance planning.

The variable line rating demonstrated the further reduction of risk based on the actual fault current affecting the safety of the pipeline maintenance personnel has demonstrated the insufficient consideration of possible risk reduction in the past. The soil resistivity monitoring opened the gate to unleash the possibility of exploring additional opportunities for probability reduction. As a result, pipeline asset operators now have more information for considering various methods of mitigating the risk of exposure to touch voltage hazards. They can engage in effective discussions with transmission system operators to coordinate the temporary reduction of fault levels. This shift from a reactive to a proactive stance enables stakeholders to manage and mitigate risks proactively, contributing to improved safety and more informed decision-making in pipeline system management.

Chapter 7 - Touch Voltage Prediction for Emergency Maintenance

The previous chapter has discussed maintenance planning using the *PRF* to improve the accuracy of probabilistic risk assessment. However, during emergency maintenance of the pipeline, this approach may not be directly applicable. In the context of assessing the hazards associated with emergency maintenance, each event must be treated as an independent occurrence. Unlike routine maintenance, which follows a planned and structured strategy, emergency maintenance arises unexpectedly and often requires immediate action.

In such scenarios, the primary focus shifts to quickly determining whether touch voltage hazards could exist and ensuring the safety of workers performing the emergency repair or intervention. The touch voltage profile was calculated in Chapter 5 using historical soil resistivity data collected during the 12-month soil resistivity monitoring. The resulting touch voltage profile can be used to predict future touch voltage hazards with suitably chosen predictors. The soil resistivity data collected is used to explain past conditions and predict future variations, providing a basis for assessing potential touch voltage hazards. This assessment helps determine the presence of touch voltage hazards and informs appropriate mitigation measures during emergency maintenance.

7.1 Touch Voltage Prediction Using Multiple Linear Regression

A comprehensive analysis was conducted using multiple linear regression to understand and quantify the factors influencing the touch voltage of the case study. Touch voltage often depends on various environmental variables. Among these variables were soil temperatures and rainfall obtained from the NIWA database.

This analysis sought to establish an equation for touch voltage prediction that considers the complex interplay between these environmental factors. A series of predictor candidates listed in Appendices B and E were tested to observe how well the selected predictors explain the variance of the touch voltages from the simulation result of a 9 kA fault. The soil temperature at a depth

of 10 cm, the 24-hour cumulative rainfall, the 3-day cumulative rainfall, and the ambient temperature had failed as their p-values were above the predefined alpha level of 0.05 [88] of the t-test, indicating no significant relationship with the touch voltages.

The results of the multiple linear regression analysis found a robust and statistically significant relationship between three key variables: soil temperature at a depth of 5 cm, count of rainy days between data collection points, and touch voltage ($F(2, 90) = 46.13$, $p < .001$, $R^2 = 0.51$, $R^2_{adj} = 0.5$). The soil temperature at a depth of 5 cm and the count of rainy days had the p-values of 2.5×10^{-13} and 0.017, respectively, considerably less than the alpha level. Therefore, the null hypothesis was rejected, which suggests no significant relationship between the predictor variables.

Instead, the alternative hypothesis, supported by the multiple linear regression model, indicates a meaningful and quantifiable relationship between soil temperature, the count of rainy days, and touch voltage. The alternative hypothesis is mathematically represented by the touch voltage equation using the multiple linear regression model as expressed in (36).

$$Y = 245.10 + 1.45\,X_1 - 2.32X_2 \quad (V) \tag{36}$$

where,

Y is the touch voltageX_1 is the soil temperature at a depth of 5cm, and X_2 is the count of rainy days between data collection.

Upon closer examination of the individual predictors, the soil temperature ($t = 8.585$, $p < 0.01$) and the rainy days count ($t = -2.439$, $p = .017$) represent significant predictors within the model. These findings indicate that soil temperature and the count of rainy days contribute significantly to the touch voltage equation.

Several diagnostic plots have been used to validate the robustness of the linear regression model. These include the quantile-to-quantile plot (Q-Q plot), residuals plot, and predicted Y plot, all presented in Figure 8-1, Figure 8-2, and Figure 8-3, respectively. These plots serve as crucial tools for assessing the model's goodness of fit and the validity of the underlying assumptions.

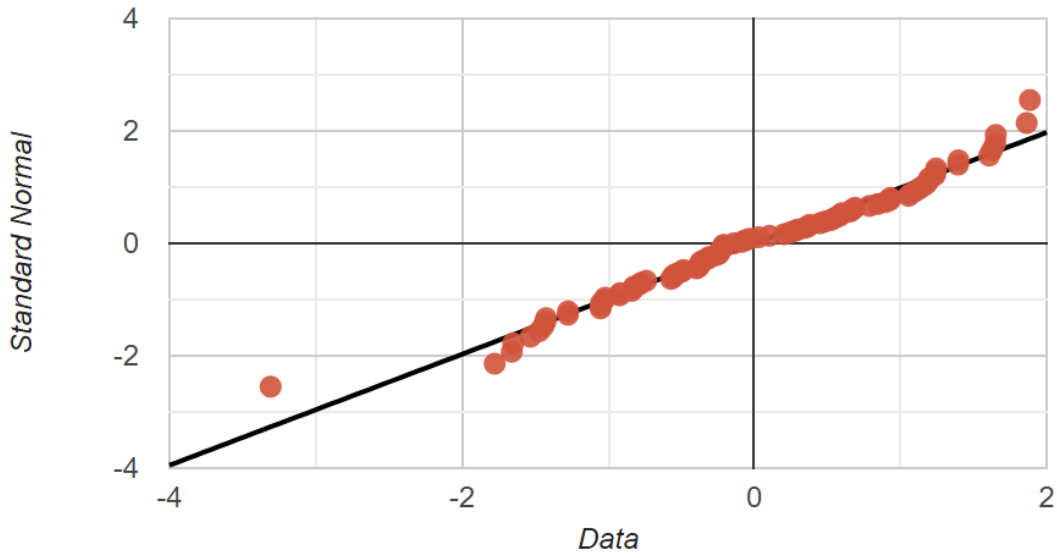

Figure 8-1 The Q-Q plot of the observed data to the quantiles of the standard distribution. The Standard Normal points in orange closely followed the 45-degree line; it indicated a good fit between the data used for multiple linear regression and the standard normal distribution.

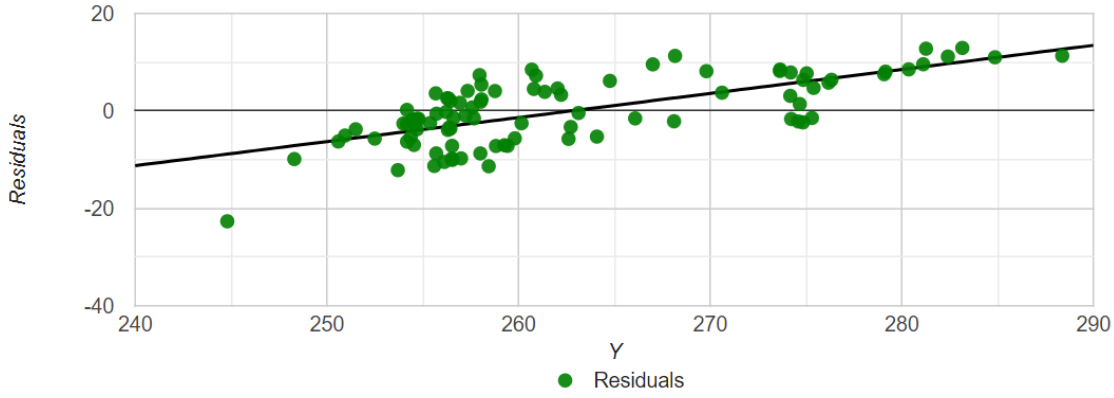

Figure 8-2 The residual versus actual data plot for the multiple linear regression analysis for predictors of soil temperature and rainy days count. The residual is the difference between the actual data and the predicted value. The units for both axes are in (V).

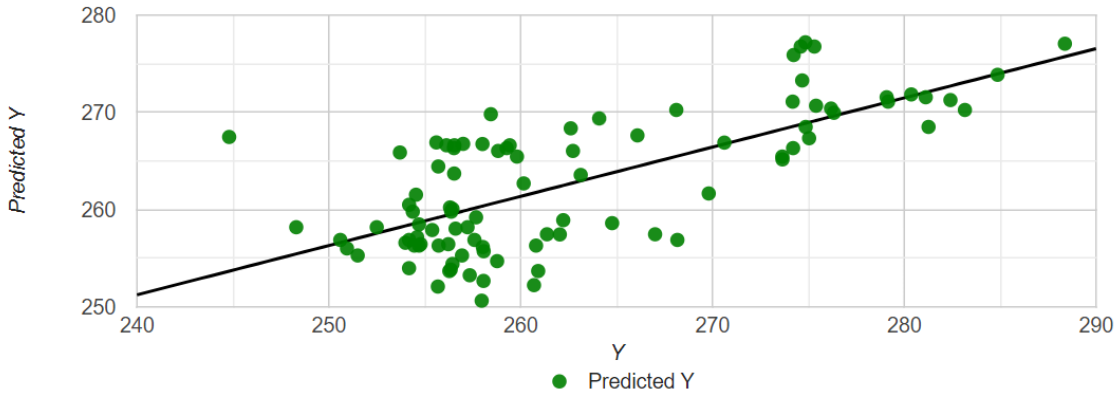

Figure 8-3 The simulated touch voltage plot against the predicted value using (36). The plot showed that the predicted value has a maximum deviation of approximately ±10 V. The units for both axes are in (V).

Despite the potential ±10 V error associated with the touch voltage predictors; the regression equation can be a valuable tool for predicting worst-case touch voltages. This tool is particularly advantageous because the predictors can be easily obtained on-site, so pipeline maintenance workers can predict touch voltage using readily available data. Additionally, by averaging the measured resistivities from a short traverse consisting of Wenner spacings of 0.1, 0.2, and 0.5 m, workers can quickly determine the soil resistivity for the top layer. This information lets them immediately assess touch voltage hazards by comparing the predicted touch voltage with the tolerable touch voltage using (12).

7.2 Using Bottom Layer Soil Resistivity to Improve Touch Voltage Estimation

Using the resistivity of the bottom layer to predict the touch voltage required the use of specialised software. Therefore, this predictor may not be easily obtainable on-site. However, considering gas pipelines are often buried at depths of at least 2 m, the bottom layer of soil resistivity can directly relate to the touch voltage. Another multiple linear regression analysis was conducted to test this argument, including the bottom layer soil resistivity and the soil temperature at a depth of 5 cm, which was previously identified as a strong predictor.

Results of the multiple linear regression indicated that there was a very strong collective significant effect between the soil temperature, bottom layer resistivity, and touch voltage ($F(2, 90) = 129.8$, $p < .001$, $R^2 = 0.74$, $R^2_{adj} = 0.74$). The individual predictors were examined further and indicated that the soil temperature ($t = 5.691$, $p < 0.01$) and bottom layer resistivity ($t = 9.697$, $p < 0.01$) were significant predictors in the model.

Overall regression with right-tailed, $F(2,90) = 129.80$, had a p-value much smaller than the alpha level of 0.05 [88]; therefore, the null hypothesis is rejected. The linear regression model is expressed in (37) shown below:

$$Y = 220.34 + 0.80\,X_1 + 0.25\,X_2 \quad (V) \tag{37}$$

where,

Y is the touch voltage,
X_1 is the soil temperature at a depth of 5cm, and
X_2 is the bottom layer resistivity.

The robustness of the linear regression model was validated using the Q-Q plot, residuals plot, and predicted Y plot, all presented in Figure 8-4, Figure 8-5, and Figure 8-6, respectively. These plots show positive results toward the goodness of fit.

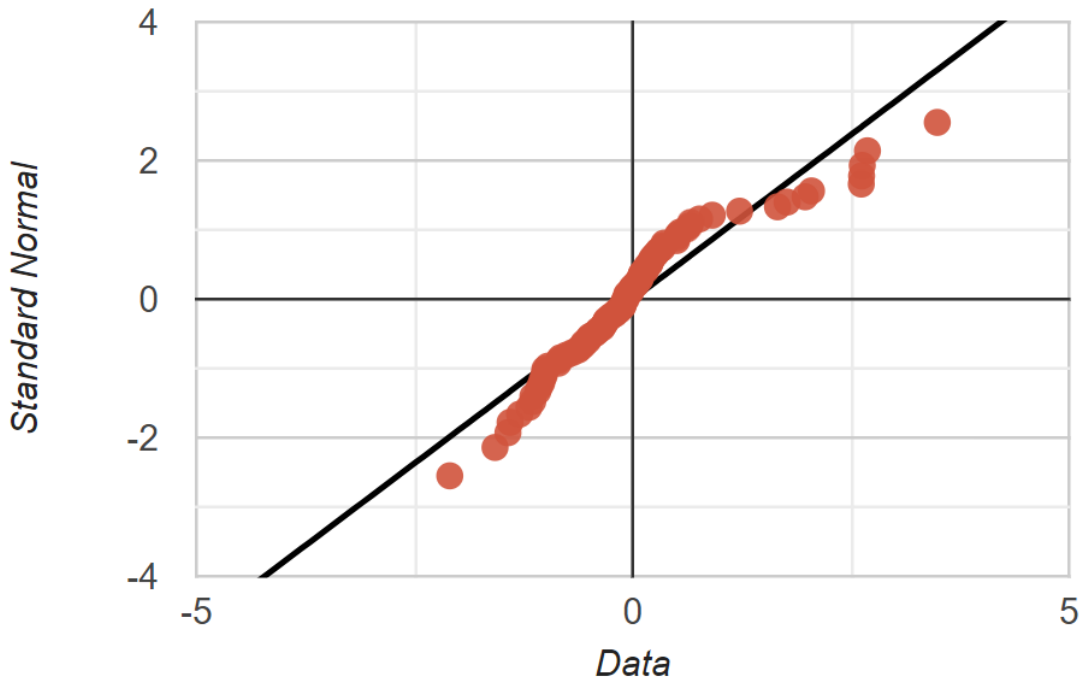

Figure 8-4 The Q-Q plot for the regression with bottom layer resistivity as a predictor: The residuals are distributed along the diagonal line means a good fit between the data and the multiple linear regression result with the error terms are normally distributed.

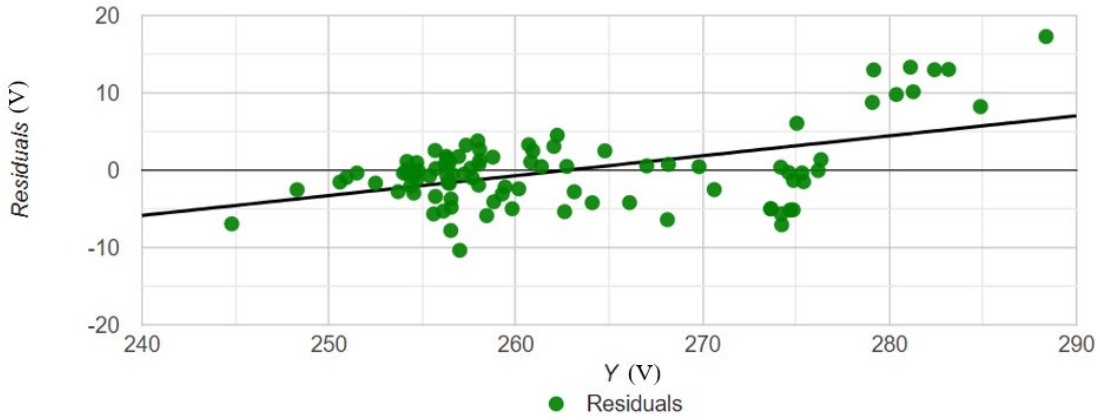

Figure 8-5 The residual versus actual data plot for the multiple linear regression analysis for predictors of soil temperature and bottom layer resistivity.

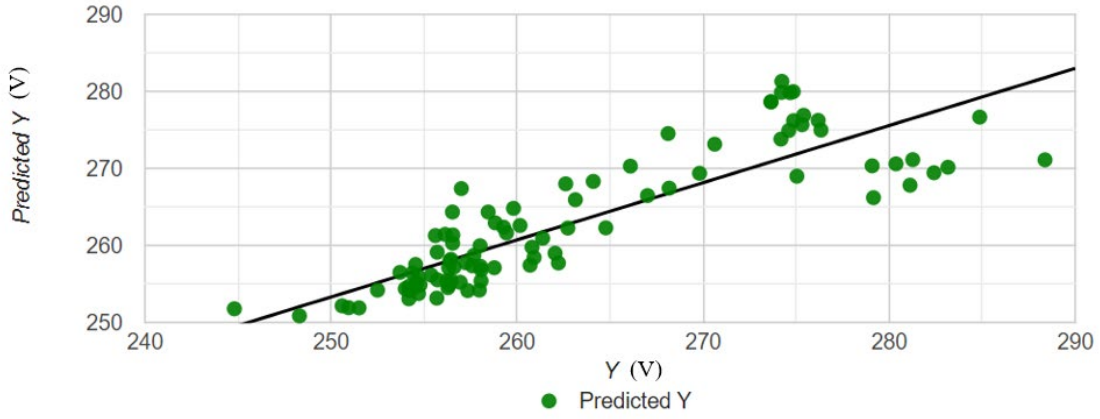

Figure 8-6 The simulated touch voltage plot against the predicted value using Equation (37).

Both sets of predictors have their strengths and weaknesses. For touch voltages below 270 V, utilizing (37) can provide estimates closer to the actual values. However, when dealing with touch voltages higher than 270 V, (36) tends to yield more accurate results. Both methods can offer reasonable estimations, and with knowledge of the error margins, this margin can be incorporated into touch voltage hazard identification to create a conservative result. Therefore, it is acceptable to use either regression equation for estimating touch voltages based on the specific circumstances and desired level of accuracy.

Both sets of predictors have their strengths and weaknesses. According to Figure 8-7, for touch voltages below 270 V, utilizing (33) can provide estimates closer to the actual values. However, when dealing with touch voltages higher than 270 V, (32) tends to yield more accurate results. Both methods can offer reasonable estimations, and with knowledge of the error margins, this margin can be incorporated into touch voltage hazard identification to create a conservative result. Therefore, it is acceptable to use either regression equation for estimating touch voltages based on the specific circumstances and desired level of accuracy.

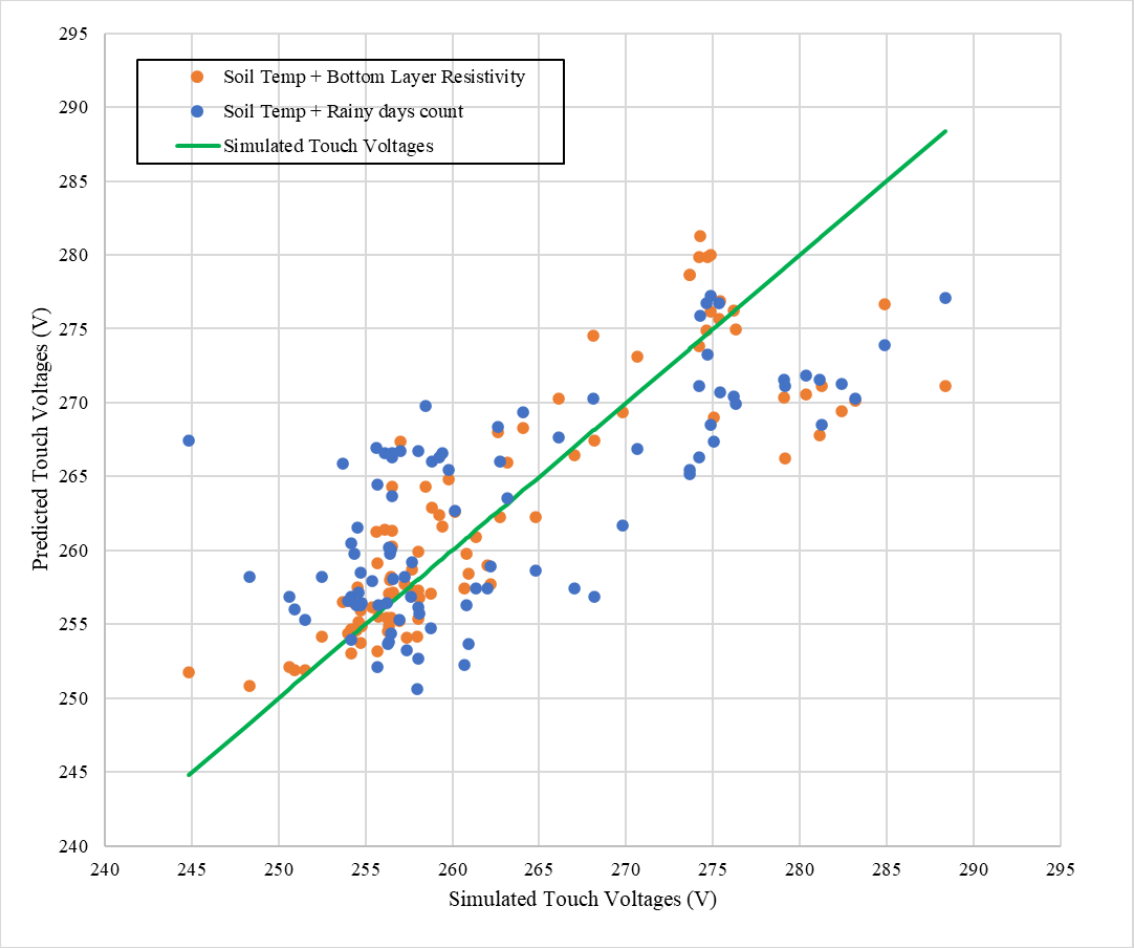

Figure 8-7 The comparison of two sets of predictors for touch voltage estimation.

The transformation of system model simulation outcomes into an annualized probability of hazardous days has shown an essential connection between fault levels and the occurrence of such

days in Table E-1. This relationship holds significant implications for predicting the variability of touch voltage hazards on the pipeline, particularly in anticipation of future upgrades in electricity network demand. Presently, available tools and methodologies do not empower pipeline asset operators to proactively manage these risks and hazards, primarily relying on information from the electricity network.

Therefore, understanding the threshold fault level beyond which no hazardous days are expected to occur becomes a valuable asset. This knowledge enables pipeline asset operators to engage with the electricity network more efficiently and effectively, fostering improved safety measures and communication protocols in requesting a temporary lower fault level. Hence, the worker could work in a touch voltage hazards-free environment.

The capability to address touch voltage concerns on-site using Equations such as (36) and (37) is undoubtedly valuable for enhancing pipeline maintenance safety. However, it is essential to note that this study represents the local soil characteristics of the test site. Soil structures and compositions can vary significantly in other locations, so similar equations may not always be applicable. Hence, pipeline asset operators still need to incorporate probabilistic risk analysis into their maintenance plans for some locations where touch voltages are difficult to predict.

7.3 Linear Regression Equation Validation

A total of 108 soil resistivity models were collected during the twelve-month soil resistivity monitoring period. The initial 90 datasets were utilized in Table E-1 to develop the touch voltage equations. The remaining 18 datasets between 16/03/2021 and 15/05/2021 were reserved for validating (36) and (37).

To assess the statistical significance of the touch voltage predictions, a paired-sample t-test was conducted. The null hypothesis posits that there is no statistically significant difference between the outcomes of the simulation and estimation methods. In other words, any disparities observed between these two touch voltage prediction approaches are attributed to random chance or sampling variability, and there is no systematic distinction between them. The objective was to

test this null hypothesis and ascertain whether there is enough evidence to support the use of Equations (36) and (37) for touch voltage prediction.

The results of the paired-sample t-tests yielded p-values of 0.9105 for (37) and 0.2231 for (36). In the case of (37), the t-test results indicated a very small effect size (d=0.027) and a high p-value (0.9105), suggesting that (37) closely resembles the system model simulation, with only a negligible practical difference. On the other hand, the t-test results for (36) showed a larger effect size (d=0.3), making (37) the method that closely aligns with the system model simulation.

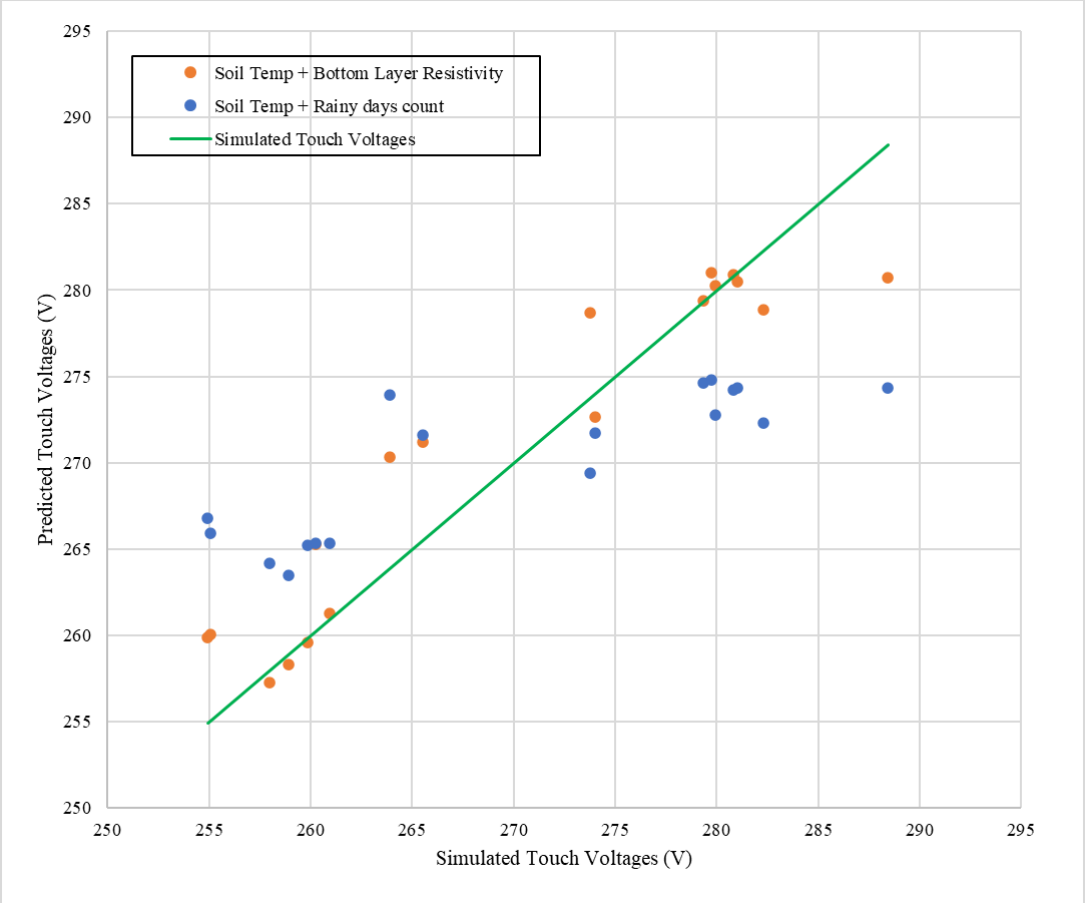

Figure 8-8 The scatter plots show that (37) in blue is superior to (36) in orange. The green line is the system model simulation result.

7.4 Emergency Maintenance Risk Considerations

In the context of assessing the risk associated with emergency maintenance work, it is important to treat each emergency maintenance event as an independent occurrence. Unlike routine

maintenance, which is part of a planned and structured maintenance strategy, emergency maintenance situations can arise unexpectedly, demanding immediate attention. In such scenarios, the primary focus is on rapidly addressing critical issues and ensuring the safety of workers involved in the immediate repair or intervention. Therefore, the primary objective of electrical safety assessment for emergency maintenance is the elimination of touch voltage hazards.

The response to an emergency maintenance situation typically involves hazard identification using the touch voltage equations (36) or (37) to estimate the touch voltage. This estimated value is then compared to the tolerable touch voltage, which is determined using Dalziel's equation (12) with conservative soil resistivity. An accurate soil resistivity measurement becomes irrelevant once excavation is undertaken to access the pipeline.

During emergency maintenance, speed and precision are of the essence. The conservative approach of using soil resistivity values that are not site-specific but rather reflect a worst-case scenario ensures that safety is prioritized in situations where immediate action is required. This approach takes into account the uncertainties introduced by excavation and the removal of the topsoil layer, as the actual soil properties can change rapidly during such work.

By using conservative soil resistivity values, the safety assessment remains robust, and potential touch voltage hazards are more likely to be identified, even in scenarios where the actual soil resistivity might differ from the initial measurements. This precautionary approach is aligned with the primary goal of emergency maintenance, which is to rapidly eliminate touch voltage hazards and ensure the safety of workers involved in the intervention.

In cases where the assessment cannot confirm the safety of the site from touch voltage hazards, the pipeline asset operator should initiate communication with the transmission system operator. This communication is intended to request a temporary reduction in the fault level setting, a measure that, as indicated by the *PRF*, has the potential to eliminate the touch voltage hazard. The case study illustrated in Figure 6-3**.** serves as a practical example, demonstrating that when the fault level is set at 12.5 kA, no touch voltage hazards are present.

The ability to communicate to the transmission system operator efficiently with the known purpose is a valuable safety measure, especially in emergency maintenance situations where immediate action is required to protect the workers and maintain the integrity of the electrical network. This approach, based on the *PRF*, offers an effective and practical solution for mitigating touch voltage hazards, providing a safer working environment during maintenance operations. It underscores the adaptability of electrical safety measures in response to specific site conditions and requirements, ultimately enhancing the overall safety of maintenance work.

When assessing the risk associated with emergency maintenance, the conventional probabilistic risk analysis may not be entirely suitable. This is because emergency maintenance situations can vary significantly in terms of the contact scenario and the duration of exposure to touch voltage hazards. These variations are often unknown and unpredictable. Therefore, an approach that is more immediate to the specific hazards of emergency maintenance becomes critical to address touch voltage risks in these serious situations effectively.

Emergency maintenance is considered an independent event in terms of probabilistic risk analysis. It does not inherently increase the risk associated with any pre-existing maintenance plan that may have been in place. Instead, the developed voltage prediction equations and *PRF* in emergency maintenance situations becomes a useful tool for rapid hazard identification and elimination of touch voltage hazards, with a paramount focus on ensuring the safety of workers in times of crisis. This focused and immediate approach is essential to address the unique challenges and uncertainties presented by emergency maintenance scenarios, ultimately minimising risks and safeguarding the well-being of those involved.

7.5 Summary

To provide historical insights, a sufficient quantity of reliable touch voltage data points has been mathematically analysed. The equations derived from multiple linear regression clearly illustrate the influence of climate on the magnitude of touch voltages on the pipeline at various times. The capacity to explain the past lays the foundation for predicting the future. The remaining touch voltage data points were used to validate the equations. The capability to forecast touch voltages

accurately makes these equations a significant tool for conducting site safety assessments before maintenance procedures begin.

The touch voltage prediction method provides a straightforward yet effective tool for quick safety assessments. (*33*), which utilizes the bottom-layer resistivity and soil temperature as predictors, offers enhanced accuracy compared to (*36*), where rainy day count and soil temperature are used. A predictor in (*33*) is the resistivity of the bottom-layer soil, which may only be accessible using specialized equipment such as an earth resistance tester. This reliance on additional tools can make (*36*) a more practical choice for touch voltage estimation, especially in emergency maintenance scenarios. Both equations, however, can validate each other, offering complementary methods for assessing touch voltage hazards in varying circumstances.

Regular reviews of the touch voltage equations are essential to ensure that the updated fault level is incorporated into the system model simulation for obtaining touch voltages through multiple linear regression. These periodic evaluations also help verify that the touch voltage prediction deviations remain within an acceptable range and that the accuracy of touch voltage assessments is maintained over time. This ongoing assessment is crucial for ensuring the continued reliability of these equations in evaluating touch voltage hazards.

Chapter 8 - Contributions and Future Research Opportunities

8.1 Original and Significant Contribution to the knowledge

This thesis has introduced a novel risk-based approach to characterising and modelling shared corridor scenarios involving gas pipelines and transmission lines. The primary objective is to integrate seasonal variation in soil resistivity into a pipeline–transmission-line system model, enhancing the existing probabilistic risk analysis for fatalities arising from touch voltages. The research has provided original and significant contributions to understanding soil resistivity fluctuations in a subtropical district, thereby improving the accuracy of touch voltage hazard identification and risk assessment.

The findings provide gas pipeline asset operators with a more comprehensive framework for both routine and emergency maintenance planning. Furthermore, the research establishes a foundation for refining industry standards on touch voltage assessment, potentially encouraging regulatory bodies to consider incorporating this novel probabilistic risk analysis into official guidelines. By demonstrating the feasibility of this approach, the work presents an opportunity for industry practitioners, regulators, and standardisation committees to evolve current safety protocols beyond deterministic models towards a more robust, risk-based methodology.

8.1.1 Obtaining Reliable Touch Voltages

A year-long data collection effort was undertaken to measure and record soil resistivities, forming the basis for a series of soil resistivity models that capture continuous variations in local soil properties. The key contribution of this part of the research lies in the proposed method for improving soil resistivity modelling accuracy. A well-calibrated soil resistivity model ensures reliable touch voltage estimations in system simulations, which, in turn, subsequently enhances the accuracy of the existing risk model. By providing continuous profiles for soil resistivity parameters, this research advances the understanding of an essential aspect of touch voltage safety assessment in shared corridor scenarios.

A significant opportunity is the standardisation of soil resistivity modelling techniques in safety regulations. Current industry standards assume worst-case scenarios, but the introduction of seasonal soil resistivity variations provides a more accurate and dynamic risk evaluation. Future collaborations with regulatory bodies, such as IEEE and IEC, could enable the integration of probabilistic soil resistivity modelling into formal industry standards, helping infrastructure operators make informed decisions while maintaining compliance with safety regulations.

8.1.2 Enhancing Predictive Hazard Identification through Touch Voltage Modelling

This research makes a significant contribution to knowledge by introducing a linear regression-based predictive model for touch voltage estimation, which enhances the accuracy of hazards identification and subsequently risk assessment in shared corridor scenarios. By systematically analysing year-long touch voltage data, the study establishes mathematical relationships between environmental factors—such as seasonal soil resistivity variations, soil temperature, and rainfall patterns—and their impact on touch voltage magnitudes. The derived equations provide a quantitative framework for predicting touch voltages under different climatic conditions, allowing gas pipeline operators to conduct proactive risk assessments before undertaking maintenance activities. Unlike conventional industry practices that depend on worst-case assumptions and fixed soil resistivity values, this approach dynamically incorporates real-world variations of the hazard into probabilistic risk analysis, improving the accuracy of safety evaluations.

A key advancement of this research is the validation of these predictive equations using independent datasets, confirming their reliability for real-world applications. This validation process ensures that the predictive model remains robust across different seasonal conditions, enhancing its usability for industry professionals. Additionally, the study highlights a practical trade-off between equation complexity and accessibility of input parameters. While the most accurate equation requires bottom-layer soil resistivity measurements—obtained using specialised equipment such as an earth resistance tester—a more practical alternative relies on readily available meteorological data, making it suitable for rapid safety assessments, particularly in emergency maintenance situations. This adaptability allows for flexible implementation depending on operational constraints and available resources.

8.1.3 Enhancing the Accuracy of Probabilistic Risk Analysis

This research makes a significant contribution to the knowledge by introducing the *PRF*, a novel approach to refining the probabilistic risk analysis of touch voltage-related fatalities. Existing probabilistic analyses for touch voltage-related fatalities have been widely adopted, with established case studies, risk acceptance methods, and criteria documented across various jurisdictions. However, a key challenge in practical applications has been the hesitation among engineers to propose risk acceptance under the ALARP principle, primarily due to concerns over potential legal liability in the event of a fatality. A major barrier to confident decision-making has been the lack of sufficient quantitative information regarding touch voltage variations, leading to a reliance on conservative assumptions. Consequently, engineers have often opted for temporary outages of the affected circuits during pipeline maintenance as a precautionary measure, despite the operational and economic impacts.

The *PRF* addresses this gap by incorporating ventricular fibrillation probability from the Dalziel equation and eliminating unnecessary conservatism. This results in a more statistically sound framework that provides a realistic assessment of fatal incident likelihood. The extensive development and validation of the *PRF*, published in the *IET Science, Measurement & Technology Journal* [99], demonstrates its ability to define ALARP risk acceptance boundaries more clearly. This allows for a more precise, justifiable approach to risk assessment, balancing safety concerns with operational efficiency. An application case study further illustrates how integrating variable line ratings into *PRF* enhances the accuracy of probabilistic risk evaluation.

8.1.4 Empowering Pipeline Operators with Risk Control Capabilities

Another important contribution is the introduction of using *PRF* as a practical decision-making tool for pipeline operators, allowing them to move beyond a traditionally passive role in negotiating safe working conditions with the electricity grid operator. In the shared corridor environments, risk is often managed through national grid protection settings and pipeline operator work plans, which often leave pipeline operators reacting to externally determined safety measures rather than proactively identifying and mitigating hazards. The *PRF* provides a quantitative method for pipeline operators to assess the impact of different fault conditions and

operational scenarios, thereby enabling them to pinpoint hazard control points and advocate for risk mitigation strategies.

By leveraging the *PRF*, pipeline operators can conduct scenario-based evaluations to determine the acceptable risk levels for maintenance activities, instead of relying solely on worst-case deterministic assumptions. This enables a more balanced risk management approach, where mitigation measures—such as adjusting maintenance schedules, implementing protective barriers, or negotiating alternative power system configurations—can be explored based on actual probabilistic risk insights. The *PRF* effectively shifts pipeline operators from a reactive to a proactive role in risk management, ensuring that safety measures are both practical and evidence based.

The contribution of this research lies in the potential for the *PRF* to enhance the existing simple risk models with a data-driven methodology. The subsequent step is the integration of the *PRF* into industry standards. By transitioning to a probabilistic safety management approach, this framework will allow operators to make better-informed, risk-based decisions. The goal is for the *PRF* to be formally recognised and incorporated into regulatory frameworks, providing operators with a powerful tool to confidently manage touch voltage risks and ensure the safety of maintenance operations.

8.1.5 Preparing for the Future Pipelines for Renewable Energy

The development of predictive risk models for touch voltage has extensive applications, particularly as pipeline infrastructure evolves to meet the growing demand for renewable energy. One emerging area of focus is the development of high-pressure steel gas pipelines designed for the transport of compressed or liquid hydrogen, which presents unique safety challenges due to its highly reactive properties and extreme operational conditions. The research presented in this thesis demonstrates the potential of the *PRF* to adapt to future scenarios, providing a flexible and robust framework for managing touch voltage risks in this new energy pipeline.

Unlike fault current studies, long-term soil resistivity monitoring is not a mandated industry practice. However, this study demonstrates its critical role in hazard identification. The findings highlight the importance of:

- Incorporating Long-Term Soil Resistivity Trends into Risk Assessments – Current standards rely on one-time or periodic soil resistivity measurements [2, 5], which may not capture seasonal variations. Guidelines should encourage utilities to consider soil resistivity variation over time, particularly in shared corridors where touch voltage hazards may be mis-estimated.
- Periodic Review of Touch Voltage Thresholds – Although periodic reviews of touch voltage thresholds are conducted, soil resistivity measurements are typically taken during a single-day site visit. This limited approach may not capture worst-case conditions over a year. To improve accuracy, regulatory bodies should consider incorporating long-term soil resistivity monitoring data into the review process.
- Adapting Risk Models for Future Grid Expansion – As electricity demand increases, fault levels may rise, potentially intensifying touch voltage hazards that were previously undetected under lower fault conditions. These higher fault levels can worsen hazards, especially in areas where soil resistivity and environmental conditions contribute to touch voltage variations.

By addressing the unique challenges posed by future pipeline infrastructures, such as those used for liquid hydrogen transport, the PRF can play a vital role in ensuring the safety and reliability of these critical renewable energy systems. The tools developed in this research contribute to the sustainability of future energy networks by enabling safer, more efficient risk management strategies, which are key to supporting the transition to clean energy solutions. The insights offered by this research have the potential to influence policy development, standardisation efforts, and regulatory frameworks, ensuring that safety measures keep pace with technological advancements in the energy sector.

8.2 Future Research Opportunities

This research provides a foundation for further exploration and development in the field of probabilistic risk analysis for touch voltage hazards in shared corridor scenarios. Several areas for future research can be identified, each offering opportunities to refine, expand, and adapt the methodologies developed in this thesis for broader applications. The following sections identify key opportunities for future work, focusing on improvements to existing models, addressing emerging challenges, and broadening the scope of touch voltage risk assessment across diverse infrastructure contexts.

8.2.1 Expanding the Scope of Soil Resistivity Modelling

While this thesis focused on seasonal variations in soil resistivity within a subtropical district, the approach can be expanded to other geographic regions, particularly those with varying soil types and climates. Future research could aim to develop a large-scale soil resistivity information database that accounts for geographic and climatic diversity, incorporating additional environmental factors such as vegetation types, underground water table levels, and seasonal fluctuations in temperature and humidity. Furthermore, more advanced soil resistivity modelling techniques, such as incorporating machine learning algorithms, could improve prediction accuracy by identifying complex non-linear relationships between environmental factors and soil resistivity variations.

Integrating soil resistivity data from various regions could create a more comprehensive probabilistic model, improving touch voltage risk assessments across diverse terrains. Collaboration with local authorities and regulatory bodies could facilitate the collection of diverse soil resistivity data, enabling the development of safety standards that are more representative of diverse environmental scenarios.

8.2.2 Refining the Predictive Model for Touch Voltage Estimation

The predictive model for touch voltage estimation developed in this research represents a significant advancement, but there are opportunities to enhance its predictive power. Future research could explore the use of more sophisticated statistical and machine learning techniques,

such as neural networks or support vector machines, to improve the model's ability to account for interactions between environmental variables and their combined impact on touch voltage.

Additionally, the model could also incorporate other environmental variables, such as atmospheric pressure and moisture levels, which might influence soil resistivity and, consequently, touch voltages. The integration of real-time data streams from weather stations and remote sensing technologies could provide more dynamic, up-to-date risk assessments, enabling operators to take immediate action when pipeline maintainers are on site.

8.2.3 Validation of the Probability Reduction Factor (*PRF*) in Real-World Scenarios

While the *PRF* has shown promise in refining probabilistic risk assessments, its real-world application and validation at existing sites remain key areas for future research. Validation efforts could focus on sites where hazardous touch voltages have already been identified, allowing for the comparison of *PRF*-based risk assessments with actual parameters. This would help assess the accuracy and reliability of the *PRF* in practical, real-world settings.

Further research could involve developing a comprehensive database of touch voltage-related incidents, facilitating a deeper evaluation of the *PRF*'s predictive ability. Long-term monitoring of touch voltage occurrences at these locations would provide substantial data, helping refine the *PRF* methodology and ensuring its applicability across various operational and geographical conditions.

8.2.4 Integrating Advanced Touch Voltage Detection and Mitigation Techniques

To further enhance the practical application of this research, future studies could focus on integrating advanced fault detection and mitigation technologies into the risk assessment process. For example, the use of smart sensors and real-time monitoring systems to detect and record fault currents, soil resistivity changes, and touch voltage levels could provide pipeline operators with the tools to make proactive decisions regarding risk management.

Research could also consider the development of automated control systems that dynamically adjust safety measures based on real-time risk assessments. These systems could be integrated with existing pipeline monitoring infrastructure, offering immediate responses to changes in fault

conditions or environmental variables. Moreover, predictive maintenance strategies based on the *PRF* and predictive touch voltage models could be implemented to optimise resource allocation and reduce the likelihood of accidents during maintenance activities.

8.2.5 Collaborative Efforts to Standardise Risk-Based Safety Protocols

Finally, a major opportunity for future research lies in the continued collaboration with industry stakeholders, regulatory bodies, and standardisation committees to establish risk-based safety protocols as a formal industry standard. Future research could focus on conducting pilot studies with major pipeline operators, energy companies, and regulators to implement and test the *PRF*-based risk assessment methodologies in real-world environments.

Moreover, future research could also integrate touch voltage risk management into broader safety and regulatory frameworks, linking it with other aspects of touch voltage safety, environmental impact assessments, and operational efficiency. The goal is to support the development of universally accepted safety standards that incorporate probabilistic risk analysis, ensuring that future pipeline operations are safer, more reliable, and better equipped to handle the challenges posed by evolving energy infrastructure.

Chapter 9 - Conclusion

This thesis has introduced a novel approach to risk assessment for touch voltage hazards in shared corridor environments involving gas pipelines and transmission lines. By integrating seasonal variations in soil resistivity into a probabilistic risk model, the research has significantly enhanced the accuracy of touch voltage hazard identification and risk evaluation. This work provides new insights into the role of soil resistivity fluctuations in shaping touch voltage risks and highlights the potential of dynamic, data-driven methodologies to improve safety practices.

The research highlights the importance of collaboration with regulatory bodies, standardisation committees, and industry stakeholders to formalise and adopt risk-based safety protocols across the sector. Integrating the probabilistic models developed in this study into broader safety frameworks will help the industry advance towards more robust and reliable safety protocols, better equipped to address the evolving challenges of modern energy infrastructure.

Ultimately, the contributions of this thesis offer substantial benefits to the safety and efficiency of pipeline operations, particularly as the energy sector adapts to the growing demand for renewable energy. Future research will build upon these foundations, refining models, validating methodologies, and developing comprehensive safety standards to minimise touch voltage risks in shared corridor environments.

At last, this research not only advances the understanding of touch voltage hazards in shared corridors but also provides a clear path forward for improving risk management practices in pipeline maintenance operations. The potential for this work to influence both industry protocols and regulatory frameworks represents a significant step towards ensuring the safety and resilience of infrastructure systems in the face of emerging energy challenges.

Chapter 10 - References

[1] ENA vol. EG-0, Ver 1, *Power System Earthing Guide Part 1: Management Principles,* Energy Network Association, 2010.

[2] *IEEE Std 80: IEEE Guide for Safety in AC Substation Grounding,* IEEE, 2013.

[3] *IEC 60479-1: Effects of current on human beings and livestock - Part 1: General aspects,* IEC, 2018.

[4] G. Biegelmeier and W. R. Lee, " New considerations on the threshold of ventricular fibrillation for a.c.shocks at 50-60 Hz," *A - Physical Science, Measurement and Instrumentation, Management and Education - Reviews,* vol. 127, no. 2, pp. 103-110, 1980.

[5] Electricity Engineers' Association, *Guide to Power System Earthing Practice,* EEA, June 2009..

[6] B. Bessen, J. Coult, J. Blackwood, C. Hsu, P. Kudenchuk, T. R. and H. Kwok, "Insights From the Ventricular Fibrillation Waveform Into the Mechanism of Survival Benefit From Bystander Cardiopulmonary Resuscitation," *Journal of the American Heart Association,* vol. 10, no. 19, 2021.

[7] Health and Safety Executive: Reducing Risks, Protecting People HSE's Decision-Making Process, Suffolk, UK: Health and Safety Executive, 2001.

[8] "Health and Safety Executive: Risk management: Expert guidance," [Online]. Available: https://www.hse.gov.uk.. [Accessed 24 June 2021].

[9] M. T. L. Kotek, "HAZOP study with qualitative risk analysis for prioritization of corrective and preventive actions," *Procedia Engineering,* vol. 42, pp. 808-815, 2012.

[10] F. C. A. Shafaghi, “Application of a Hazard & Operability Study to Hazard Evaluation of an Absorption Heat Pump,” *IEEE Transactions on Reliability,* vol. 37, no. 2, pp. 159-166, June 1988.

[11] J. P. J. Hewitt, “Qualitative Versus Quantitative Methods in Safety Risk Management,” in *2018 Annual Reliability and Maintainability Symposium (RAMS)*, Reno, NV, USA, 2018.

[12] AS/NZS Standard, AS/NZS 4853: Electrical hazards on metallic pipelines, Standards New Zealand, Ministry of Business, Innovation and Employment (MBIE), 2012.

[13] BS EN ISO 18086:2020 Corrosion of metals and alloys - Determination of AC corrosion - Protection criteria, BSI, 2020.

[14] I. B. M. Malekzadeh, “Making an ALARP decision of sufficient testing,” in *2014 IEEE 15th International Symposium on High-Assurance Systems Engineering*, 2014.

[15] N. Abdullah, A. Marican, M. Osman and N. Abdul, “Case study on impact of seasonal variations of soil resistivities on substation grounding system safety in tropic country,” in *7th Asia-Pacific International Conference on Lightning*, Chengdu, China, 2011.

[16] E. Juhlin and R. Braunlich, “AC Corrosion on Metallic Pipelines due to Interference from AC Power Lines - Phenomenon, Modelling and,” eCIGRE , 2006.

[17] SES & Technologies Limited, “Software Packages,” 2023. [Online]. Available: https://www.sestech.com/en/Product/PackageOverview. [Accessed 07 2023].

[18] BSI Vol. BS EN 505222:2010, *Earthing of power installations exceeding 1 kV a.c.,* BSI Standards Publication, 2010.

[19] S. P. K. Suresh, “Transferred Potential—A Hidden Killer of Many Linemen,” *IEEE Transactions on Industry Applications,* vol. 51, no. 3, pp. 2691-2699, May-June 2015.

[20] R. N. Deo, R. M. Azoor and J. K. Kodikara, “Proof of concept using numerical simulations for pipe corrosion inferences using ground penetrating radar,” in *9th International Workshop on Advanced Ground Penetrating Radar (IWAGPR)*, Edinburgh, 2017.

[21] SLB, “1870s–1910s: An Early Passion,” SLB, 2023. [Online]. Available: https://www.slb.com/about/who-we-are/our-history/1870-1910s. [Accessed 1 10 2023].

[22] IEEE Std 81: IEEE Guide for Measuring Earth Resistivity, Ground Impedance, and Earth Surface Potentials of a Grounding System, IEEE, 2012.

[23] W. e. a. Ruan, “Effective sounding depths for HVDC grounding electrode,” in *IEEE/PES Transmission & Distribution Conference & Exposition: Asia and Pacific (2005)*, 2005.

[24] Telecommunication Standardization Sector of ITU, “Series K: Protection Against Interference,” International Telecommunication Union , 1996.

[25] IEEE Std 80-2000, *IEEE Guide for Safety in AC Substation Grounding,* IEEE, 2000.

[26] New Zealand, “Electricity (Safety) Regulation,” 2010. [Online]. Available: https://www.legislation.govt.nz/regulation/public/2010/0036/latest/DLM2763732.html. [Accessed July 2023].

[27] C. Dalziel, “Miniature differential circuit breaker”. United States Patent US-3213321-A, 19 October 1965.

[28] C. F. Dalziel, “Effects of Electric Current on Man,” *Electrical Engineering,* vol. 60, no. 2, 1941.

[29] C. F. Dalziel, “Effects of Electric Shock on Man,” *IRE Transactions on Medical Electronics,* Vols. PGME-5, 1956.

[30] C. K. Das, et al., “Renewable and Sustainable Energy Reviews,” *Journal of Energy Storage,* vol. 91, pp. 1205-1230, 2018.

[31] BS EN 50321: Electrically insulating footwear for working on low voltage installations, BSI, 2018.

[32] BS 7354: , “BS 7354: Code of practice for Design of high-voltage ope-terminal stations,” BSi, 1990.

[33] Ministry of Transport, “The number of road deaths — daily, quarterly, historically and over holiday periods,” New Zealand Government, [Online]. Available: https://www.transport.govt.nz/statistics-and-insights/road-transport/sheet/vehicle-kms-travelled-vkt. [Accessed 1 09 2023].

[34] One News, “National wants to spend at least $30 million to reverse speed limit ...,” TVNZ, [Online]. Available: https://www.1news.co.nz/2023/09/24/national-to-spend-at-least-30m-to-reverse-speed-limit-changes-if-elected/. [Accessed 1 10 2023].

[35] Pennington, P., “Wellington hostel fire: Firefighters ‘pretty cut up’ they couldn’t rescue more people as second ladder truck unavailable,” NZME, [Online]. Available: https://www.nzherald.co.nz/nz/wellington-hostel-fire-firefighters-pretty-cut-up-they-couldnt-rescue-more-people-as-second-ladder-truck-unavailable/37JYISHKZ5GYDLPXAD2EAYKR7A/. [Accessed 1 7 2023].

[36] OECD, “New Zealand Road Safety - International Transport Forum,” OECD, [Online]. Available: https://www.itf-oecd.org/sites/default/files/new-zealand-road-safety.pdf. [Accessed 1 9 2023].

[37] NIWA, “NIWA Weather,” National Institute of Water and Atmospheric Research, [Online]. Available: https://weather.niwa.co.nz/. [Accessed 1 7 2023].

[38] A. Amin et al., “Assessing electrocution risks in transmission substations using probabilistic criteria,” in *48th International Universities' Power Engineering Conference (UPEC)*, Dublin, Ireland, 2013.

[39] A. Madikizela, M. Kabeya and I. E. Davidson, “Seasonal Variation of Soil Resistivity and Corrective Factor for Optimal Substation Earth Grid Design in Eastern Cape,” in *30th Southern African Universities Power Engineering Conference (SAUPEC)*, Durban, South Africa, 2022.

[40] C. Prabhakar and R. A. Deshpande, “Evaluation Of Soil Resistivity And Design Of Grounding System For Hydroelectric Generating Station In A Hilly Terrain — A Case Study,” in *International Conference on Advances in Energy Conversion Technologies (ICAECT)*, 2014.

[41] Wang, C., Liang, X., Freschi, F., “Investigation of factors affecting induced voltages on underground pipelines due to inductive coupling with nearby transmission lines,” *IEEE Transaction in Industrial Applications,* vol. 2, no. 56, pp. 1266-1274, 2020.

[42] Christy Thomas, Eskom Holdings SOC Ltd, “Seasonal variation of soil resistivity and the correction factor,” in *Cigre 8th Southern Africa Regional Conference*, 2017.

[43] F. E. Asimakopoulou, G. J. Tsekouras and I. F. Gonos, “An Artificial Neural Network For Estimating The Ground Resistance,” in *International Conference on Grounding and Earthing & 4th International Conference on Lightning Physics and Effects*, 2001.

[44] F. E. Asimakopoulou, G. J. Tsekouras, I. F. Gonos and I. A. Stathopulos, “Artificial Neural Network Approach On The Seasonal Variation Of Soil Resistance,” in *IEEE 7th Asia-Pacific International Conference on Lightning*, 2011.

[45] F. ASIMAKOPOULOU, E. KOURNI, V. KONTARGYRI, G. TSEKOURAS and I. STATHOPULOS, “Artificial Neural Network Methodology For The Estimation Of Ground Resistance,” in *Recent Researches in System Science, WSEAS Conference*, 2011.

[46] F. E. Asimakopouloua, G. J. TsekourasbIoannis, F. GonosaIoannis and A. Stathopulos, “Estimation Of Seasonal Variation Of Ground Resistance Using Artificial Neural Networks,” *Electric Power Systems Research,* vol. 94, pp. 113-121, 2013.

[47] F. E. Asimakopoulou, V. T. Kontargyri, G. J. Tsekouras and I. F. Gonos, “Estimation Of The Earth Resistance By Artificial Neural Network Model,” *IEEE Transactions on Industry Applications,* vol. 51, no. 6, 2015.

[48] F. King, R. Given and G. V. Boven, “Effect of Transitions in the Water Table and Soil Moisture Content on the Cathodic Protection of Buried Pipelines,” in *Journal of Pressure Vessel Technology 133*, 2006.

[49] J. He, R. Zeng, Y. Gao, Y. Tu, W. Sun, J. Zou and Z. Guan, “Seasonal influences on safety of substation grounding system,” *IEEE Transactions on Power Delivery,* vol. 18, no. 3, 2003.

[50] J. He, G. Yu, J. Yuan, R. Zeng, B. Zhang, J. Zou and Z. Guan, “Decreasing grounding resistance of substation by deep-ground-well method,” *IEEE Transactions on Power Delivery,* vol. 20, no. 2, 2005.

[51] J. He, Y. Gao, R. Zeng, W. Sun, J. Zou and Z. Guan, “Optimal design of grounding system considering the influence of seasonal frozen soil layer,” *IEEE Transactions on Power Delivery,* vol. 20, no. 1, 2005.

[52] R. Zeng, J. He, Z. Wang, Y. Gao, W. Sun and Q. Su, “Analysis on influence of long vertical grounding electrodes on grounding system for substation,” in *PowerCon 2000. 2000 International Conference on Power System Technology. Vol 3.*, 2000.

[53] J. T. Afa and C. Anaele, “Seasonal Variation of Soil Resistivity and Soil Temperature in Bayelsa State,” *American J. of Engineering and Applied Sciences ,* vol. 3, pp. 704-709, 2010.

[54] K. K. M. Rezende, L. Rodrigues, P. H. M. Campos, W. P. Calixto and G. P. Furriel, “Technique development to improve electrical grounding systems performance,” in *2017 CHILEAN Conference on Electrical, Electronics Engineering, Information and Communication Technologies (CHILECON)*, 2017.

[55] L. Li, X. Cui, T. Lu and H. Yin, “Influence of soil and conductor of ground grid on safety of the grounding system,” in *IEEE International Symposium on Electromagnetic Compatibility. Vol 2.*, 2000.

[56] M. G. Unde and B. E. Kushare, “Impact of seasonal variation of soil resistivity on safety of substation grounding system,” in *Fifth International Conference on Advances in Recent Technologies in Communication and Computing*, 2013.

[57] P. Lagace, M. H. Vuong, M. Lefebvre and J. Fortin, “Multilayer resistivity interpretation and error estimation using electrostatic images,” *IEEE Transactions on Power Delivery,* vol. 21, no. 4, 2006.

[58] Q. Louw and P. Bokoro, “Soil resistivity: Field tests and estimation of zero-sequence currents,” in *2017 IEEE AFRICON*, 2017.

[59] Gustafson, R.J.; Pursley, R.; Albertson, V.D., “Seasonal grounding resistance variations on distribution systems,” *IEEE Transactions on Power Delivery,* vol. 5, no. 2, 1990.

[60] S. Sakamoto, “Alma Memo No. 346 Spatial Distribution Of Near-Surface Soil Resistivity In The Cerro Chasc´On Science Preserve,” National Astronomical Observatory of Japan Mitaka, Tokyo 181-8588, Japan, 2001.

[61] S. Sakamoto, “Alma Memo No. 369 Seasonal And Diurnal Variation Of Upper Soil Resistivity In The Cerro Chasc´On Science Preserve,” National Astronomical Observatory of Japan, 2001.

[62] T. A. Papadopoulos, O. Ceylan and G. K. Papagiannis, “Two-layer earth structure parameter estimation and seasonal analysis,” in *2018 53rd International Universities Power Engineering Conference (UPEC)*, 2018.

[63] Androvitsaneas, V. P.; Gonos, I. F.; Stathopulos, I. A., “Wavelet Neural Network For Ground Resistance Estimation,” in *2014 ICHVE International Conference on High Voltage Engineering and Application*, 2014.

[64] V. P. Androvitsaneas, G. J. Tsekouras, I. F. Gonos and I. A. Stathopulos, “Design Of An Artificial Neural Network For Ground Resistance Forecasting,” in *MedPower 2014-9th Mediterranean Conference on Power Generation, Transmission, Distribution and Energy Conversion*, 2014.

[65] V. P. Androvitsaneas and I. F. Gonos, “Ground Resistance Estimation Using Inductive Machine Learning,” in *The 19th International Symposium on High Voltage Engineering*, Pilsen, Czech Republic, 2015.

[66] V. P. Androvitsaneas, G. J. Tsekouras, Ioannis and F. Gonos, “Seasonal Variation and Timeless Evolution of Ground Resistance,” in *2018 IEEE International Conference on High Voltage Engineering and Application (ICHVE)*, 2018.

[67] W. Fieltsch, F. Shahinas, E. Gudino and T. Wymenga, “Effects of Seasonal Variation on AC Interference and Mitigation Design,” in *NACE-2018-11231*, 2018.

[68] X. Long, M. Dong, W. Xu and Y. W. Li, “Online Monitoring Of Substation Grounding Grid Conditions Using Touch And Step Voltage Sensors,” *IEEE Transactions on Smart Grid ,* vol. 3, no. 2, 2012.

[69] Operations Technology, Inc. (OTI), “ETAP,” 17 Goodyear, Suite 100, Irvine, CA, 92618-1812.

[70] Electric Power Research Institute (EPRI), “SGW,” 3412 Hillview Avenue, Palo Alto, CA, 94304.

[71] Electric Power Research Institute (EPRI), “SDWorkstation,” 3412 Hillview Avenue, Palo Alto, CA 94304.

[72] Krishnav Bhatia; Pranav B. Darji ; Hitesh R. Jariwala, “Evaluation of sustainability of microgrid grounding grid design under varying soil conditions through estimation of touch, step voltages and novel methods of earthing,” *IET Science, Measurement & Technology,* vol. 14, no. 5, pp. 621-632, 2020.

[73] K. Adedeji, A. Ponnle, B. Abe and A. Jimoh, “Effect of increasing energy demand on the corrosion rate of buried pipelines in the vicinity of high voltage overhead transmission lines,” in *2015 Intl Aegean Conference on Electrical Machines & Power Electronics (ACEMP), 2015 Intl Conference on Optimization of Electrical & Electronic Equipment (OPTIM) & 2015 Intl Symposium on Advanced Electromechanical Motion Systems (ELECTROMOTION)*, 2015.

[74] Stet, D., Ponnle, A., Abe, B., Jimoh A., “Case studies on electromagnetic interference between HVPL and buried pipelines.,” in *International Conference and Exposition on Electrical and Power Engineering (EPE)*, 2014.

[75] M.A. El-Kady; M.Y. Vainberg, “Risk assessment of grounding hazards due to step and touch potentials near transmission line structures,” *IEEE Transactions on Power Apparatus and Systems,* Vols. PAS-102, no. 9, pp. 3080-3087, 1983.

[76] NetworkRail, “Safe by Design Groups / Health and Safety by Design groups,” Network Rail, 2023. [Online]. Available: https://safety.networkrail.co.uk/safety/prevention-through-engineering-and-design/safe-by-design-groups/. [Accessed 11 10 2023].

[77] Safe Work Australia, “Managing health and safety,” Safe Work Australia, 2023. [Online]. Available: https://www.safeworkaustralia.gov.au/safety-topic/managing-health-and-safety/safe-design. [Accessed 11 10 2023].

[78] Worksafe Mahi Haumaru Aotearoa, “Health and safety by design: an introduction,” New Zealand Government, 2023. [Online]. Available: https://www.worksafe.govt.nz/topic-and-industry/health-and-safety-by-design/health-and-safety-by-design-gpg/. [Accessed 11 10 2023].

[79] DIgSILENT, “DIGSILENT | Power System Solution,” [Online]. Available: https://www.digsilent.de/en/powerfactory.html. [Accessed 1 7 2020].

[80] FirstGas, “Network Map,” [Online]. Available: https://firstgas.co.nz/our-network/network-map/. [Accessed 11 09 2023].

[81] Electricity Authority Te Mana Hiko, “Wholesale datasets DIgSILENT Powerfactory case files,” [Online]. Available: emi.ea.govt.nz/Wholesale/Datasets/Transmission/PowerSystemAnalysis/PowerFactoryCaseFiles. [Accessed 1 6 2023].

[82] “Local Government Local Government,” Council Auckland: Retrolens Historic Image Resource, 2015. [Online]. Available: https://retrolens.co.nz.. [Accessed 1 4 2021].

[83] Institute of Geological and Nuclear Science Limited, “1:250 000 geological map 3,” Institute of Geological and Nuclear Science, Auckland, New Zealand, 2001.

[84] Smith, I., O’Connor, B., Roland, J, “Geology Rocks & Minerals,” The University of Auckland, 2005. [Online]. Available: https://flexiblelearning.auckland.ac.nz/rocks_minerals/rocks/limestone.html. [Accessed 21 3 2021].

[85] Transpower (NZ) Limited, “Maps and GIS Data,” [Online]. Available: https://www.transpower.co.nz/our-work/industry/our-grid/maps-and-gis-data. [Accessed 11 09 2023].

[86] AEMC Instruments , “Ground Resistance Tester Model 6471,” 09 2023. [Online]. Available: https://www.aemc.com/userfiles/files/resources/usermanuals/Ground-Testers/6471_EN.pdf. [Accessed 30 09 2023].

[87] Duoyi Instrument, “DY4300B DIGITAL 4-TERMINAL EARTH RESISTANCE AND SOIL RESISTIVITY TESTER,” 2023. [Online]. Available: https://www.dyinstrument.com/duoyi/DY4300b_digital_earth_resistance_and_soil_resistivity_tester. [Accessed 30 09 2023].

[88] J.W. Cohen, Statistical Power Analysis for Behavioral Science @nd Ed., NJ: Lawrence Erlbaum Associates, 1988.

[89] IBM Corp. , “IBM SPSS Statistics for Windows (Version 27.0) [Computer software],” IBM Corp, 2020.

[90] R. C. Fraley et al., “The N-pact factor: Evaluating the quality of empirical journals with respect to sample size and statistical power,” *PLOS One,* vol. 9, no. 10, 2014.

[91] National Institute of Water and Atmospheric Research, “Software tools,” [Online]. Available: https://niwa.co.nz/our-services/software-tools. [Accessed 1 7 2023].

[92] Transpower (NZ) Limited, “Variable Line Ratings.xlsx,” [Online]. Available: https://static.transpower.co.nz/public/bulk-upload/documents/Variable%20Line%20Ratings.xlsx?VersionId=L8cT3GaGUkSO7.xDmVkOCcOXsR6DHeRu. [Accessed 1 6 2023].

[93] Transpower (NZ) Limited, “Lines Asset Drawings - NL2,” [Online]. Available: https://static.transpower.co.nz/public/plain-page/attachments/Lines_Asset_Drawings_NL2.pdf?VersionId=derBbndCgioMgEGJ6xGMRuht5OXpt1LX. [Accessed 1 6 2023].

[94] Electricity Authority Te Mana Hiko NZ, “Wholesale datasets DIgSILENT Powerfactory case files,” NZ Government , 2023. [Online]. Available: https://www.emi.ea.govt.nz/Wholesale/Datasets/Transmission/PowerSystemAnalysis/PowerFactoryCaseFiles. [Accessed 09 2023].

[95] M. Boas, Mathematical Methods in the Physical Sciences, 3rd Ed., New York: John Wiley & Sons, 2005.

[96] Koo, T.K., Li, M.Y., “A guideline of selecting and reporting intraclass correlation,” *J. Chiropractic Med.,* vol. 15, no. 2, pp. 155-163, 2016.

[97] G. R. Cooper, “Aspects of chaotic dynamics in the least-squares inversion of gravity data,” *Computer & Graphics,* vol. 25, no. 4, pp. 691-697, August 2001.

[98] J. Hohnson, et al., “Dynamic line rating oncor electric delivery smart grid program,” Oncor Electric Delivery Company Llc, 2013.

[99] Chan, K.M.K.; Baguley, C.A.; Madawala, U.K., “A novel approach to touch voltage risk assessment for gas pipelines in shared transmission corridors,” *IET Sci. Meas. Technol.,* vol. 17, pp. 27-36, 2023.

[100] B. M. Vasantrao, P. J. Bhaskarrao and B. A. Mukund, “Comparative study of Wenner and Schlumberger electrical resistivity method for groundwater

investigation: a case study from Dhule district(M.S.), India," *Applied Water Science,* vol. 7, 2017.

[101] Jinliang He et al., "Seasonal influences on safety of substation grounding system," *IEEE Transactions on Power Delivery,* vol. 18, no. 3, pp. 788-795, 2003.

[102] Google Earth Pro, "Whakamaru Hydroelectric Power Station 38°25'1.07"S 175°48'1.45"E," [Online]. Available: http://www.google.com/earth/index.html. [Accessed 1 6 2023].

[103] New Zealand Legislation, "Electricity (Safety) Regulations," Parliamentary Counsel Office, New Zealand, 2010.

[104] R.D. Southey, et al., "Using Fall-of-Potential Measurements to Improve Deep Soil Resistivity Estimates," *IEEE Transactions on Industry Applications,* vol. 51, no. 6, pp. 5023-5029, 2015.

Appendix A – Reduction of Wenner Test Traverse

The maximum spacing was reduced iteratively to identify soil resistivity modelling from the soil resistivity data collected in the Pre-test survey with a maximum test spacing of 40 m. This process aimed to identify the shortest Wenner test traverse that could maintain the integrity and accuracy of the soil model while avoiding distortion. The iterative steps are shown in Figures A-1 to A-4.

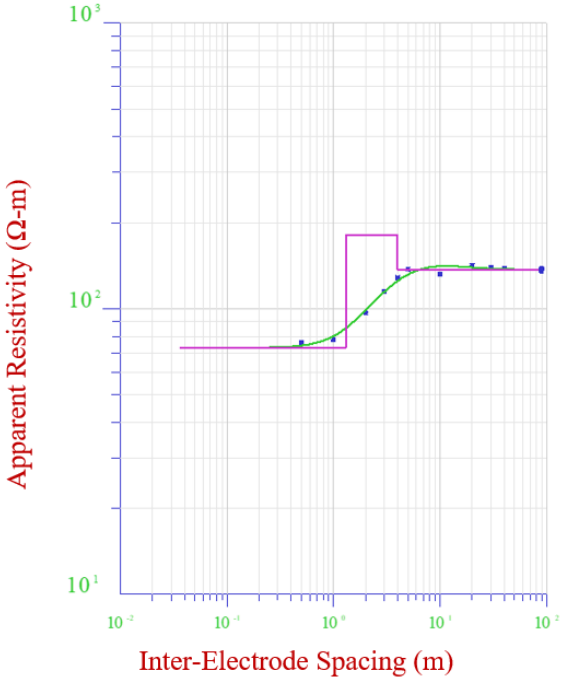

Measurement Method : Wenner

RMS error : 3.02%

Layer #	Resistivity (Ω-m)	Thickness (m)
Air	Infinite	Infinite
2	73.05	1.31
3	180.49	2.69
4	136.74	Infinite

Figure A-1 Soil resistivity model for Traverse 6 with a maximum spacing of 40 m.

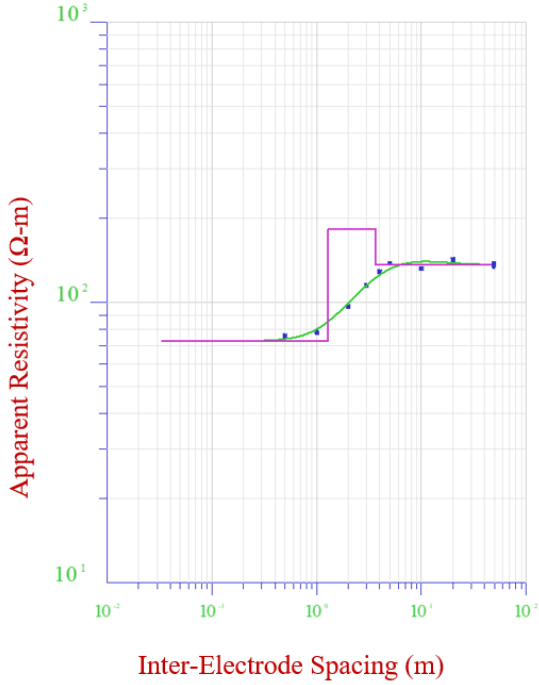

Measurement Method : Wenner

RMS error : 3.31%

Layer #	Resistivity (Ω-m)	Thickness (m)
Air	Infinite	Infinite
2	72.65	1.28
3	182.42	2.39
4	135.79	Infinite

Figure A-2 Soil resistivity model for Traverse 6 with a maximum spacing of 30 m.

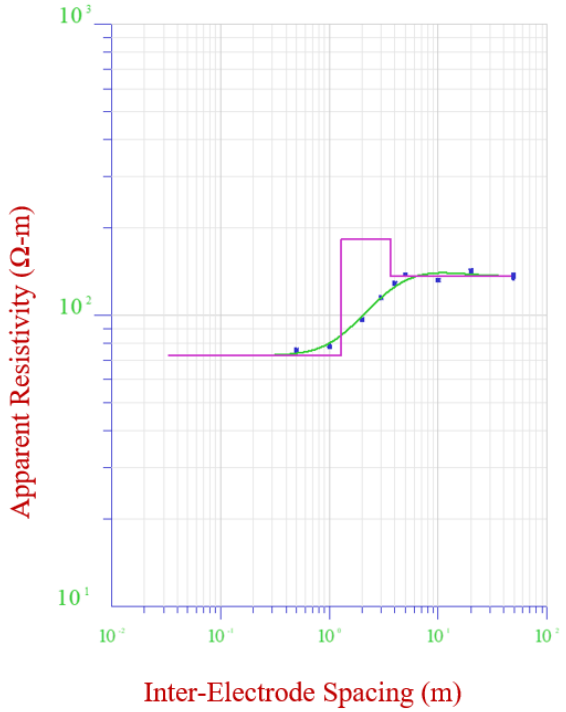

Measurement Method : Wenner

RMS error : 3.43%

Layer #	Resistivity (Ω-m)	Thickness (m)
Air	Infinite	Infinite
2	71.61	1.28
3	182.41	2.29
4	132.71	Infinite

Figure A-3 Soil resistivity model for Traverse 6 with a maximum spacing of 20 m.

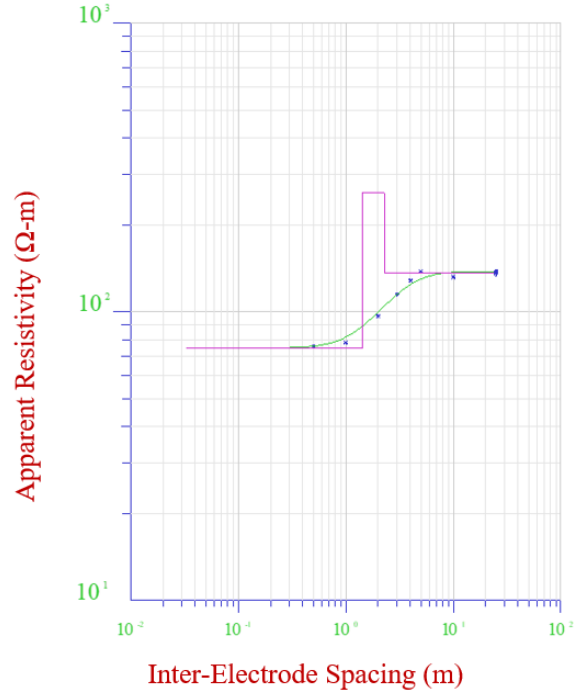

Measurement Method : Wenner

RMS error : 3.53%

Layer #	Resistivity (Ω-m)	Thickness (m)
Air	Infinite	Infinite
2	74.83	1.44
3	258.23	0.85
4	136.27	Infinite

Figure A-4 Soil resistivity model (distorted) for Traverse 6 with a maximum spacing of 10 m.

Appendix B - Data Collection and Data Processing

The twice-weekly soil resistivity data collection was begun on 16/07/2020 and finished on 15/05/2021. The collected data was measured. The measured apparent soil resistance, calculated apparent soil resistivity, soil resistivity model (unadjusted), soil resistivity model (warm-starting), and climate information from NIWA [37] are shown in Table B-1.

Table B-1 Twelve-month data collection. Soil resistances are measured in (Ω), and soil resistivities are calculated in (Ω-m).

Date	26/07/2020	29/07/2020	1/08/2020	5/08/2020	9/08/2020	12/08/2020
Soil Resistance Measurement						
Wenner Spacing (m)						
0.1	95.49	96.29	95.81	101.50	96.60	92.37
0.2	49.34	48.54	48.54	51.10	48.62	46.55
0.5	21.65	21.71	21.68	22.14	21.06	20.43
1	13.37	13.37	13.32	13.83	13.23	13.12
2	7.96	8.12	8.16	8.95	8.71	8.71
3	5.41	5.46	5.47	6.39	6.28	6.28
4	4.10	4.14	4.14	4.81	4.73	4.72
5	3.31	3.28	3.28	3.77	3.71	3.68
10	1.59	1.59	1.62	1.71	1.65	1.61
15	1.00	1.00	1.07	1.09	1.04	1.02
20	0.72	0.72	0.80	0.81	0.77	0.75
Calculated Soil Resistivity						
Wenner Spacing (m)						
0.1	60.00	60.50	60.20	63.77	60.70	58.04
0.2	62.00	61.00	61.00	64.21	61.10	58.50
0.5	68.00	68.20	68.10	69.57	66.15	64.17
1	84.00	84.00	83.70	86.92	83.10	82.42
2	100.00	102.00	102.50	112.44	109.40	109.50
3	102.00	103.00	103.20	120.53	118.38	118.34
4	103.00	104.00	104.10	120.83	118.98	118.57
5	104.00	103.00	103.10	118.51	116.53	115.71
10	100.00	100.00	102.00	107.23	103.44	101.36
15	94.00	94.00	100.50	103.04	98.33	95.88
20	91.00	91.10	100.10	101.44	96.37	93.82
Soil Model Unadjusted						
Layer-0 Resitivity (Ω-m)						
Layer-0 Thickness (m)						
Layer-1 Resitivity (Ω-m)	60.86	60.36	61.23	63.71	60.64	57.97
Layer-1 Thickness (m)	0.75	0.66	0.72	0.73	0.76	0.72
Layer-2 Resitivity (Ω-m)	222.11	212.78	218.32	212.58	221.67	225.87
Layer-1 Thickness (m)	1.17	1.45	1.12	1.12	1.16	1.17
Bottom Resitivity (Ω-m)	92.18	94.62	97.44	99.43	93.97	91.31
RMS Error	2.4%	3.4%	3.2%	2.1%	2.1%	3.7%
Soil Model (warm-start)						
Layer-0 Resitivity (Ω-m)						
Layer-0 Thickness (m)						
Layer-1 Resitivity (Ω-m)	60.86	61.74	61.52	63.92	60.22	57.24
Layer-1 Thickness (m)	0.75	0.75	0.72	0.68	0.67	0.67
Layer-2 Resitivity (Ω-m)	222.11	178.06	166.66	186.60	193.03	201.22
Layer-1 Thickness (m)	1.17	1.03	0.98	1.03	1.05	1.07
Bottom Resitivity (Ω-m)	92.18	90.80	97.16	102.40	97.27	94.02
RMS Error	2.4%	3.5%	3.2%	2.1%	2.1%	3.7%
Climate info from NIWA						
3-day culmulative rain (mm)	0.2	0	0.2	0	3.6	14.4
Soil Temperature 5 cm (°C)	9.8	8.4	10.9	8.1	9.1	11.7
Soil Temperature 10 cm (°C)	10.4	9.4	11.2	9.5	10.1	11.8

Continue Table B-1 Twelve-month data collection. Soil resistances are measured in (Ω), and soil resistivities are calculated in (Ω-m).

Date	16/08/2020	19/08/2020	22/08/2020	26/08/2020	29/08/2020	1/09/2020
Soil Resistance Measurement						
Wenner Spacing (m)						
0.1	97.24	94.11	93.20	89.41	93.33	93.62
0.2	49.00	47.42	46.95	45.09	47.03	47.22
0.5	21.45	20.76	20.52	19.90	20.62	20.84
1	13.61	13.31	13.13	12.88	13.18	13.42
2	8.85	8.91	8.75	8.56	8.67	8.79
3	6.32	6.45	6.31	6.17	6.22	6.28
4	4.75	4.84	4.74	4.63	4.67	4.71
5	3.73	3.74	3.70	3.62	3.64	3.68
10	1.69	1.54	1.60	1.59	1.61	1.64
15	1.09	0.94	1.00	1.01	1.02	1.05
20	0.80	0.68	0.73	0.74	0.75	0.77
Calculated Soil Resistivity						
Wenner Spacing (m)						
0.1	61.10	59.13	58.56	56.18	58.64	58.82
0.2	61.58	59.58	59.00	56.66	59.10	59.34
0.5	67.39	65.22	64.48	62.52	64.77	65.48
1	85.50	83.60	82.49	80.93	82.80	84.30
2	111.15	111.92	109.90	107.62	109.00	110.48
3	119.15	121.62	119.00	116.21	117.24	118.35
4	119.48	121.56	119.20	116.44	117.28	118.26
5	117.26	117.59	116.12	113.70	114.48	115.54
10	106.46	96.68	100.51	100.04	101.12	103.06
15	102.46	88.26	94.50	94.84	96.14	98.52
20	100.94	85.11	92.24	92.89	94.28	96.82
Soil Model Unadjusted						
Layer-0 Resitivity (Ω-m)						
Layer-0 Thickness (m)						
Layer-1 Resitivity (Ω-m)	61.03	59.06	58.50	56.11	58.57	58.75
Layer-1 Thickness (m)	0.70	0.72	0.74	0.70	0.71	0.69
Layer-2 Resitivity (Ω-m)	209.97	216.90	231.19	219.68	217.75	214.97
Layer-1 Thickness (m)	1.11	1.58	1.20	1.17	1.16	1.13
Bottom Resitivity (Ω-m)	99.01	81.54	89.54	90.50	91.99	94.71
RMS Error	2.3%	3.2%	2.2%	3.2%	2.3%	2.7%
Soil Model (warm-start)						
Layer-0 Resitivity (Ω-m)						
Layer-0 Thickness (m)						
Layer-1 Resitivity (Ω-m)	59.24	58.33	57.33	53.74	55.62	56.42
Layer-1 Thickness (m)	0.66	0.66	0.67	0.69	0.68	0.68
Layer-2 Resitivity (Ω-m)	203.80	227.01	227.35	223.20	224.37	224.96
Layer-1 Thickness (m)	1.08	1.16	1.16	1.15	1.16	1.16
Bottom Resitivity (Ω-m)	97.11	85.75	88.72	89.49	90.47	91.30
RMS Error	2.4%	3.2%	2.2%	3.2%	2.3%	2.8%
Climate info from NIWA						
3-day culmulative rain (mm)	0	7.6	6.6	8	0	0
Soil Temperature 5 cm (°C)	7	12.2	11.3	10.7	10.2	12.2
Soil Temperature 10 cm (°C)	8.6	12	11.7	11.4	10.7	12.3

Continue Table B-1 Twelve-month data collection. Soil resistances are measured in (Ω), and soil resistivities are calculated in (Ω-m).

Date	6/09/2020	9/09/2020	13/09/2020	16/09/2020	19/09/2020	23/09/2020
Soil Resistance Measurement						
Wenner Spacing (m)						
0.1	99.89	99.42	103.26	100.79	99.70	102.53
0.2	50.25	50.07	51.96	50.76	50.21	51.61
0.5	21.63	21.78	22.44	22.09	21.85	22.31
1	13.38	13.69	13.93	13.87	13.76	13.87
2	8.66	8.88	8.97	8.98	8.96	8.95
3	6.22	6.35	6.41	6.41	6.42	6.43
4	4.71	4.78	4.83	4.83	4.84	4.87
5	3.71	3.75	3.79	3.79	3.80	3.86
10	1.70	1.70	1.73	1.73	1.73	1.80
15	1.09	1.09	1.11	1.11	1.11	1.16
20	0.81	0.81	0.82	0.82	0.82	0.86
Calculated Soil Resistivity						
Wenner Spacing (m)						
0.1	62.76	62.47	64.88	63.33	62.65	64.42
0.2	63.14	62.91	65.30	63.79	63.10	64.85
0.5	67.96	68.43	70.51	69.39	68.65	70.10
1	84.06	86.03	87.51	87.18	86.47	87.12
2	108.79	111.60	112.71	112.82	112.58	112.42
3	117.29	119.72	120.82	120.90	121.08	121.14
4	118.26	120.13	121.28	121.28	121.66	122.46
5	116.54	117.93	119.17	119.10	119.53	121.20
10	106.76	107.06	108.63	108.41	108.53	113.05
15	102.91	103.00	104.68	104.44	104.35	109.79
20	101.41	101.44	103.16	102.92	102.75	108.51
Soil Model Unadjusted						
Layer-0 Resitivity (Ω-m)						
Layer-0 Thickness (m)						
Layer-1 Resitivity (Ω-m)	62.71	62.40	64.82	63.26	62.58	64.36
Layer-1 Thickness (m)	0.76	0.72	0.74	0.72	0.72	0.73
Layer-2 Resitivity (Ω-m)	205.40	211.08	209.92	211.82	215.30	205.64
Layer-1 Thickness (m)	1.11	1.11	1.11	1.10	1.11	1.07
Bottom Resitivity (Ω-m)	99.50	99.48	101.24	101.00	100.72	106.83
RMS Error	2.6%	3.2%	3.0%	2.2%	2.3%	2.2%
Soil Model (warm-start)						
Layer-0 Resitivity (Ω-m)						
Layer-0 Thickness (m)						
Layer-1 Resitivity (Ω-m)	60.82	62.40	60.82	60.82	60.82	62.40
Layer-1 Thickness (m)	0.69	0.72	0.64	0.66	0.68	0.68
Layer-2 Resitivity (Ω-m)	221.25	211.08	200.76	207.26	209.51	200.06
Layer-1 Thickness (m)	1.15	1.11	1.11	1.11	1.13	1.11
Bottom Resitivity (Ω-m)	97.27	99.48	101.89	101.26	100.99	106.92
RMS Error	2.6%	3.2%	3.0%	2.2%	2.3%	2.2%
Climate info from NIWA						
3-day culmulative rain (mm)	0	0	0	3	5.4	0
Soil Temperature 5 cm (°C)	11.3	9.3	11	12.4	11.5	12.1
Soil Temperature 10 cm (°C)	11.5	10.1	11.2	12.6	11.8	12.2

Continue Table B-1 Twelve-month data collection. Soil resistances are measured in (Ω), and soil resistivities are calculated in (Ω-m).

Date	26/09/2020	30/09/2020	3/10/2020	7/10/2020	11/10/2020	12/10/2020
Soil Resistance Measurement						
Wenner Spacing (m)						
0.1	103.05	101.14	105.62	135.90	281.83	191.50
0.2	51.82	50.86	53.03	68.01	135.84	94.61
0.5	22.25	21.81	22.39	27.53	42.45	33.87
1	13.73	13.48	13.43	14.57	16.72	14.20
2	8.92	8.84	8.74	8.43	8.80	7.78
3	6.42	6.40	6.37	6.10	6.15	6.01
4	4.85	4.85	4.84	4.72	4.68	4.89
5	3.82	3.82	3.82	3.80	3.76	4.08
10	1.73	1.72	1.71	1.83	1.88	2.07
15	1.10	1.10	1.08	1.19	1.25	1.35
20	0.81	0.81	0.79	0.88	0.94	1.00
Calculated Soil Resistivity						
Wenner Spacing (m)						
0.1	64.75	63.55	66.36	85.39	177.08	120.32
0.2	65.12	63.91	66.64	85.46	170.70	118.89
0.5	69.91	68.53	70.34	86.47	133.37	106.40
1	86.29	84.69	84.37	91.57	105.08	89.21
2	112.12	111.07	109.83	105.91	110.65	97.75
3	121.07	120.71	120.06	114.93	115.95	113.30
4	121.93	121.95	121.74	118.57	117.67	122.96
5	119.87	120.01	119.96	119.37	118.15	128.06
10	108.44	108.08	107.35	115.01	117.99	130.34
15	103.95	103.21	101.92	112.10	117.76	127.13
20	102.22	101.31	99.76	110.78	117.64	125.05
Soil Model Unadjusted						
Layer-0 Resitivity (Ω-m)					178.21	120.57
Layer-0 Thickness (m)					0.36	0.51
Layer-1 Resitivity (Ω-m)	64.69	63.50	66.33	85.39	63.14	51.38
Layer-1 Thickness (m)	0.78	0.79	0.87	1.30	0.54	0.75
Layer-2 Resitivity (Ω-m)	219.12	225.91	226.96	183.65	263.23	234.14
Layer-1 Thickness (m)	1.12	1.13	1.18	1.17	0.28	1.52
Bottom Resitivity (Ω-m)	100.03	98.92	97.07	108.89	117.51	121.45
RMS Error	2.3%	2.3%	2.1%	4.3%	6.3%	6.5%
Soil Model (warm-start)						
Layer-0 Resitivity (Ω-m)					177.86	120.89
Layer-0 Thickness (m)					0.36	0.48
Layer-1 Resitivity (Ω-m)	62.40	62.40	62.40	84.88	69.15	53.78
Layer-1 Thickness (m)	0.70	0.75	0.75	1.11	0.61	0.77
Layer-2 Resitivity (Ω-m)	209.35	215.75	215.68	163.77	156.48	239.98
Layer-1 Thickness (m)	1.14	1.18	1.19	1.14	0.98	1.23
Bottom Resitivity (Ω-m)	100.53	99.16	97.96	110.61	116.57	123.41
RMS Error	2.3%	2.3%	2.1%	4.3%	3.2%	2.9%
Climate info from NIWA						
3-day culmulative rain (mm)	0	0.8	0.2	0	0	0
Soil Temperature 5 cm (°C)	13.3	11.1	10.9	14.9	14.3	15.4
Soil Temperature 10 cm (°C)	13.4	12	12	15.2	14.6	15.5

Continue Table B-1 Twelve-month data collection. Soil resistances are measured in (Ω), and soil resistivities are calculated in (Ω-m).

Date	14/10/2020	17/10/2020	21/10/2020	25/10/2020	28/10/2020	29/10/2020
Soil Resistance Measurement						
Wenner Spacing (m)						
0.1	280.11	94.72	111.35	632.06	2187.96	1389.14
0.2	140.09	47.72	55.93	169.63	979.76	574.72
0.5	56.28	20.86	23.70	25.58	180.47	84.12
1	28.79	13.29	14.18	12.62	26.49	17.72
2	15.29	8.81	9.01	8.00	10.27	9.51
3	10.34	6.38	6.47	6.18	7.43	7.17
4	7.49	4.83	4.89	4.96	5.65	5.69
5	5.62	3.81	3.85	4.08	4.46	4.62
10	2.01	1.73	1.74	1.99	1.97	2.09
15	1.14	1.11	1.11	1.27	1.23	1.26
20	0.80	0.82	0.82	0.93	0.90	0.90
Calculated Soil Resistivity						
Wenner Spacing (m)						
0.1	176.00	59.52	69.96	397.14	1374.74	872.82
0.2	176.05	59.97	70.29	213.17	1231.20	722.22
0.5	176.80	65.52	74.46	80.37	566.97	264.27
1	180.91	83.53	89.12	79.27	166.43	111.35
2	192.20	110.66	113.24	100.49	129.08	119.47
3	194.93	120.18	121.99	116.44	140.05	135.21
4	188.20	121.43	122.96	124.72	142.09	142.94
5	176.71	119.65	120.99	128.19	140.09	145.07
10	126.39	108.69	109.43	124.79	124.06	131.08
15	106.99	104.26	104.72	119.44	116.27	119.21
20	100.16	102.53	102.87	116.57	113.13	113.40
Soil Model Unadjusted						
Layer-0 Resitivity (Ω-m)				501.14	1402.72	908.71
Layer-0 Thickness (m)				0.11	0.30	0.23
Layer-1 Resitivity (Ω-m)	176.00	59.45	69.92	68.23	83.50	84.19
Layer-1 Thickness (m)	1.56	0.73	0.80	1.23	1.01	1.27
Layer-2 Resitivity (Ω-m)	299.44	223.48	193.23	256.18	266.32	261.22
Layer-1 Thickness (m)	1.77	1.11	1.38	1.33	1.26	1.91
Bottom Resitivity (Ω-m)	93.42	100.34	100.51	112.27	109.39	105.63
RMS Error	3.1%	2.3%	2.1%	8.5%	6.7%	9.3%
Soil Model (warm-start)						
Layer-0 Resitivity (Ω-m)	176.72			300.03	1398.16	797.52
Layer-0 Thickness (m)	0.82			0.27	0.30	0.26
Layer-1 Resitivity (Ω-m)	127.25	59.10	68.72	49.98	77.10	67.95
Layer-1 Thickness (m)	0.44	0.67	0.67	0.71	0.87	0.90
Layer-2 Resitivity (Ω-m)	346.16	192.93	190.64	186.37	227.43	251.67
Layer-1 Thickness (m)	1.61	1.34	1.33	1.41	1.72	1.86
Bottom Resitivity (Ω-m)	94.82	100.72	100.49	104.90	107.91	108.12
RMS Error	3.1%	2.3%	2.1%	3.0%	2.2%	4.3%
Climate info from NIWA						
3-day culmulative rain (mm)	5	0	0	0	0	0
Soil Temperature 5 cm (°C)	13.6	10.9	16.5	17.8	17.6	18
Soil Temperature 10 cm (°C)	14.2	12	16.3	17.5	17.8	18.1

Continue Table B-1 Twelve-month data collection. Soil resistances are measured in (Ω), and soil resistivities are calculated in (Ω-m).

Date	31/10/2020	7/11/2020	8/11/2020	11/11/2020	14/11/2020	18/11/2020
Soil Resistance Measurement						
Wenner Spacing (m)						
0.1	899.01	122.04	93.31	87.03	106.56	118.48
0.2	301.18	61.11	46.87	43.75	53.32	59.26
0.5	39.36	24.95	19.89	18.73	21.55	23.84
1	15.76	13.67	12.12	11.63	11.43	12.34
2	9.71	8.37	8.12	7.88	6.92	7.06
3	7.36	6.18	6.08	5.92	5.37	5.35
4	5.80	4.81	4.74	4.63	4.41	4.38
5	4.67	3.87	3.81	3.75	3.72	3.70
10	2.07	1.82	1.79	1.80	1.96	2.02
15	1.25	1.17	1.15	1.17	1.29	1.36
20	0.89	0.86	0.85	0.87	0.96	1.02
Calculated Soil Resistivity						
Wenner Spacing (m)						
0.1	564.86	76.68	58.63	54.68	66.96	74.44
0.2	378.48	76.80	58.90	54.98	67.00	74.47
0.5	123.65	78.38	62.50	58.85	67.71	74.89
1	99.01	85.89	76.13	73.07	71.79	77.53
2	121.97	105.18	101.99	99.08	86.93	88.67
3	138.65	116.56	114.57	111.65	101.19	100.81
4	145.79	120.93	119.05	116.47	110.90	110.02
5	146.86	121.63	119.71	117.69	116.84	116.29
10	129.96	114.44	112.68	113.34	123.38	126.76
15	117.75	109.82	108.27	110.18	121.76	127.89
20	111.99	107.74	106.31	108.73	120.22	127.82
Soil Model Unadjusted						
Layer-0 Resitivity (Ω-m)	632.73					
Layer-0 Thickness (m)	0.15					
Layer-1 Resitivity (Ω-m)	83.55	76.67	91.52	54.64	66.95	73.57
Layer-1 Thickness (m)	1.17	1.16	1.91	0.82	1.57	0.99
Layer-2 Resitivity (Ω-m)	263.38	200.25	181.30	207.22	207.14	106.98
Layer-1 Thickness (m)	1.89	1.37	1.65	1.17	1.64	1.36
Bottom Resitivity (Ω-m)	104.57	104.86	102.39	106.70	116.96	133.54
RMS Error	13.5%	1.5%	1.4%	4.4%	4.2%	5.6%
Soil Model (warm-start)						
Layer-0 Resitivity (Ω-m)	471.67	76.74				
Layer-0 Thickness (m)	0.19	0.76				
Layer-1 Resitivity (Ω-m)	64.24	91.52	58.59	54.85	66.77	74.44
Layer-1 Thickness (m)	0.78	0.63	0.85	0.84	1.48	1.39
Layer-2 Resitivity (Ω-m)	258.37	201.57	201.91	200.06	195.51	202.22
Layer-1 Thickness (m)	1.86	1.48	1.38	1.37	1.46	1.29
Bottom Resitivity (Ω-m)	106.16	103.23	103.63	105.58	119.18	126.95
RMS Error	7.1%	1.5%	1.4%	0.5%	1.5%	2.0%
Climate info from NIWA						
3-day culmulative rain (mm)	0	0.2	18.8	20	0	0
Soil Temperature 5 cm (°C)	18	18	18.2	16	17.8	19.2
Soil Temperature 10 cm (°C)	18.1	18.2	18.5	16.5	18.1	19.5

Continue Table B-1 Twelve-month data collection. Soil resistances are measured in (Ω), and soil resistivities are calculated in (Ω-m).

Date	21/11/2020	25/11/2020	28/11/2020	2/12/2020	5/12/2020	9/12/2020
Soil Resistance Measurement						
Wenner Spacing (m)						
0.1	1205.09	117.71	94.13	127.42	169.85	280.55
0.2	564.23	58.98	47.20	63.73	84.87	136.72
0.5	132.97	24.28	19.60	25.61	33.70	43.91
1	23.79	13.40	11.33	13.18	16.48	15.43
2	7.53	7.81	7.41	7.40	8.24	7.87
3	5.55	5.55	5.69	5.54	5.76	6.06
4	4.48	4.27	4.59	4.49	4.55	4.98
5	3.76	3.44	3.83	3.77	3.80	4.23
10	2.08	1.73	2.03	1.99	2.11	2.38
15	1.42	1.15	1.37	1.31	1.45	1.64
20	1.08	0.86	1.03	0.97	1.10	1.25
Calculated Soil Resistivity						
Wenner Spacing (m)						
0.1	757.18	73.96	59.15	80.06	106.72	176.27
0.2	709.03	74.12	59.31	80.08	106.65	171.81
0.5	417.74	76.27	61.59	80.45	105.86	137.94
1	149.50	84.17	71.18	82.80	103.55	96.94
2	94.59	98.20	93.13	93.01	103.54	98.94
3	104.57	104.62	107.28	104.41	108.65	114.23
4	112.67	107.20	115.48	112.96	114.45	125.25
5	118.22	108.22	120.32	118.48	119.42	132.86
10	130.42	108.60	127.71	124.72	132.34	149.62
15	133.96	108.35	128.84	123.02	136.78	154.87
20	135.38	108.22	129.11	121.41	138.73	157.09
Soil Model Unadjusted						
Layer-0 Resitivity (Ω-m)	765.62					
Layer-0 Thickness (m)	0.36					
Layer-1 Resitivity (Ω-m)	65.24	73.94	59.13	80.06	106.74	177.03
Layer-1 Thickness (m)	1.72	0.85	0.96	1.94	0.84	0.44
Layer-2 Resitivity (Ω-m)	199.89	129.39	161.30	205.66	89.44	48.60
Layer-1 Thickness (m)	0.24	1.07	1.42	1.60	1.27	0.63
Bottom Resitivity (Ω-m)	137.60	108.01	129.29	117.99	141.80	160.48
RMS Error	6.1%	8.1%	3.6%	3.2%	3.8%	9.6%
Soil Model (warm-start)						
Layer-0 Resitivity (Ω-m)	768.28					174.04
Layer-0 Thickness (m)	0.36					0.43
Layer-1 Resitivity (Ω-m)	72.83	74.55	59.16	79.36	105.55	55.97
Layer-1 Thickness (m)	1.18	1.03	1.00	1.33	1.43	0.72
Layer-2 Resitivity (Ω-m)	200.46	141.79	174.80	138.93	94.34	125.63
Layer-1 Thickness (m)	1.32	1.21	1.34	1.30	1.32	1.20
Bottom Resitivity (Ω-m)	134.45	106.77	128.19	124.80	144.40	161.16
RMS Error	4.2%	2.1%	3.6%	3.2%	3.8%	5.1%
Climate info from NIWA						
3-day culmulative rain (mm)	0	14.6	0	0	0	0
Soil Temperature 5 cm (°C)	18.7	18.1	15.9	15.3	17.6	20.2
Soil Temperature 10 cm (°C)	19.1	17.8	16.8	16.2	18	20.2

Continue Table B-1 Twelve-month data collection. Soil resistances are measured in (Ω), and soil resistivities are calculated in (Ω-m).

Date	12/12/2020	16/12/2020	19/12/2020	26/12/2020	30/12/2020	2/01/2021
Soil Resistance Measurement						
Wenner Spacing (m)						
0.1	309.89	1205.09	534.57	692.75	714.82	146.81
0.2	149.18	564.23	266.77	344.43	345.08	73.44
0.5	44.71	132.97	104.00	128.33	104.07	29.56
1	15.49	23.79	46.24	50.41	32.91	15.26
2	8.46	7.53	17.34	17.24	14.13	8.37
3	6.52	5.55	10.07	10.08	9.74	6.03
4	5.34	4.48	7.31	7.27	7.48	4.81
5	4.51	3.76	5.87	5.74	6.06	4.07
10	2.51	2.08	3.07	2.83	3.10	2.56
15	1.72	1.42	2.08	1.88	2.08	1.98
20	1.31	1.08	1.57	1.41	1.56	1.64
Calculated Soil Resistivity						
Wenner Spacing (m)						
0.1	194.71	757.18	335.88	435.27	449.14	92.24
0.2	187.47	709.03	335.24	432.83	433.64	92.28
0.5	140.45	417.74	326.72	403.15	326.95	92.88
1	97.30	149.50	290.56	316.74	206.78	95.88
2	106.25	94.59	217.85	216.61	177.57	105.13
3	122.97	104.57	189.81	190.06	183.65	113.61
4	134.12	112.67	183.74	182.84	187.97	120.96
5	141.62	118.22	184.39	180.41	190.46	127.89
10	157.67	130.42	193.17	177.94	194.72	160.88
15	162.47	133.96	196.38	177.58	195.69	187.06
20	164.46	135.38	197.77	177.49	196.01	205.78
Soil Model Unadjusted						
Layer-0 Resitivity (Ω-m)		639.04	335.97	435.69	451.78	
Layer-0 Thickness (m)		0.26	1.08	0.72	0.40	
Layer-1 Resitivity (Ω-m)	195.96	49.53	110.88	154.25	121.06	92.25
Layer-1 Thickness (m)	0.39	0.57	0.84	0.70	0.64	1.22
Layer-2 Resitivity (Ω-m)	49.14	142.86	158.43	183.23	240.70	124.67
Layer-1 Thickness (m)	0.56	0.20	0.20	0.20	0.20	5.01
Bottom Resitivity (Ω-m)	167.45	167.67	199.87	177.35	196.50	271.33
RMS Error	12.2%	10.3%	7.2%	5.1%	5.5%	2.3%
Soil Model (warm-start)						
Layer-0 Resitivity (Ω-m)	164.01	754.63	763.85	762.70	451.10	
Layer-0 Thickness (m)	0.60	0.37	0.36	0.37	0.40	
Layer-1 Resitivity (Ω-m)	69.82	65.62	65.29	62.93	127.58	94.04
Layer-1 Thickness (m)	1.16	1.19	1.09	1.03	0.87	1.85
Layer-2 Resitivity (Ω-m)	145.25	119.12	120.90	122.23	148.43	102.70
Layer-1 Thickness (m)	1.20	1.20	1.20	1.20	1.19	1.20
Bottom Resitivity (Ω-m)	179.62	141.24	138.91	138.72	197.86	222.35
RMS Error	6.2%	5.2%	3.9%	4.2%	6.5%	2.3%
Climate info from NIWA						
3-day culmulative rain (mm)	0	0	0	1.4	0	0
Soil Temperature 5 cm (°C)	17.2	19.9	21.4	18.5	17.9	22
Soil Temperature 10 cm (°C)	18	20.3	21.4	19.4	18.6	22.2

Continue Table B-1 Twelve-month data collection. Soil resistances are measured in (Ω), and soil resistivities are calculated in (Ω-m).

Date	5/01/2021	10/01/2021	13/01/2021	17/01/2021	20/01/2021	24/01/2021
Soil Resistance Measurement						
Wenner Spacing (m)						
0.1	185.09	564.42	705.77	1068.05	111.73	980.85
0.2	92.52	265.41	320.38	424.50	56.46	421.41
0.5	36.85	69.28	71.83	64.68	24.42	73.57
1	18.06	18.86	19.72	19.53	13.76	17.10
2	8.77	7.65	9.27	10.75	7.86	7.71
3	6.03	5.63	6.68	7.99	5.81	5.46
4	4.84	4.73	5.31	6.49	4.75	4.40
5	4.17	4.16	4.41	5.50	4.07	3.77
10	2.68	2.69	2.39	3.16	2.43	2.31
15	2.00	1.99	1.63	2.21	1.74	1.67
20	1.59	1.57	1.23	1.69	1.34	1.31
Calculated Soil Resistivity						
Wenner Spacing (m)						
0.1	116.30	354.64	443.45	671.08	70.20	616.29
0.2	116.26	333.53	402.60	533.44	70.95	529.55
0.5	115.76	217.64	225.65	203.19	76.72	231.13
1	113.48	118.47	123.88	122.70	86.43	107.46
2	110.15	96.19	116.48	135.07	98.81	96.93
3	113.66	106.13	126.00	150.53	109.46	102.83
4	121.65	118.87	133.40	163.01	119.27	110.60
5	131.06	130.73	138.70	172.83	127.75	118.39
10	168.70	169.15	150.08	198.47	152.97	145.00
15	188.92	187.35	153.34	208.04	163.59	157.52
20	200.41	197.23	154.68	212.52	168.87	164.14
Soil Model Unadjusted						
Layer-0 Resitivity (Ω-m)		358.52	451.72	708.68		635.81
Layer-0 Thickness (m)		0.33	0.28	0.23		0.25
Layer-1 Resitivity (Ω-m)	107.72	90.25	87.63	88.13	70.08	80.32
Layer-1 Thickness (m)	1.84	0.33	0.28	0.99	0.40	0.25
Layer-2 Resitivity (Ω-m)	93.09	79.05	97.97	120.06	96.63	90.03
Layer-1 Thickness (m)	0.21	1.95	1.05	0.21	2.07	2.65
Bottom Resitivity (Ω-m)	179.78	218.42	156.68	191.76	178.59	177.49
RMS Error	2.3%	9.5%	5.1%	4.9%	5.3%	8.3%
Soil Model (warm-start)						
Layer-0 Resitivity (Ω-m)		356.91	448.05	602.26		554.55
Layer-0 Thickness (m)		0.34	0.29	0.23		0.11
Layer-1 Resitivity (Ω-m)	116.31	77.88	87.59	88.83	70.58	85.69
Layer-1 Thickness (m)	1.23	1.01	0.86	0.76	0.62	0.61
Layer-2 Resitivity (Ω-m)	88.11	94.42	136.88	163.04	105.77	100.63
Layer-1 Thickness (m)	1.97	1.67	1.56	1.51	2.03	1.73
Bottom Resitivity (Ω-m)	227.07	221.74	157.94	217.82	177.22	177.44
RMS Error	1.9%	3.5%	3.2%	3.0%	5.5%	3.7%
Climate info from NIWA						
3-day culmulative rain (mm)	0	0	0	0	7.2	0
Soil Temperature 5 cm (°C)	20.5	21.2	21.4	21.6	19.3	19.8
Soil Temperature 10 cm (°C)	21.1	21.7	22.1	22.5	21	20.3

Continue Table B-1 Twelve-month data collection. Soil resistances are measured in (Ω), and soil resistivities are calculated in (Ω-m).

Date	27/01/2021	31/01/2021	4/02/2021	6/02/2021	9/02/2021	13/02/2021
Soil Resistance Measurement						
Wenner Spacing (m)						
0.1	341.24	223.79	276.26	684.37	243.25	534.88
0.2	163.95	110.22	133.89	302.54	120.97	258.92
0.5	48.15	39.35	42.00	58.40	45.60	77.74
1	15.11	17.20	15.50	15.23	19.85	22.18
2	7.33	9.28	8.71	8.90	9.49	9.09
3	5.74	6.96	6.78	6.90	6.87	6.78
4	4.82	5.65	5.58	5.64	5.54	5.53
5	4.17	4.75	4.73	4.76	4.67	4.67
10	2.48	2.63	2.66	2.65	2.61	2.60
15	1.75	1.81	1.84	1.82	1.80	1.79
20	1.34	1.37	1.40	1.38	1.37	1.36
Calculated Soil Resistivity						
Wenner Spacing (m)						
0.1	214.41	140.61	173.58	430.00	152.84	336.08
0.2	206.03	138.51	168.25	380.18	152.01	325.36
0.5	151.28	123.63	131.96	183.47	143.26	244.24
1	94.95	108.08	97.39	95.70	124.73	139.38
2	92.06	116.67	109.40	111.87	119.25	114.25
3	108.12	131.23	127.76	130.10	129.48	127.76
4	121.25	141.91	140.23	141.75	139.34	138.87
5	131.10	149.36	148.75	149.63	146.84	146.62
10	155.66	165.47	167.39	166.34	164.11	163.61
15	164.60	170.36	173.15	171.23	169.64	168.89
20	168.74	172.41	175.58	173.28	172.02	171.09
Soil Model Unadjusted						
Layer-0 Resitivity (Ω-m)			174.49	440.46		337.88
Layer-0 Thickness (m)			0.41	0.27		0.44
Layer-1 Resitivity (Ω-m)	215.86	140.98	47.57	55.30	152.99	67.24
Layer-1 Thickness (m)	0.38	0.41	0.52	0.63	0.61	0.82
Layer-2 Resitivity (Ω-m)	58.50	82.12	168.33	148.36	84.19	142.19
Layer-1 Thickness (m)	1.08	0.89	0.20	0.20	0.96	0.20
Bottom Resitivity (Ω-m)	175.73	175.47	179.29	176.34	175.66	174.45
RMS Error	4.3%	2.2%	6.6%	7.2%	2.3%	6.1%
Soil Model (warm-start)						
Layer-0 Resitivity (Ω-m)	226.09		183.43	542.92		
Layer-0 Thickness (m)	0.13		0.12	0.11		
Layer-1 Resitivity (Ω-m)	78.21	120.53	83.03	82.12	152.99	337.17
Layer-1 Thickness (m)	0.64	0.66	0.55	0.49	0.61	0.17
Layer-2 Resitivity (Ω-m)	113.19	118.39	147.25	141.69	99.56	131.32
Layer-1 Thickness (m)	1.25	1.16	1.09	1.10	1.00	1.59
Bottom Resitivity (Ω-m)	178.37	178.69	176.95	175.30	175.66	173.32
RMS Error	4.3%	2.2%	3.1%	2.1%	2.7%	2.4%
Climate info from NIWA						
3-day culmulative rain (mm)	0	0	0	0	0.2	0
Soil Temperature 5 cm (°C)	21.2	19.4	21.8	21.8	22.1	17.9
Soil Temperature 10 cm (°C)	21.7	20.7	22.4	22.7	22.8	19.2

Continue Table B-1 Twelve-month data collection. Soil resistances are measured in (Ω), and soil resistivities are calculated in (Ω-m).

Date	16/02/2021	20/02/2021	24/02/2021	28/02/2021	3/03/2021	6/03/2021
Soil Resistance Measurement						
Wenner Spacing (m)						
0.1	2890.36	2809.92	4916.17	4807.25	139.86	96.28
0.2	1222.30	1202.22	1950.79	1930.72	70.02	48.59
0.5	167.07	172.47	199.32	207.46	28.50	21.40
1	18.34	18.48	16.36	17.37	15.33	13.39
2	8.83	8.36	8.81	8.98	8.98	8.75
3	6.88	6.57	6.87	6.99	6.58	6.69
4	5.64	5.42	5.67	5.75	5.21	5.45
5	4.79	4.62	4.84	4.89	4.31	4.62
10	2.69	2.63	2.73	2.75	2.29	2.61
15	1.85	1.81	1.88	1.89	1.55	1.81
20	1.40	1.38	1.43	1.44	1.17	1.38
Calculated Soil Resistivity						
Wenner Spacing (m)						
0.1	1816.07	1765.53	3088.92	3020.48	87.88	60.50
0.2	1535.98	1510.75	2451.43	2426.21	87.99	61.06
0.5	524.86	541.83	626.18	651.74	89.53	67.23
1	115.24	116.13	102.79	109.13	96.32	84.11
2	111.00	105.08	110.68	112.91	112.84	109.97
3	129.77	123.91	129.57	131.72	124.10	126.03
4	141.84	136.25	142.56	144.44	131.06	137.04
5	150.42	145.16	151.98	153.65	135.51	145.01
10	168.90	165.06	171.62	172.82	144.13	164.10
15	174.21	171.01	177.41	178.35	146.42	170.63
20	176.56	173.67	180.11	180.92	147.32	173.55
Soil Model Unadjusted						
Layer-0 Resitivity (Ω-m)	1877.21	1819.80	3244.13	3162.34		
Layer-0 Thickness (m)	0.26	0.27	0.23	0.23		
Layer-1 Resitivity (Ω-m)	50.50	49.33	43.77	47.21	87.87	60.41
Layer-1 Thickness (m)	0.62	0.67	0.55	0.58	1.02	0.59
Layer-2 Resitivity (Ω-m)	154.64	141.26	155.72	160.32	147.10	136.01
Layer-1 Thickness (m)	0.20	0.20	0.19	0.20	1.40	1.46
Bottom Resitivity (Ω-m)	180.16	177.85	184.11	184.74	148.59	178.21
RMS Error	5.9%	7.1%	9.2%	6.5%	3.1%	2.3%
Soil Model (warm-start)						
Layer-0 Resitivity (Ω-m)	2398.96	2263.40	3112.43	4236.49		
Layer-0 Thickness (m)	0.20	0.09	0.10	0.08		
Layer-1 Resitivity (Ω-m)	102.05	103.62	86.78	95.18	88.76	64.15
Layer-1 Thickness (m)	0.58	0.58	0.57	0.57	0.44	0.46
Layer-2 Resitivity (Ω-m)	107.72	96.95	100.75	111.66	128.18	163.38
Layer-1 Thickness (m)	1.90	1.89	1.85	1.82	1.62	1.36
Bottom Resitivity (Ω-m)	179.39	178.01	194.32	180.87	157.00	171.57
RMS Error	3.6%	3.8%	3.2%	3.2%	3.4%	4.7%
Climate info from NIWA						
3-day culmulative rain (mm)	26.8	0	0	1.8	0.9	0
Soil Temperature 5 cm (°C)	20.8	19.3	20.3	20.5	19.2	20.1
Soil Temperature 10 cm (°C)	20.3	20.1	21.2	21.7	20.4	21.2

Continue Table B-1 Twelve-month data collection. Soil resistances are measured in (Ω), and soil resistivities are calculated in (Ω-m).

Date	10/03/2021	13/03/2021	16/03/2021	20/03/2021	23/03/2021	27/03/2021
Soil Resistance Measurement						
Wenner Spacing (m)						
0.1	99.65	81.19	101.50	96.60	92.37	97.24
0.2	50.31	42.51	51.10	48.62	46.55	49.00
0.5	22.12	21.62	22.14	21.06	20.43	21.45
1	13.53	13.83	13.83	13.23	13.12	13.61
2	8.52	8.38	8.95	8.71	8.71	8.85
3	6.42	6.19	6.39	6.28	6.28	6.32
4	5.22	5.01	4.81	4.73	4.72	4.75
5	4.42	4.25	3.77	3.71	3.68	3.73
10	2.53	2.47	1.71	1.65	1.61	1.69
15	1.76	1.74	1.09	1.04	1.02	1.09
20	1.35	1.34	0.81	0.77	0.75	0.80
Calculated Soil Resistivity						
Wenner Spacing (m)						
0.1	62.61	51.01	63.77	60.70	58.04	61.10
0.2	63.22	53.41	64.21	61.10	58.50	61.58
0.5	69.48	67.91	69.57	66.15	64.17	67.39
1	85.03	86.88	86.92	83.10	82.42	85.50
2	107.10	105.34	112.44	109.40	109.50	111.15
3	121.00	116.77	120.53	118.38	118.34	119.15
4	131.12	125.94	120.83	118.98	118.57	119.48
5	138.84	133.50	118.51	116.53	115.71	117.26
10	158.84	155.23	107.23	103.44	101.36	106.46
15	166.24	164.07	103.04	98.33	95.88	102.46
20	169.66	168.34	101.44	96.37	93.82	100.94
Soil Model Unadjusted						
Layer-0 Resitivity (Ω-m)						
Layer-0 Thickness (m)						
Layer-1 Resitivity (Ω-m)	62.52	50.57	62.71	62.40	64.82	63.26
Layer-1 Thickness (m)	0.55	0.31	0.76	0.72	0.74	0.72
Layer-2 Resitivity (Ω-m)	123.22	112.23	205.40	211.08	209.92	211.82
Layer-1 Thickness (m)	1.75	2.19	1.11	1.11	1.11	1.10
Bottom Resitivity (Ω-m)	175.37	175.89	174.91	178.89	177.22	178.31
RMS Error	2.9%	5.1%	10.1%	6.3%	4.4%	6.5%
Soil Model (warm-start)						
Layer-0 Resitivity (Ω-m)						
Layer-0 Thickness (m)						
Layer-1 Resitivity (Ω-m)	66.35	60.66	65.00	62.40	64.82	63.26
Layer-1 Thickness (m)	0.29	0.21	0.66	0.72	0.74	0.72
Layer-2 Resitivity (Ω-m)	122.59	112.27	133.42	211.08	209.92	211.82
Layer-1 Thickness (m)	1.59	1.56	1.67	1.11	1.11	1.10
Bottom Resitivity (Ω-m)	175.19	173.98	199.23	178.89	177.22	178.31
RMS Error	2.9%	5.2%	9.5%	5.1%	4.9%	5.3%
Climate info from NIWA						
3-day culmulative rain (mm)	0	0	0.2	0	0.2	0
Soil Temperature 5 cm (°C)	20.2	19.8	18.3	19	20.1	20
Soil Temperature 10 cm (°C)	21.7	20.7	19.3	20	21.1	21

Continue Table B-1 Twelve-month data collection. Soil resistances are measured in (Ω), and soil resistivities are calculated in (Ω-m).

Date	30/03/2021	3/04/2021	6/04/2021	10/04/2021	13/04/2021
Soil Resistance Measurement					
Wenner Spacing (m)					
0.1	94.11	93.20	89.41	93.33	93.62
0.2	47.42	46.95	45.09	47.03	47.22
0.5	20.76	20.52	19.90	20.62	20.84
1	13.31	13.13	12.88	13.18	13.42
2	8.91	8.75	8.56	8.67	8.79
3	6.45	6.31	6.17	6.22	6.28
4	4.84	4.74	4.63	4.67	4.71
5	3.74	3.70	3.62	3.64	3.68
10	1.54	1.60	1.59	1.61	1.64
15	0.94	1.00	1.01	1.02	1.05
20	0.68	0.73	0.74	0.75	0.77
Calculated Soil Resistivity					
Wenner Spacing (m)					
0.1	59.13	58.56	56.18	58.64	58.82
0.2	59.58	59.00	56.66	59.10	59.34
0.5	65.22	64.48	62.52	64.77	65.48
1	83.60	82.49	80.93	82.80	84.30
2	111.92	109.90	107.62	109.00	110.48
3	121.62	119.00	116.21	117.24	118.35
4	121.56	119.20	116.44	117.28	118.26
5	117.59	116.12	113.70	114.48	115.54
10	96.68	100.51	100.04	101.12	103.06
15	88.26	94.50	94.84	96.14	98.52
20	85.11	92.24	92.89	94.28	96.82
Soil Model Unadjusted					
Layer-0 Resitivity (Ω-m)					
Layer-0 Thickness (m)					
Layer-1 Resitivity (Ω-m)	62.58	64.36	64.69	63.50	66.33
Layer-1 Thickness (m)	0.72	0.73	0.78	0.79	0.87
Layer-2 Resitivity (Ω-m)	215.30	205.64	219.12	225.91	226.96
Layer-1 Thickness (m)	1.11	1.07	1.12	1.13	1.18
Bottom Resitivity (Ω-m)	169.24	176.39	177.52	171.19	145.52
RMS Error	7.8%	5.5%	1.7%	7.8%	6.7%
Soil Model (warm-start)					
Layer-0 Resitivity (Ω-m)					
Layer-0 Thickness (m)					
Layer-1 Resitivity (Ω-m)	62.58	64.36	64.69	63.50	66.33
Layer-1 Thickness (m)	0.72	0.73	0.78	0.79	0.87
Layer-2 Resitivity (Ω-m)	215.30	205.64	219.12	225.91	226.96
Layer-1 Thickness (m)	1.11	1.07	1.12	1.13	1.18
Bottom Resitivity (Ω-m)	169.24	176.39	177.52	171.19	145.52
RMS Error	8.3%	4.3%	2.2%	6.6%	7.2%
Climate info from NIWA					
3-day culmulative rain (mm)	3.6	14.4	0	7.6	6.6
Soil Temperature 5 cm (°C)	20.3	20.1	20.4	20.3	19.9
Soil Temperature 10 cm (°C)	21.3	21.1	21.4	21.3	20.9

Continue Table B-1 Twelve-month data collection. Soil resistances are measured in (Ω), and soil resistivities are calculated in (Ω-m).

Date	17/04/2021	20/04/2021	24/04/2021	27/04/2021	1/05/2021	5/05/2021
Soil Resistance Measurement						
Wenner Spacing (m)						
0.1	99.89	99.42	103.26	100.79	99.70	102.53
0.2	50.25	50.07	51.96	50.76	50.21	51.61
0.5	21.63	21.78	22.44	22.09	21.85	22.31
1	13.38	13.69	13.93	13.87	13.76	13.87
2	8.66	8.88	8.97	8.98	8.96	8.95
3	6.22	6.35	6.41	6.41	6.42	6.43
4	4.71	4.78	4.83	4.83	4.84	4.87
5	3.71	3.75	3.79	3.79	3.80	3.86
10	1.70	1.70	1.73	1.73	1.73	1.80
15	1.09	1.09	1.11	1.11	1.11	1.16
20	0.81	0.81	0.82	0.82	0.82	0.86
Calculated Soil Resistivity						
Wenner Spacing (m)						
0.1	62.76	62.47	64.88	63.33	62.65	64.42
0.2	63.14	62.91	65.30	63.79	63.10	64.85
0.5	67.96	68.43	70.51	69.39	68.65	70.10
1	84.06	86.03	87.51	87.18	86.47	87.12
2	108.79	111.60	112.71	112.82	112.58	112.42
3	117.29	119.72	120.82	120.90	121.08	121.14
4	118.26	120.13	121.28	121.28	121.66	122.46
5	116.54	117.93	119.17	119.10	119.53	121.20
10	106.76	107.06	108.63	108.41	108.53	113.05
15	102.91	103.00	104.68	104.44	104.35	109.79
20	101.41	101.44	103.16	102.92	102.75	108.51
Soil Model Unadjusted						
Layer-0 Resitivity (Ω-m)						
Layer-0 Thickness (m)						
Layer-1 Resitivity (Ω-m)	85.39	73.94	59.13	80.06	106.74	176.00
Layer-1 Thickness (m)	1.30	0.85	0.96	1.94	0.84	1.56
Layer-2 Resitivity (Ω-m)	183.65	129.39	161.30	205.66	89.44	299.44
Layer-1 Thickness (m)	1.17	1.07	1.42	1.60	1.27	1.77
Bottom Resitivity (Ω-m)	136.49	145.09	125.00	102.87	100.21	109.06
RMS Error	3.5%	5.6%	7.1%	6.6%	10.4%	6.0%
Soil Model (warm-start)						
Layer-0 Resitivity (Ω-m)						
Layer-0 Thickness (m)						
Layer-1 Resitivity (Ω-m)	85.39	73.94	59.13	80.06	106.74	176.00
Layer-1 Thickness (m)	1.30	0.85	0.96	1.94	0.84	1.56
Layer-2 Resitivity (Ω-m)	183.65	129.39	161.30	205.66	89.44	299.44
Layer-1 Thickness (m)	1.17	1.07	1.42	1.60	1.27	1.77
Bottom Resitivity (Ω-m)	136.49	145.09	125.00	102.87	100.21	109.06
RMS Error	2.3%	6.1%	5.9%	7.1%	9.2%	6.5%
Climate info from NIWA						
3-day culmulative rain (mm)	8	0	0	0	0	0
Soil Temperature 5 cm (°C)	19.8	18.2	17.1	17.5	18.1	17.1
Soil Temperature 10 cm (°C)	20.8	19.2	18.1	18.5	19.1	18.1

Continue Table B-1 Twelve-month data collection. Soil resistances are measured in (Ω), and soil resistivities are calculated in (Ω-m).

Date	8/05/2021	12/05/2021	15/05/2021
Soil Resistance Measurement			
Wenner Spacing (m)			
0.1	103.05	101.14	105.62
0.2	51.82	50.86	53.03
0.5	22.25	21.81	22.39
1	13.73	13.48	13.43
2	8.92	8.84	8.74
3	6.42	6.40	6.37
4	4.85	4.85	4.84
5	3.82	3.82	3.82
10	1.73	1.72	1.71
15	1.10	1.10	1.08
20	0.81	0.81	0.79
Calculated Soil Resistivity			
Wenner Spacing (m)			
0.1	64.75	63.55	66.36
0.2	65.12	63.91	66.64
0.5	69.91	68.53	70.34
1	86.29	84.69	84.37
2	112.12	111.07	109.83
3	121.07	120.71	120.06
4	121.93	121.95	121.74
5	119.87	120.01	119.96
10	108.44	108.08	107.35
15	103.95	103.21	101.92
20	102.22	101.31	99.76
Soil Model Unadjusted			
Layer-0 Resitivity (Ω-m)			
Layer-0 Thickness (m)			
Layer-1 Resitivity (Ω-m)	59.45	69.92	87.87
Layer-1 Thickness (m)	0.73	0.80	1.02
Layer-2 Resitivity (Ω-m)	223.48	193.23	147.10
Layer-1 Thickness (m)	1.11	1.38	1.40
Bottom Resitivity (Ω-m)	102.54	101.23	100.63
RMS Error	4.3%	1.8%	4.1%
Soil Model (warm-start)			
Layer-0 Resitivity (Ω-m)			
Layer-0 Thickness (m)			
Layer-1 Resitivity (Ω-m)	59.45	69.92	87.87
Layer-1 Thickness (m)	0.73	0.80	1.02
Layer-2 Resitivity (Ω-m)	223.48	193.23	147.10
Layer-1 Thickness (m)	1.11	1.38	1.40
Bottom Resitivity (Ω-m)	102.54	101.23	100.63
RMS Error	3.1%	2.3%	2.9%
Climate info from NIWA			
3-day culmulative rain (mm)	3	5.4	0
Soil Temperature 5 cm (°C)	17	15.8	14.7
Soil Temperature 10 cm (°C)	18	16.8	15.7

Appendix C - Variable Line Ratings for OTA-WKM-1

Table C-1 Variable Line Rating for the Transmission Line Under Study.

TRANSPOWER

Branch Details	
Line	OTA-WKM-A
Circuit	OTA-WKM-1
Branch ID	OTA_WKM1.1
Nominal Voltage (kV)	220
Effective Start Date	24-Nov-11

Version Information	
Version	2
Revisions	Updated to 12 changes per day
Revision Date	19-Sep-18
Publication Date	19-Sep-18

iVLR Ratings (MW)

Month	Time of day (NZ Local Time)/ iVLR Rating (MW)											
Jan	1-3	3-5	5-7	7-9	9-11	11-13	13-15	15-17	17-19	19-21	21-23	23-25
	347.14	352.47	352.47	320.08	296.46	305.60	314.37	323.13	352.47	362.38	374.57	379.15
Feb	1-3	3-5	5-7	7-9	9-11	11-13	13-15	15-17	17-19	19-21	21-23	23-25
	352.47	347.14	349.80	323.13	299.51	283.88	286.93	296.46	342.18	367.33	379.15	367.33
Mar	1-3	3-5	5-7	7-9	9-11	11-13	13-15	15-17	17-19	19-21	21-23	23-25
	354.76	352.47	360.09	331.51	308.65	293.41	317.42	323.13	344.85	371.91	390.58	374.57
Apr DT	1-3	3-5	5-7	7-9	9-11	11-13	13-15	15-17	17-19	19-21	21-23	23-25
	364.67	376.86	357.43	362.38	320.08	308.65	308.65	331.51	344.85	374.57	386	364.67
Apr ST	0-2	2-4	4-6	6-8	8-10	10-12	12-14	14-16	16-18	18-20	20-22	22-24
	364.67	376.86	357.43	362.38	320.08	308.65	308.65	331.51	344.85	374.57	386	364.67
May	0-2	2-4	4-6	6-8	8-10	10-12	12-14	14-16	16-18	18-20	20-22	22-24
	362.38	379.15	383.72	381.43	342.18	323.13	323.13	334.18	360.09	369.62	357.43	371.91
Jun	0-2	2-4	4-6	6-8	8-10	10-12	12-14	14-16	16-18	18-20	20-22	22-24
	367.33	367.33	367.33	362.38	344.85	336.85	334.18	336.85	362.38	367.33	379.15	367.33
Jul	0-2	2-4	4-6	6-8	8-10	10-12	12-14	14-16	16-18	18-20	20-22	22-24
	383.72	388.29	374.57	374.57	349.80	336.85	334.18	354.76	367.33	401.63	390.58	392.86
Aug	0-2	2-4	4-6	6-8	8-10	10-12	12-14	14-16	16-18	18-20	20-22	22-24
	405.82	399.34	399.34	383.72	344.85	331.51	376.86	395.15	395.15	405.82	414.2	416.49
Sep ST	0-2	2-4	4-6	6-8	8-10	10-12	12-14	14-16	16-18	18-20	20-22	22-24
	390.58	386.00	392.86	362.38	328.47	325.80	360.09	390.58	388.29	414.2	410.01	395.15
Sep DT	1-3	3-5	5-7	7-9	9-11	11-13	13-15	15-17	17-19	19-21	21-23	23-25
	390.58	386.00	392.86	362.38	328.47	325.80	360.09	390.58	388.29	414.2	410.01	395.15
Oct	1-3	3-5	5-7	7-9	9-11	11-13	13-15	15-17	17-19	19-21	21-23	23-25
	374.57	379.15	383.72	336.85	320.08	352.47	374.57	383.72	418.39	422.59	426.78	405.82
Nov	1-3	3-5	5-7	7-9	9-11	11-13	13-15	15-17	17-19	19-21	21-23	23-25
	371.91	364.67	360.09	328.47	308.65	314.37	320.08	344.85	381.43	395.15	390.58	395.15
Dec	1-3	3-5	5-7	7-9	9-11	11-13	13-15	15-17	17-19	19-21	21-23	23-25
	371.91	352.47	360.09	323.13	323.13	328.47	323.13	331.51	367.33	392.86	386	381.43

Min.	Max.
283.88	426.78

DT = Daylight Savings Time (section of month within daylight savings period)
ST = NZ Standard Time (section of month outside of daylight savings period)

Appendix D - Research Flow Chart

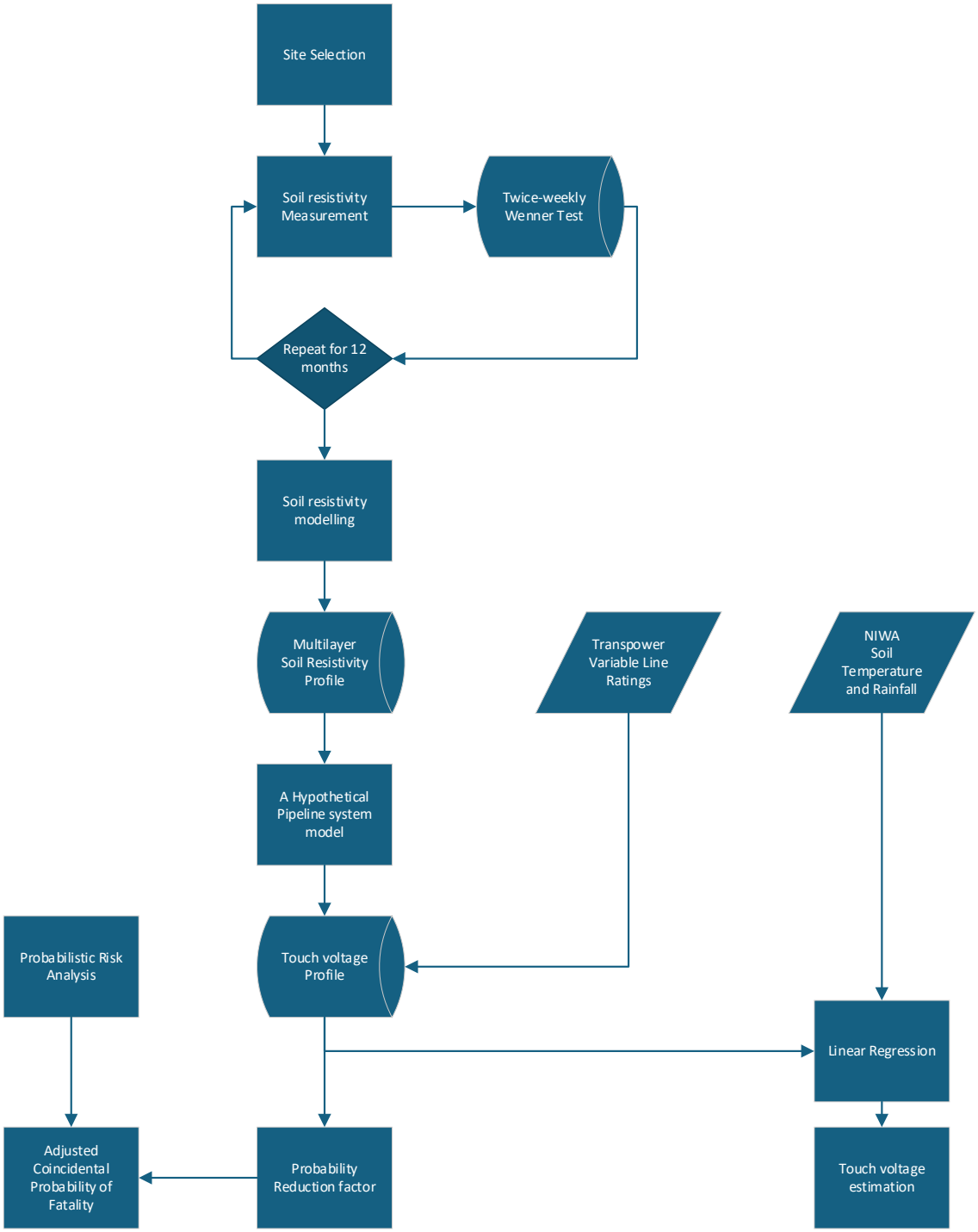

Figure D-1 The Research flowchart

Appendix E – Touch voltage profile

The touch voltage values obtained from the pipeline–transmission line system model, considering the soil resistivity values listed in Table E-1. The system model was developed to assess the touch voltage hazards under various fault conditions, incorporating the influence of soil resistivity on the electrical potential distribution.

Table E-1 Touch Voltage Results Calculated from the Pipeline-Transmission Line System Model

Date	Touch Voltage Limit (V)	Touch voltage under different fault levels (V)				
		10 kA	12 kA	12.5 kA	13 kA	14 kA
2/05/2020	386.66	300.69	360.83	375.87	390.90	420.97
6/05/2020	379.53	297.97	357.57	372.46	387.36	417.16
9/05/2020	381.59	299.79	359.75	374.74	389.72	419.70
13/05/2020	382.69	286.31	343.57	357.89	372.20	400.83
16/05/2020	381.87	296.68	356.02	370.85	385.68	415.35
17/05/2020	382.62	282.43	338.92	353.04	367.16	395.40
20/05/2020	384.03	294.19	353.03	367.74	382.45	411.87
23/05/2020	383.01	291.16	349.39	363.95	378.51	407.62
27/05/2020	384.42	282.83	339.40	353.54	367.68	395.96
31/05/2020	386.37	284.87	341.84	356.09	370.33	398.82
3/06/2020	385.40	284.70	341.64	355.88	370.11	398.58
6/06/2020	386.33	284.64	341.57	355.80	370.03	398.50
10/06/2020	386.33	284.84	341.81	356.05	370.29	398.78
13/06/2020	385.67	286.75	344.10	358.44	372.78	401.45
17/06/2020	386.65	284.14	340.97	355.18	369.38	397.80
20/06/2020	386.67	284.76	341.71	355.95	370.19	398.66
24/06/2020	386.41	286.22	343.46	357.77	372.08	400.70
27/06/2020	386.58	284.94	341.93	356.18	370.43	398.92
1/07/2020	386.46	285.94	343.13	357.43	371.73	400.32
5/07/2020	386.18	284.94	341.93	356.18	370.43	398.92
8/07/2020	386.52	285.49	342.59	356.87	371.14	399.69
11/07/2020	386.49	284.10	340.92	355.12	369.33	397.74
15/07/2020	386.53	283.77	340.52	354.71	368.90	397.27
18/07/2020	385.87	285.82	342.98	357.27	371.56	400.14
22/07/2020	385.92	286.70	344.04	358.38	372.71	401.38
26/07/2020	385.90	287.53	345.03	359.41	373.79	402.54
29/07/2020	385.68	286.74	344.09	358.42	372.76	401.43
1/08/2020	385.80	289.78	347.74	362.23	376.72	405.70
5/08/2020	385.79	289.67	347.60	362.08	376.56	405.53
9/08/2020	385.29	289.91	347.89	362.38	376.88	405.87
12/08/2020	385.23	287.64	345.17	359.55	373.93	402.70
16/08/2020	383.20	286.63	343.96	358.29	372.62	401.29
19/08/2020	382.16	275.89	331.07	344.87	358.66	386.25
22/08/2020	381.87	278.44	334.13	348.05	361.98	389.82
26/08/2020	380.61	278.83	334.60	348.54	362.48	390.36
29/08/2020	381.91	279.45	335.34	349.32	363.29	391.23
1/09/2020	382.00	280.56	336.67	350.70	364.72	392.78
6/09/2020	384.08	282.43	338.91	353.04	367.16	395.40

Continue Table E-1 Touch Voltage Results Calculated from the Pipeline-Transmission Line System Model

Date	Touch Voltage Limit (V)	Touch voltage under different fault levels (V)				
		10 kA	12 kA	12.5 kA	13 kA	14 kA
9/09/2020	383.92	282.43	338.91	353.03	367.15	395.40
13/09/2020	385.20	283.10	339.72	353.87	368.03	396.34
16/09/2020	384.38	283.00	339.60	353.75	367.90	396.20
19/09/2020	384.02	282.90	339.48	353.62	367.76	396.05
23/09/2020	384.96	285.12	342.15	356.40	370.66	399.17
26/09/2020	385.13	282.64	339.17	353.30	367.44	395.70
30/09/2020	384.50	282.22	338.66	352.77	366.88	395.10
3/10/2020	385.99	283.01	339.61	353.76	367.91	396.21
7/10/2020	396.03	286.68	344.02	358.35	372.68	401.35
11/10/2020	407.80	281.90	338.28	352.37	366.47	394.66
12/10/2020	400.42	272.01	326.41	340.01	353.61	380.81
14/10/2020	399.40	284.80	341.76	356.00	370.24	398.72
17/10/2020	382.37	282.73	339.28	353.42	367.55	395.83
21/10/2020	387.88	284.12	340.95	355.15	369.36	397.77
25/10/2020	490.19	288.08	345.70	360.10	374.51	403.31
28/10/2020	657.15	291.92	350.31	364.90	379.50	408.69
29/10/2020	670.58	288.26	345.91	360.32	374.74	403.56
31/10/2020	477.08	285.05	342.06	356.32	370.57	399.07
7/11/2020	391.44	284.59	341.51	355.74	369.97	398.43
8/11/2020	381.92	284.01	340.81	355.01	369.21	397.61
11/11/2020	379.84	285.04	342.05	356.30	370.55	399.06
14/11/2020	386.32	285.03	342.03	356.29	370.54	399.04
18/11/2020	390.26	291.80	350.15	364.74	379.33	408.51
21/11/2020	754.23	295.66	354.79	369.57	384.35	413.92
25/11/2020	390.00	285.56	342.67	356.95	371.23	399.79
28/11/2020	382.20	292.37	350.85	365.47	380.08	409.32
2/12/2020	393.22	289.07	346.88	361.34	375.79	404.70
5/12/2020	408.10	287.59	345.10	359.48	373.86	402.62
9/12/2020	526.43	287.17	344.60	358.96	373.31	402.03
12/12/2020	508.03	288.68	346.41	360.85	375.28	404.15
16/12/2020	586.50	293.44	352.13	366.80	381.47	410.82
19/12/2020	517.57	311.52	373.82	389.40	404.98	436.13
26/12/2020	533.41	307.52	369.02	384.40	399.78	430.53
30/12/2020	531.83	292.40	350.88	365.50	380.12	409.36
2/01/2021	555.44	294.59	353.51	368.24	382.97	412.43
5/01/2021	398.28	293.23	351.88	366.54	381.20	410.52
10/01/2021	492.92	313.79	376.55	392.24	407.93	439.30
13/01/2021	491.37	312.36	374.83	390.45	406.07	437.30
17/01/2021	482.16	311.52	373.82	389.40	404.98	436.13

Continue Table E-1 Touch Voltage Results Calculated from the Pipeline-Transmission Line System Model

Date	Touch Voltage Limit (V)	Touch voltage under different fault levels (V)				
		10 kA	12 kA	12.5 kA	13 kA	14 kA
20/01/2021	386.97	301.61	361.93	377.01	392.09	422.25
21/01/2021	386.32	300.78	360.93	375.97	391.01	421.09
22/01/2021	387.07	298.04	357.65	372.55	387.45	417.26
23/01/2021	401.97	300.44	360.52	375.55	390.57	420.61
24/01/2021	643.95	305.69	366.83	382.12	397.40	427.97
27/01/2021	464.29	304.70	365.64	380.88	396.12	426.59
31/01/2021	401.24	298.97	358.76	373.71	388.66	418.56
4/02/2021	442.95	305.91	367.09	382.38	397.68	428.27
6/02/2021	583.01	305.12	366.14	381.40	396.65	427.16
9/02/2021	431.32	305.39	366.46	381.73	397.00	427.54
13/02/2021	417.90	302.19	362.63	377.74	392.85	423.07
16/02/2021	386.00	306.00	367.20	382.51	397.81	428.41
20/02/2021	387.36	305.40	366.48	381.76	397.03	427.57
24/02/2021	699.67	306.87	368.25	383.59	398.93	429.62
28/02/2021	710.73	307.04	368.45	383.80	399.15	429.85
3/03/2021	380.68	300.73	360.87	375.91	390.95	421.02
6/03/2021	380.96	299.16	358.99	373.95	388.90	418.82
10/03/2021	386.99	299.62	359.54	374.52	389.50	419.46
13/03/2021	381.87	294.28	353.13	367.84	382.56	411.99
17/03/2021	380.97	295.28	354.33	369.09	383.86	413.39
20/03/2021	388.23	296.28	355.53	370.34	385.16	414.79
24/03/2021	563.21	297.28	356.73	371.59	386.46	416.19
27/03/2021	555.26	298.28	357.93	372.84	387.76	417.59
31/03/2021	386.82	297.11	356.53	371.39	386.24	415.95
3/04/2021	388.06	297.52	357.02	371.90	386.78	416.53
7/04/2021	383.09	296.21	355.45	370.26	385.07	414.69
10/04/2021	384.23	288.00	345.60	360.00	374.40	403.20
14/04/2021	384.48	296.25	355.50	370.31	385.13	414.75
17/04/2021	386.37	294.35	353.22	367.94	382.66	412.09
21/04/2021	384.46	299.28	359.13	374.09	389.06	418.99
24/04/2021	385.64	296.22	355.47	370.28	385.09	414.71
28/04/2021	385.50	295.18	354.21	368.97	383.73	413.25
2/05/2021	385.40	296.38	355.65	370.47	385.29	414.93

.